Mechanisms of Tissue-Specific Regeneration in Planarians

by

Samuel Alexander LoCascio

B.S., Biology, Emmanuel College, 2009

Submitted to the Department of Brain and Cognitive Sciences
in partial fulfillment of the requirements for the degree of

DOCTOR OF PHILOSOPHY IN NEUROSCIENCE

at the

MASSACHUSETTS INSTITUTE OF TECHNOLOGY

September 2017

Signature redacted

Author.....
Samuel A. LoCascio
Department of Brain and Cognitive Sciences
July 27, 2017

Signature redacted

Certified by. .....
Peter W. Reddien
Professor of Biology
Thesis Supervisor

Signature redacted

Approved by... .....
Matthew A. Wilson
Professor of Neuroscience
Director of Graduate Education for Brain and Cognitive Sciences

Mechanisms of Tissue-Specific Regeneration in Planarians

by

Samuel Alexander LoCascio

Submitted to the Department of Brain and Cognitive Sciences on July 27th, 2017
in partial fulfillment of the requirements for the degree of

Doctor of Philosophy in Neuroscience

ABSTRACT

How animals establish and maintain the sizes of myriad tissues and organs in tight proportion to one another is a fundamental question of developmental biology. Planarian flatworms regenerate from diverse injuries, in each case precisely restoring body parts to their appropriate proportions. Underlying this ability is a pluripotent population of dividing cells called neoblasts, which are required for homeostatic maintenance and regeneration of all planarian tissues. Whether neoblasts restore proportion by sensing and responding to the presence or absence of specific tissues during regeneration is unknown. We used the planarian eye lineage to address this problem. Following decapitation, neoblasts normally give rise to a large number of eye progenitors, facilitating eye regeneration. Remarkably, we found that eye absence alone was not sufficient to induce this response. Tissue-specific eye regeneration was achieved by homeostatic eye progenitor production accompanied by a decreased rate of cell death specifically in the regenerating eye. Conversely, large head wounds were sufficient to increase eye progenitors, even in the presence of intact eyes. Therefore, eye absence is not sufficient or necessary for neoblasts to increase eye progenitor production. Our findings suggest a "target-blind" model for planarian regeneration in which progenitor production by neoblasts does not depend on feedback from the presence or absence of specific target tissues to be regenerated.

Thesis Supervisor: Peter W. Reddien
Title: Professor of Biology

ACKNOWLEDGEMENTS

It is a great fortune to have had Peter as a mentor. His boundless curiosity and unwavering kindness are lessons in themselves. Our many hours discussing experimental detail or great mysteries of nature have been invaluable to my education.

I thank my lab mates for their skepticism and support. Each day at the bench has been an absolute joy.

I am indebted to my committee for insightful feedback and candid advice that provided a foundation for progress. Troy's dedication to graduate student education has opened doors for myself and others.

Many mentors have generously nurtured my scientific growth: Susan Krassnig, Todd Williams, Joel Kowit, Joey Kurtz, Uwe Beffert, Megan Sykes, and Feng Zhang. In turn, I am thankful for the mentees with whom I have had the privilege of sharing the beauty of science.

I am grateful for my wife Danielle, who reminds me of the pieces of life that matter, and for our dog Jimi, whose companionship is an enduring source of joy.

Thank you Mom, Dad, and Monica for your love and support that span many years and time zones.

TABLE OF CONTENTS

Chapter 1

INTRODUCTION

FEEDBACK CONTROL OF TISSUE PROPORTION IN METAZOANS

Adult animals are composed of myriad cell types, tissues, and organ systems that are established in size during development and maintained in tight proportion to one another for up to hundreds of years. Many animals also restore proportion in adulthood by regenerating body parts lost to injury. These abilities imply the existence of feedback mechanisms that modulate processes affecting the sizes of specific tissues, including cellular proliferation and death, in response to aberrations in proportion. Characterizing how such feedback mechanisms are implemented on the molecular, cellular and organismal level has revealed a diversity of strategies for maintaining and restoring tissue size across the animal kingdom.

Autoregulation of tissue size: the chalone hypothesis

How are the sizes of various tissues reached, restored, and maintained in proportion to one another over the lifespan of an animal? A long-standing hypothesis is that tissues produce factors that specifically limit their own growth. This tissue-specific negative feedback strategy would facilitate maintenance of a homeostatic target tissue size, limiting or promoting growth in response to deviation. Early experimental evidence for autoregulation of growth was reported in 1937, when it was found that aorta extracts inhibit the proliferation of chicken aorta tissue in vitro (Simms and Stillman, 1937). The authors postulated that this inhibition "plays a role in restraining growth in the adult animal body, thereby keeping the cells in their normal dormant state." However, whether the suppressive effects of aorta extract were specific to aorta tissue growth was not

determined. Evidence for such specificity was later provided in Saetren's "A principle of autoregulation of growth." The kidney and liver of young rats exhibit increased mitosis after their respective partial resection. Saetren found that spreading dissociated kidney cells in the peritoneal cavity reduced the mitotic response to partial nephrectomy (kidney resection) but not hepatectomy (liver resection). Conversely, dissociated hepatocytes inhibited the mitotic response to hepatectomy, whereas dissociated cells of the liver, brain, spleen or testes had no effect on the mitotic response to nephrectomy (Figure 1A) (Saetren, 1956). These data indicated that tissues may act as autospecific mitotic inhibitors, a finding that was shortly thereafter extended to the epidermis (Bullough and Laurence, 1960), and proposed as a general principle of size control (Bullough, 1962; Weiss and Kavanau, 1957). Bullough formalized this notion in 1962, introducing the term *chalone* to describe secreted molecules with specific mitotic autoregulatory properties, proposing that "each tissue produces and contains its own specific mitotic inhibitor... they evidently act most strongly to slow growth when the adult state is reached" (Figure 1B) (Bullough, 1962).

Given the likely existence of chalone-like molecules, attempts were made at their isolation and characterization. Inhibitory activity of aorta extract and kidney macerate was abolished by heating, suggesting that inhibitors might be denaturable proteins (Saetren, 1956; Simms and Stillman, 1937). The inhibitory activity of kidney macerate was rapidly degraded in vivo, a property that would allow tissue absence to result in a rapid decline in inhibitor concentration, thus facilitating growth soon after tissue loss (Saetren, 1956). Elegant studies of liver regeneration also suggested that chalones might be circulated factors. A technique called parabiosis was used to join the circulatory

system of two rats, one containing an intact liver, and the other having undergone partial hepatectomy. Remarkably, increased hepatocyte proliferation was observed in the rat with an intact liver, consistent with dilution of the hypothetical inhibitor by shared circulation (Moolten and Bucher, 1967). That a tissue-specific inhibitor might be circulated in the blood stream was theoretically significant, because distribution throughout the body would allow inhibition to be coordinated with the relative size of an animal – larger animals would require more tissue to produce a given concentration of inhibitor.

Despite these important insights into the nature of tissue-specific inhibition, and the demonstration of growth inhibition by extracts of many different tissues (Elgjo and Reichelt, 2004), the identification of specific molecules with chalone-like activity remained elusive for some time. In the 1980s, an oligopeptide named Granulopoiesis Inhibiting Factor was isolated from human leukocytes that specifically inhibited proliferation of myeloid lineages of the hematopoietic system in mice (Paukovits and Laerum, 1982). Identification of similar oligopeptides from other tissues followed, each with autoinhibitory properties. However, a convincing physiological role for these oligopeptides in development or adult homeostasis was not demonstrated. In hindsight, it is not surprising that some concentrated components of cell extracts might affect tissue growth, regardless of their true role in vivo.

Feedback control of skeletal muscle mass by myostatin

A landmark in the understanding of autoregulatory size control was the discovery of Growth / Differentiation Factor-8 (GDF8), now appropriately known as myostatin for its

role in skeletal muscle mass regulation (McPherron et al., 1997). *myostatin* null mice develop normally except for a dramatic and specific overgrowth of skeletal muscle, resulting from both hyperplasia and hypertrophy of muscle cells (Figure 2A). In the adult, *myostatin* expression is exclusive to skeletal muscle, and embryos express *myostatin* in the myotome compartment of developing somites. The muscle-restricted expression and striking muscle-specific overgrowth phenotype strongly suggested myostatin as a long-sought chalone-like molecule, opening the door to a molecular understanding of tissue size autoregulation.

Soon after its initial discovery, myostatin was found to have a conserved role in limiting skeletal muscle mass across vertebrates. Multiple cattle breeds, such as the Belgian Blue, exhibit a "double-muscling" phenotype (Figure 2B), and virtually all breeds with this phenotype harbor loss-of-function *myostatin* mutations (Grobet et al., 1997; Grobet et al., 1998; Kambadur et al., 1997; McPherron and Lee, 1997). *myostatin* mutations also underlie hypermuscular phenotypes in sheep (Clop et al., 2006), dogs (Figure 2C) (Mosher et al., 2007), and humans (Figure 2D) (Schuelke et al., 2004).

Myostatin is a member of the transforming growth factor β (TGF-β) superfamily of secreted ligands (McPherron et al., 1997). It is translated as an inactive propeptide that circulates in the blood in a latent complex, requiring proteolytic processing to reach its active signaling form (Lee, 2004, 2008). Bone morphogenic protein-1/tolloid (BMP-1/TLD) family metalloproteases are at least partly responsible for proteolytic activation of myostatin in vivo, and members of this family are expressed in skeletal muscle (Lee, 2008). Myostatin signals through activin type II receptors, resulting in phosphorylation and activation of intracellular Smad transcription factors (Lee et al., 2005). Myostatin can

be bound and antagonized by multiple proteins including Follistatin, a well-established inhibitor of TGF-β family signaling ligands. *follistatin* is expressed in developing muscle, though not exclusively, and its overexpression in muscle phenocopies *myostatin* null mice (Lee and McPherron, 2001), whereas Follistatin deficiency reduces muscle mass (Matzuk et al., 1995).

Myostatin regulates the proliferation and differentiation of satellite cells, which are quiescent muscle stem cells that proliferate and fuse with myocytes to promote muscle growth (McCroskery et al., 2003; Thomas et al., 2000). Cultured adult satellite cells show decreased proliferation when exposed to recombinant myostatin, which prevents S-phase entry and increases expression of the cyclin-dependent kinase inhibitor p21 (Thomas et al., 2000). *myostatin* mutant mice exhibit an increased density of satellite cells lining muscle fibers, as well as an increased proportion of satellite cells actively cycling in vivo (McCroskery et al., 2003). Cultured satellite cells from *myostatin* mutants, upon being placed in differentiation medium, exhibit delayed but prolonged expression of myogenic transcription factors such as MyoD and Myogenin (McCroskery et al., 2003). Together, these results suggest that the hypermuscular *myostatin* mutant phenotype results from enhanced and/or prolonged proliferation and delayed differentiation of muscle progenitors.

Feedback control of neurogenesis in the olfactory epithelium

The mammalian olfactory epithelium (OE) is a powerful experimental system for investigating how feedback control of adult neurogenesis maintains a constant population size over time (Calof et al., 2002). The OE contains a single major neuronal cell type,

olfactory receptor neurons (ORNs), which are relatively unique among mammalian neurons in that they undergo continuous turnover in adults and are regenerated after ablation. ORNs develop from a well-characterized multistage progenitor lineage, consisting of *Sox2*$^+$ stem cells, *Mash1*$^+$ neural-committed early progenitors, *Neurog1*$^+$ immediate neuronal precursors (INPs), and finally *Ncam1*$^+$ post-mitotic ORNs. Progenitors migrate from their stem cell source to the OE, such that in addition to possessing specific molecular markers, each stage occupies a unique spatial domain. It is immediately apparent from the characteristics of this multistage lineage that opportunities for regulation of neurogenesis are present at multiple developmental stages and locations. OE explants show continued proliferation, migration and differentiation of the ORN lineage in vitro, facilitating detailed studies of factors regulating these neurogenic processes.

Ongoing control of ORN population size in the adult mouse OE was revealed by the fact that ORNs regenerate after ablation (Matulionis, 1975), facilitated by proliferation and increased neurogenesis (Schwartz Levey et al., 1991; Schwob et al., 1992). Purified *Neurog1*$^+$ INPs form colonies producing differentiated neurons in vitro, and the formation of neuron-producing colonies is inhibited by addition of ORNs, but not by addition of non-neuronal OE stromal cells, indicating that a signal from ORNs might limit their own production by INPs (Mumm et al., 1996). Experiments applying recombinant proteins to in vitro cultures implicate TGF-β family bone morphogenic proteins (BMPs) as potential mediators of this negative feedback in the OE (Shou et al., 1999). Interestingly, BMP4 at high concentration decreases neurogenesis by inhibiting lineage progression of *Mash1*$^+$ progenitors, but at low concentration promotes survival of

differentiated ORNs (Shou et al., 2000; Shou et al., 1999), suggesting an intriguing dual feedback mechanism for a single molecule that might promote or inhibit ORN population growth according to the current population size. The relevance of this mechanism in vivo is unknown.

Soon after the discovery of myostatin, the closely related TGF-β superfamily member GDF11 was identified in rats (Nakashima et al., 1999). Although expressed in a number of tissues in mice, within the nasal mucosa, *Gdf11* is restricted to ORNs, and recombinant GDF11 suppresses ORN progenitor proliferation in vitro (Wu et al., 2003). Unlike BMP4, which suppresses neurogenesis at high concentrations by affecting *Mash1*$^{+}$ progenitors (Shou et al., 1999), GDF11 specifically inhibits proliferation of *Neurog1*$^{+}$ INPs (Figure 2F), suggesting that ORN neurogenesis is regulated by different factors at multiple stages of development. Although *Gdf11* mutants exhibit a variety of developmental defects and die within 24 hours of birth, embryos show increased incorporation of progenitors into ORNs, as well as an expanded progenitor population and thickened OE. *follistatin* is expressed in the OE and suppresses the effects of GDF11 on INPs in culture, and *follistatin* mutant embryos display decreased neurogenesis and a thinner OE, in direct contrast to the phenotype observed in *Gdf11* mutant embryos (Wu et al., 2003).

A later study found that the *follistatin* mutant phenotype of decreased OE thickness was not rescued in *follistatin* / *Gdf11* double mutants, indicating that Follistatin might be necessary for the suppression of an additional anti-neurogenic TGF-β in the OE. Indeed, activin βB (ACTβB) is expressed in the OE, and limits neurogenesis by inhibiting proliferation of *Sox2*$^{+}$ and *Mash1*$^{+}$ progenitors, in contrast to GDF11, which

acts on later *Neurog1*$^{+}$ INPs. The study also provided evidence that GDF11 and ACTβB influence neuron/glia lineage choice in *Sox2*$^{+}$ stem cells, implicating progenitor fate choice as a potential feedback point in the autoregulation of tissue size (Gokoffski et al., 2011). In summary, studies of the OE have revealed that multiple developmental stages can serve as distinct targets of feedback for size control, each of which might be regulated through different cellular process, such as fate choice, proliferation, differentiation, or survival.

Comparison of the molecular and cellular strategies used for myogenic and neurogenic feedback control by GDF8/myostatin and GDF11 reveal striking parallels (Figures 2E and 2F) (Gamer et al., 2003). First, GDF8 and GDF11 are closely related, sharing 90% amino acid identity, and define a distinct subgroup within the TGF-β superfamily. Second, each molecule suppresses growth of the tissue from which it is secreted. Third, the cellular mechanism of growth control involves inhibition of progenitor proliferation. Fourth, Follistatin is expressed in skeletal muscle and ORNs, promoting myogenesis or neurogenesis by inhibiting GDF8 and GDF11. One interesting difference is that whereas GDF8 is circulated and restricts growth of a single tissue type distributed throughout the body, GDF11 appears to act locally at multiple distinct anatomical locations. A genetic duplication event producing the paralogs GDF8 and GDF11 may have allowed similar growth inhibitors to be employed in specialized contexts.

Diverse feedback strategies in size regulation and regeneration

There is likely an underexplored diversity of molecular and cellular strategies for negative feedback control of tissues size in addition to those mediated by TGF-β ligands. An intriguing example comes from dopamine neurons of the newt midbrain (Figure 3A) (Berg et al., 2011). Not produced at an appreciable rate during adult homeostasis, these neurons are rapidly regenerated after specific chemical ablation by 6-hydroxydopamine (6-OHDA), facilitated by the proliferation of ependymoglia, which act as stem cells for midbrain neurons after injury. Provision of the dopamine precursor L-3,4-dihydroxyphenylalanine (L-dopa) inhibits regeneration of midbrain dopaminergic neurons but not regeneration of cholinergic neurons, and L-dopa decreases the proliferation of ependymoglia after dopaminergic but not cholinergic neuron ablation. Dopamine receptors are expressed by ependymoglia, and are required for the suppressive effect of L-dopa administration. Finally, administration of dopamine receptor antagonist in uninjured animals stimulates proliferation of quiescent ependymoglia and results in an excess of dopamine neurons. These results suggest that midbrain dopaminergic neurons suppress their own formation by dopamine signaling, and raise the possibility that neurons might control self-neurogenesis via neurotransmitter release. However, further tissue-specific genetic perturbation studies are necessary to confirm the direct effect of neurotransmitter release from midbrain dopaminergic neurons on ependymoglia cells, and to determine whether this mechanism is activity dependent.

The regulation of adipose (fat) tissue by leptin further highlights the diversity of potential strategies for autoregulation of tissue size (Friedman and Halaas, 1998). Leptin is expressed exclusively by adipose tissue (Zhang et al., 1994), is circulated in the blood

(Coleman, 1973), and mutants of the leptin-encoding gene *obese* develop obesity (Ingalls et al., 1950). Although these characteristics are reminiscent of the specific autoregulatory role of myostatin, the leptin receptor OB-R is expressed in diverse tissues, including the central nervous system (Tartaglia et al., 1995). Circulating leptin activates OB-R-expressing neurons in the hypothalamus, which drive increased energy expenditure and decreased food intake behavior to decrease fat stores (Figure 3B) (Friedman and Halaas, 1998; Kennedy, 1953). Thus, although leptin is a factor secreted by a specific tissue that inhibits its own growth, the autoregulatory feedback mechanism is strikingly indirect, involving regulation at the level of organismal behavior.

In contrast to examples of negative feedback control, increased relative concentrations of circulated factors may also stimulate tissue growth. A prime example is the role of bile acids in liver regeneration. Under normal conditions, the liver produces bile acids, most of which are stored in the gall bladder and secreted into the intestine upon meal ingestion. In turn, the liver reabsorbs and processes bile acids from the intestine for future use (Chiang, 2013). Partial hepatectomy considerably increases bile acid processing requirements on remaining hepatocytes, stimulating their proliferation via the nuclear bile acid receptor, FXR (Figure 3C). Supplementing diet with bile acid accelerates liver regeneration and induces liver growth in uninjured animals, whereas sequestration of bile acid delays regeneration (Huang et al., 2006). The liver therefore senses insufficient functional capacity through an elevated bile acid to liver mass ratio, adjusting its size to metabolic requirements. This mechanism is consistent with the aforementioned parabiosis liver regeneration experiments (Moolten and Bucher, 1967), but offers an alternative to the suppressive chalone model previously proposed. Sensing a

mismatch between metabolic requirement and functional capacity is also consistent with liver transplant experiments in dogs, where a liver from a small animal transplanted into an animal twice its size grows to precisely match the size of the recipient's original liver (Kam et al., 1987). Interestingly, intestinal FXR expression is also required for normal liver regeneration, and its activation following partial hepatectomy may facilitate liver regeneration by stimulating production of intestine-derived fibroblast growth factor 15 (Zhang et al., 2012a). Thus, control of liver size is achieved through monitoring of functional capacity and involves cross-talk among multiple organs.

Tissue damage indicates tissue loss and drives regeneration

The actual presence of damaged tissue, in contrast to the absence of healthy tissue, can also provide feedback signals for the regulation of tissue size, particularly in cases where regeneration is required. Acute tissue loss is traumatic and results in damage, inflammation, necrosis, and apoptosis in the remaining tissue. In turn, these processes stimulate cellular proliferation and regeneration. Although general damage signals do not necessarily carry information about the relative sizes of specific tissues, they nevertheless serve as a feedback mechanism to promote growth near wounds where tissues were lost, thus facilitating proportion restoration.

Necrosis is a stress-induced form of unprogrammed cell death that ends when cells rupture and release their contents into the extracellular space. These contents include a heterogeneous collection of normally intracellular molecules that signal the presence of tissue damage, and are collectively termed damage-associated molecular patterns (DAMPs). DAMPs include proteins (e.g., histones, heat shock proteins), nucleic

acids (e.g., adenosine, ATP) and other metabolites, and are recognized by innate immune, purinergic and other receptors. They contribute directly to tissue regeneration by recruiting and stimulating proliferation of tissue progenitors, and indirectly by immune cell recruitment and activation (Cordeiro and Jacinto, 2013; Vénéreau et al., 2015).

The immune response to tissue damage is critical for regeneration. For example, systemic depletion of macrophages during a critical time window after amputation permanently blocks limb regeneration in axolotl, impacting regeneration-associated gene expression and cytokine signaling at the wound site (Godwin et al., 2013). Macrophages and other leukocytes have been implicated in regeneration of diverse tissues, including skeletal muscle (Deng et al., 2012; Heredia et al., 2013), cardiomyocytes (Aurora et al., 2014), kidney (Zhang et al., 2012b), intestine (Lindemans et al., 2015) and hair follicle (Chen et al., 2015), facilitating regeneration by clearing debris and senescent cells (Yun et al., 2015), and by provision of cytokines that affect progenitor and stem cell proliferation (Wynn and Vannella, 2016).

Apoptosis, the orderly process of genetically programmed cell death, is not only a common consequence of traumatic tissue loss, but also a critical component of regeneration. Temporally paired waves of apoptosis and proliferation in response to injury have been observed in diverse animals with regenerative capacity (Vriz et al., 2014), and evidence for a causal relationship comes from studies employing pharmacological inhibition of apoptosis. For example, head regeneration in *Hydra* is associated with simultaneous apoptosis and proliferation at the wound site, and inhibition of apoptosis prevents wound-induced proliferation and head regeneration. In this context, apoptotic cells appear to act as a source of Wnt3, activating β-catenin in surrounding

cells to drive proliferation (Figure 3D) and head regeneration. Amazingly, heat-shock-induced apoptosis in the regenerating foot led to ectopic head regeneration (Chera et al., 2009). Inhibition of apoptosis in the zebrafish tail during an apoptotic wave that initiates around 12 hours post amputation reduces concomitant progenitor proliferation, alters wound-induced gene expression, and impedes tail regeneration (Gauron et al., 2013), and similar findings have been reported for *Xenopus* tadpole tail regeneration (Tseng et al., 2007). The details of such findings should be interpreted with caution, as organism-wide pharmacological inhibition of apoptosis likely has multiple consequences, and the inhibitors are known to be inherently toxic (Gauron et al., 2013). Additional evidence for the role of apoptosis in regeneration comes from a study in which irradiated apoptotic mouse embryonic fibroblasts (MEFs) stimulated proliferation of various stem and progenitor cell types in culture. Caspase-deficient MEFs exhibited decreased apoptosis in response to irradiation, and did not induce proliferation to the same degree as irradiated wild-type MEFs. Furthermore, mice deficient in the executioner caspase 3 showed delayed epidermal repair and liver regeneration, in association with decreased injury-induced proliferation (Li et al., 2010).

Although adult fruit flies possess little capacity for regeneration in adulthood, developing *Drosophila* wing imaginal discs in which up to 60% of cells are killed by irradiation exhibit heightened proliferation and go on to produce wings of normal size and morphology (Haynie and Bryant, 1977). Investigation of compensatory proliferation in the imaginal wing disc was facilitated by the creation of "undead" apoptosis-arrested cells, using a genetic approach to initiate apoptosis while simultaneously preventing its completion by expression of the baculovirus protein p35, an inhibitor of executioner

caspases (Huh et al., 2004; Pérez-Garijo et al., 2004; Ryoo et al., 2004). Apoptosis-arrested cells persistently express the mitogens *wingless* and *decapentaplegic* (Wnt and BMP ligands, respectively), which induce proliferation of non-apoptotic neighboring cells (Figure 3D), and lead to the development of abnormally large and deformed wings. These results offer insight into how apoptosis coordinates autonomous orderly cell death and non-autonomous compensatory proliferation, and suggest a possible feedback mechanism whereby tissue death induces proliferation to restore proportion in diverse models of regeneration.

Cell death in the limitation of tissue size

Besides the counterintuitive role of increased cell death in regenerative tissue growth, cell death can also serve as an important feedback mechanism for limiting tissue size in response to inappropriate growth or proliferation. The studies outlined above indicate that development of the *Drosophila* wing imaginal disc is robust to experimentally induced cell death, through a mechanism involving compensatory proliferation. The opposite is also true – hyperproliferation results in compensatory apoptosis, leading to the development of a morphologically normal adult wing. Clones overexpressing dMyc grow and proliferate more rapidly than neighboring wild-type cells, whereas wild-type clones grow and proliferate more rapidly than neighboring *Minute* mutant cells (containing dominant mutations in genes encoding ribosomal proteins). In each case, the juxtaposition of cells growing at different rates results in apoptosis of the slower-growing cells (whether they are wild-type or mutant), a phenomenon termed "cell competition" (de la Cova et al., 2004; Morata and Ripoll, 1975; Moreno and Basler, 2004; Vincent et

al., 2013). Competition-induced cell death ensures that the presence of hyperproliferative "super-competitors" does not lead to net overgrowth (Figure 4A).

A screen for genes upregulated in prospective "loser" cells resulting from competition in both dMyc-overexpressing and *Minute* mosaics identified Flower, a transmembrane protein expressed in the *Drosophila* wing imaginal disc that is critical for cell competition-induced apoptosis (Rhiner et al., 2010). The Flower-encoding gene *Fwe* produces three splice forms, termed fwe^{ubi}, $fwe^{Lose\text{-}A}$ and $fwe^{Lose\text{-}B}$. fwe^{ubi} is expressed at low levels in all cells of the wing imaginal disc, whereas during cell competition, fwe^{Lose} isoforms are upregulated in prospective losers. Clones with induced expression of fwe^{Lose} proliferate normally but exhibit increased apoptosis when juxtaposed with wild-type cells expressing fwe^{ubi}. In contrast, whole discs or entire flies ubiquitously expressing fwe^{Lose} do not exhibit increased apoptosis and develop normally. *fwe* RNAi in the entire disc disrupts the induction of apoptosis by dMyc-overexpressing clones and limits their hyperproliferation, thereby reducing cell competition. Thus, differential expression of Flower isoforms in neighboring cells is sufficient and necessary for normal cell competition.

Mechanical feedback is hypothesized to regulate tissue size (Shraiman, 2005), and recent evidence suggests that cell displacement is indeed a consequence of physical crowding in epithelia, implicating it as a feedback mechanism for the limitation of tissue size. The elimination of excess live epithelial cells occurs by displacement from epithelial sheets. Extrusion and delamination refer to displacement apically or basally, respectively, and unless part of a programmed epithelial to mesenchymal transition, both processes cause loss of contact-dependent survival signals and apoptosis. In one study, cultured

epithelial cells were grown to confluence on a stretched elastic surface, which was then un-stretched to induce acute crowding. Crowded epithelia exhibited increased extrusion of live, non-apoptotic cells, which subsided as the cells returned to their original confluent density by 6 hours post crowding (Figure 4B) (Eisenhoffer et al., 2012). Extrusion from crowded epithelia was dependent on Rho kinase-mediated actomyosin contraction, and required the mechanical stretch receptor Piezo1 in vivo. Interestingly, Piezo1 is also required for a proliferative response to mechanically stretching, but how Piezo1 mediates opposite effects in crowded or stretched epithelia is not fully understood (Gudipaty et al., 2017). In the developing fly notum epithelium, delamination of cells occurs almost exclusively at the midline, where cell crowding, oblong cell geometry and decreased epithelial tension are observed. Experimental induction of hyper- or hypoproliferation results in a concomitant increase or decrease in delamination at the midline, thus buffering the epithelium against aberrations in tissue growth (Marinari et al., 2012).

Classic studies on the role of cell death in neurodevelopment also demonstrate its central role in the limitation of tissue size. Extirpation of the developing chick limb bud results in a decreased population of neurons in the adult corresponding spinal segment that normally innervates the limb (Hamburger, 1934). It was initially hypothesized that the limb bud provides a neurogenic signal, and that its removal results in decreased neurogenesis in the spinal cord, thus leading to hypoplasia. Although this is partly true, a subsequent study investigated cell death as the cause of hypoplasia (Hamburger and Levi-Montalcini, 1949) pointing out that "few investigators have considered the possibility that a hypoplasia following a reduction of the periphery might be attributed, wholly or in part,

to regressive changes, that is to the atrophy and breakdown of neurons." The authors observed a "degenerative process" occurring on days 5 and 6 of embryogenesis in all spinal ganglia with the exception of the larger ganglia innervating the limbs. Ganglia corresponding to extirpated limb buds were no longer spared from this wave of cell death, resulting in their atrophy (Figures 4C and 4D). The experiments suggest that an excess of spinal neurons are produced early in development and are subsequently culled by cell death to match the size of the target they innervate. Nerve growth factor (NGF) was later identified as a target-derived secreted protein that signals via a retrograde axonal transport-dependent mechanism to promote neuronal survival (Cohen, 1960; Cohen and Levi-Montalcini, 1956; Levi-Montalcini, 1987; Oppenheim, 1991; Paravicini et al., 1975). Because NGF expression is limited, it is thought to support the survival of a finite number of competing neurons projecting to the same source, thus limiting the population to an appropriate size for the target. Additional factors with homology to NGF have now been identified, collectively termed neurotrophins, which play similar roles in determining neuronal population size, as well as diverse roles in promoting growth and shaping neural circuits (Park and Poo, 2013).

CONTROL OF TISSUE PROPORTION IN PLANARIANS

Introduction to planarian anatomy, regeneration, and proportionality

Planarians are free-living freshwater flatworms that are known for their legendary ability to regenerate body parts after diverse injuries, with even a small body fragment capable of regenerating an entire animal (Morgan, 1898; Reddien and Sánchez Alvarado, 2004). Planarians are bilaterally symmetric and possess derivatives of all three germ layers. The nervous system consists of bilobed cephalic ganglia (i.e., a brain) attached to ventral nerve cords, and includes a diversity of central and peripheral neuron types. Paired eyes on the dorsal surface consist of pigmented optic cups juxtaposed by photoreceptor neurons that project their axons ventroposteriorly to the brain. A muscular tube called the pharynx extends ventrally out of the body to ingest food and excrete waste, and is connected to a multi-branched intestinal system. The epidermis encases the animal, with ventral cilia facilitating locomotion. A basement membrane separates the outermost epidermis from a network of body-wall muscle, and mesenchymal tissue called parenchyma fills the space around the internal organs. Regardless of the injury, planarians regenerate this complex anatomy, restoring all tissues to their correct proportion and place (Figures 5A–5D) (Morgan, 1898; Reddien and Sánchez Alvarado, 2004). Planarian regeneration occurs even in the absence of food, with tissues being restored to their proper proportion without net organismal growth (Morgan, 1901). This process involves both growth and degrowth of specific tissues. For example, the eyes in a decapitated head degrow to a size proportional to the new body fragment, whereas the same fragment must grow a new pharynx (Figure 5D).

The ability of planarians to maintain and restore proportional tissue size is remarkable. Removal of a body part results in acute deviation from proportionality, and regeneration is the process by which proportionality is restored. For example, decapitation of a proportional planarian with an appropriate brain : pharynx size ratio immediately results in two disproportional fragments (Figure 6A). The body lacking a head will have a reduced brain : pharynx size ratio, necessitating brain growth and pharynx degrowth. Conversely, the head lacking a body will have an increased brain : pharynx ratio, necessitating brain degrowth and pharynx growth. Thus, planarian regeneration is not simply the replacement of body parts, but rather a coordinated adjustment in the sizes of multiple tissues that results in restoration of proportion. In response to frequent feeding, uninjured planarians exhibit uniform proportional growth of all tissues, whereas starvation induces the opposite effect, degrowth (Figures 6B and 6C). Thus, adult planarians undergo reversible changes in size by an order of magnitude while maintaining tissue proportionality within tight limits, and rapidly restore proportionality after limitless perturbations resulting from injury. These powerful abilities make planarians an ideal model for the investigation of feedback mechanisms that maintain and restore proportional tissue size.

In order to understand potential points of tissue size regulation, it is important to define the processes that contribute to the growth and degrowth of differentiated tissues. A population of dividing cells called neoblasts contains pluripotent stem cells and is required for the growth, regeneration, and homeostatic maintenance of all differentiated planarian tissues (Baguñà et al., 1989; Wagner et al., 2011). Neoblasts fuel growth by giving rise to progenitors that incorporate into pre-existing or regenerating tissue (Figure

6D). Because differentiated tissues are post-mitotic, their growth and regeneration does not involve the proliferation of the tissues themselves. Hypertrophy of existing differentiated cells has also not been observed as a growth or regeneration strategy. Therefore, neoblast-derived tissue production leading to increased cell number is the primary process directly contributing to tissue growth. Degrowth appears to be primarily mediated by cell death, as apoptosis has been characterized under homeostatic and regenerative conditions (Pellettieri et al., 2010), whereas cellular hypotrophy, dedifferentiation or transdifferentiation have not been observed. Tissue size is therefore ultimately affected by two primary processes: neoblast-derived tissue production and differentiated cell death (Figure 6D). Tissue size remains constant when the two processes are in equilibrium, whereas their imbalance results in net growth or degrowth. With this framework in mind, it is possible to consider specific mechanisms by which these primary processes might be regulated to affect tissue size.

General neoblast characteristics and heterogeneity

A number of shared features define neoblasts as a population. Neoblasts constitute approximately 20% of all cells (Baguñà et al., 1989), and reside throughout the adult animal in the parenchyma, being generally excluded only from the anterior head tip and pharynx (Figure 5B) (Newmark and Sánchez Alvarado, 2000; Reddien et al., 2005b). Morphologically, neoblasts are small (5-8 μm) and circular with a high nuclear to cytoplasmic ratio. They are transcriptionally distinct from other cell types, and express neoblast-specific genes including the PIWI protein *smedwi-1*, conveniently allowing their identification in vivo (Reddien et al., 2005b). Neoblasts are highly proliferative, and

continuous BrdU administration results in labeling of the entire population within 24 hours (Newmark and Sánchez Alvarado, 2000). As the only adult somatic dividing cells, neoblasts are specifically ablated by irradiation (Baguñà et al., 1989; Dubois, 1949; Reddien et al., 2005b), leading to loss of regenerative ability, failure of homeostatic tissue maintenance, and eventual death. Transplantation of unirradiated neoblasts (but not other cell types) from a healthy donor into neoblast-ablated animals rescues tissue maintenance and regenerative ability (Baguñà et al., 1989). Remarkably, transplantation of a single healthy adult neoblast leads to reconstitution of the entire neoblast population, and complete restoration of homeostatic tissue maintenance and regenerative ability (Wagner et al., 2011). Thus, neoblasts are pluripotent as a population, and at least some neoblasts are pluripotent stem cells. Pluripotent neoblasts with the ability to reconstitute an entire animal are termed clonogenic neoblasts, or cNeoblasts. However, the proportion of neoblasts with such capabilities is unknown, and a cNeoblast-specific marker has not been identified.

Although often analyzed at the population level, considerable heterogeneity exists within neoblasts. A large proportion of neoblasts express transcription factors that also mark specific differentiated cell types. These lineage-specific transcription factors are expressed in non-overlapping neoblast subsets (Scimone et al., 2014a) and facilitate specification of neoblasts into distinct fates, with neoblasts expressing them acting as tissue progenitors (Adler et al., 2014; Cowles et al., 2013; Currie and Pearson, 2013; Forsthoefel et al., 2011; Lapan and Reddien, 2011, 2012; März et al., 2013; Scimone et al., 2014b; Scimone et al., 2011; van Wolfswinkel et al., 2014). Among the best-characterized examples of neoblast-derived lineage-specific progenitors are eye

progenitors (Lapan and Reddien, 2011, 2012). Eye progenitors express the transcription factor *ovo*, which specifically marks the entire eye lineage and is required for the homeostatic maintenance and regeneration of the eyes. *smedwi-1*$^{+}$/*ovo*$^{+}$ progenitors appear in the head posteriorly to the eyes, then migrate forward and incorporate into existing eyes during homeostatic maintenance, or coalesce to form eyes *de novo* in the case of regeneration. Eye progenitors differentiate as they migrate, progressively upregulating genes specific to the particular eye cell type (e.g., photoreceptor neurons or pigmented optic cup cells) that they are destined to become (Lapan and Reddien, 2011). Neoblast-derived progenitors similar to those for the eye exist for most if not all differentiated planarian tissues (Scimone et al., 2014a). Thus, in addition to neoblasts being regulated as a general population, specification of neoblasts into distinct fates and the behavior of these neoblast-derived progenitors are potential points of regulation for feedback control of specific tissue size.

Behavior and regulation of neoblasts as a population

General neoblast proliferation appears to be an important point of regulation for tissue size control during regeneration. Amputation induces neoblast proliferation, a process characterized in detail by immunofluorescence (IF) for a conserved indicator of mitosis, histone H3 phosphorylated at serine 10 (H3P) (Wenemoser and Reddien, 2010). A body-wide increase in the density of mitoses occurs approximately 6 hours post amputation. This is followed by a global decrease in mitoses by 18 hours, though mitoses are still elevated in comparison to uninjured animals at this time point. A second peak of mitosis is observed at 48 hours, which contrasts with the 6-hour peak in that it is localized to the

wound site and sustained for a number of days thereafter (Figure 7A). Wounds that do not result in significant tissue loss, such as a needle poke or a non-amputating incision, elicit the 6-hour global mitotic response, but not the 48-hour local mitotic response, indicating that sustained proliferation is specific to wounds that require tissue regeneration (Figure 7B).

Forward genetic screens based on transcriptomic analysis of regenerating tissue in combination with in situ hybridization (ISH) and RNA interference (RNAi) have identified a number of genes involved in or required for the regeneration response (Reddien et al., 2005a; Wenemoser et al., 2012; Wurtzel et al., 2015). One such gene, *follistatin*, appears to play a central and specific role in the neoblast response to tissue absence (Gaviño et al., 2013; Roberts-Galbraith and Newmark, 2013). *follistatin* expression is induced at wounds, and sustained at wounds that require tissue regeneration. *follistatin(RNAi)* animals exhibit a normal 6 hour mitotic response to wounding, but fail to mount the 48 hour mitotic peak associated with tissue regeneration, and do not regenerate decapitated heads (Gaviño et al., 2013; Roberts-Galbraith and Newmark, 2013). Although Follistatin is required for regeneration of missing tissues and the proliferative response to tissue absence, uninjured *follistatin(RNAi)* animals sustain long-term homeostatic maintenance of existing tissues and do not exhibit obvious morphological abnormalities. Thus, *follistatin* is specifically required for regeneration and the increased proliferative response to tissue absence (Gaviño et al., 2013).

Planarian Follistatin appears to mediate its effects through inhibition of TGF-β ligands, namely Activins, as defects in proliferation and regeneration induced by *follistatin* RNAi are suppressed by simultaneous RNAi of either of two identified

planarian Activin genes. Despite suppressing head regeneration, *activin* is expressed primarily in the gut and pharynx of uninjured animals. Its expression is dynamic, and it is upregulated at amputations as well as incisions that do not remove tissue. Although *activin* RNAi suppresses the *follistatin* RNAi phenotype, *activin* RNAi alone does not significantly affect neoblast proliferation (Gaviño et al., 2013; Roberts-Galbraith and Newmark, 2013). These characteristics indicate that a simple TGF-β-mediated tissue-specific autoregulatory circuit (akin to those involving myostatin or GDF11 in vertebrates) wherein Activin suppresses the formation of the tissues that express it under homeostatic conditions is not likely. Further analysis of the roles of planarian TGF-β ligands in regeneration and homeostasis will be required to determine if such a circuit exists, or if an alternative autoregulatory strategy is implemented.

General neoblast proliferation is also affected by feeding, starvation, and animal size (Baguñà, 1974, 1976). Interestingly, the mitotic response to feeding parallels the response to amputation, with an early peak around 6-8 hours, followed by a second peak around 48 hours (which is global rather than local) that gradually recedes by approximately 1-2 weeks post feeding, after which mitosis remains relatively constant. The immediate increase in percentage of mitotic neoblasts in response to feeding decreases as overall animal size increases, and baseline mitotic rates in homeostatic animals also decrease with overall animal size. The effects of feeding and growth on neoblast mitosis should be revisited with current imaging tools to confirm these findings. An inverse relationship between mitosis and animal size could help limit growth and degrowth beyond organismal sizes that become disadvantageous, and these processes indeed may decelerate in very large and small animals, respectively (Baguñà and

Romero, 1981; Morgan, 1901). Whether and how overall organismal size mediates feedback on neoblast proliferation in planarians is largely unexplored.

Migration of neoblasts and their progeny also contributes to regeneration at wound sites and the homeostatic maintenance of tissues. The distal tip of the pharynx and the anterior head tip do not contain neoblasts, indicating that non-dividing progeny must migrate to these sites during homeostatic maintenance (Newmark and Sánchez Alvarado, 2000; Reddien et al., 2005b). Amputation in the anterior head tip induces recruitment of mitotic cells to this site, indicating that migration also plays a role in regeneration (Wenemoser and Reddien, 2010). Further evidence of regenerative neoblast migration comes from experiments in which irradiated planarians were partially protected by a lead shield, creating an "island" of unirradiated neoblasts in an otherwise neoblast-ablated animal. Unirradiated neoblasts generally did not migrate into the irradiated regions of uninjured animals, whereas amputation in irradiated regions induced migration of neoblasts towards the wound (Guedelhoefer and Sánchez Alvarado, 2012). Neoblast recruitment, in addition to proliferation, is therefore a likely feedback strategy for the restoration of tissue size after wounding.

Two recent studies identified a requirement for planarian integrins in the proper migration of neoblasts and their progenitors during regeneration and homeostasis (Bonar and Petersen, 2017; Seebeck et al., 2017). Integrins are transmembrane receptors that facilitate interactions between the extracellular matrix and cytoskeleton, and contribute to cellular migration in diverse contexts (Huttenlocher and Horwitz, 2011). *βI-integrin* RNAi resulted in failure of neoblasts transplanted into irradiated animals to migrate towards wounds (Seebeck et al., 2017). This failure was observed when either the host or

neoblast donor underwent *β1-integrin* RNAi, suggesting both an autonomous and non-autonomous role for integrins in neoblast migration, although this interpretation is complicated by the possibility of the effects of RNAi spreading between donor and host cells. *β1-integrin(RNAi)* regenerating heads displayed gross disorganization and mislocalization of tissues, suggesting a failure of neoblast-derived tissue progenitors to migrate to their correct locations after specification (Bonar and Petersen, 2017; Seebeck et al., 2017). These studies provide important insight into the migratory cellular machinery, but further investigation is required to determine the factors that actually guide neoblasts and their progeny towards the wound or their appropriate targets.

Neoblast heterogeneity and tissue-specific progenitors

The specification of neoblasts into distinct lineage fates is an important point of regulation for the control of tissue proportions. Consistent with this, the abundance of different specified neoblast types is reflected by the relative sizes of their corresponding differentiated tissues (Figure 8). For example, roughly a quarter of all dividing neoblasts are *zfp-1*$^{+}$ and consist largely of epidermal progenitors (van Wolfswinkel et al., 2014), and the epidermis is a highly abundant tissue that exhibits rapid turnover. By contrast, the eyes are very small in comparison to the epidermis, and their progenitors make up a tiny fraction of all neoblasts, with a total of approximately 5-10 eye progenitors being present in a homeostatic animal at a given time (Lapan and Reddien, 2011, 2012).

Disruption of gene expression affects formation of specific progenitor classes, resulting in altered tissue proportions. A clear example of this is that RNAi of some transcription factors eliminates progenitors for specific tissues altogether (e.g., *ovo*$^{+}$ eye

progenitors, *FoxA*$^{+}$ pharynx progenitors, *zfp-1*$^{+}$ epidermal progenitors), resulting in complete failure of their homeostatic maintenance and regeneration (Figure 8) (Adler et al., 2014; Lapan and Reddien, 2012; van Wolfswinkel et al., 2014). RNAi of Wnt pathway components expressed in the head increases or decreases brain progenitor numbers, resulting in corresponding alterations in brain size (Hill and Petersen, 2015). RNAi of *p66*, a component of the nucleosome remodeling and deacetylase (NuRD) complex, alters the ratio of photoreceptor neurons (PRN) to pigmented optic cup cells in the eye by specifically increasing PRN progenitor formation (Vásquez-Doorman and Petersen, 2016). Finally, *NPHP8* RNAi specifically increases the proportion of *POU2/3*$^{+}$ protonephridia progenitors, leading to disproportionately large protonephridia (Thi-Kim Vu et al., 2015). Together, these data indicate that the relative rates of neoblast-derived progenitor production are an important determinant of homeostatic tissue size.

Overall rates of progenitor specification during homeostasis are also controlled by spatial restriction of specification. For example, eye progenitors are specified in the head, whereas pharynx progenitors are specified in the trunk (Figure 8). A number of molecules associated with embryonic patterning (e.g., Wnt, BMP, FGFRL) are expressed in gradients within planarian muscle along the primary body axes, and spatially restrict the location of progenitors (Gurley et al., 2008; Petersen and Reddien, 2008; Reddien, 2011; Scimone et al., 2016; Stückemann et al., 2017; Witchley et al., 2013; Wurtzel et al., 2017). For example, *bmp4* is most strongly expressed dorsally, and its expression gradient defines the dorsoventral axis. *bmp4* RNAi results in dorsal specification of normally ventrally restricted progenitors, effectively increasing the overall rate of ventral progenitor specification (Wurtzel et al., 2017). Similarly, a Wnt signaling gradient, as

defined by β-catenin activity, defines the anteroposterior axis, and *β-catenin(RNAi)* animals no longer restrict anterior progenitors (such as *ovo*$^{+}$ eye progenitors) to the head, leading to the ectopic formation of eyes (Gurley et al., 2008; Petersen and Reddien, 2008; Stückemann et al., 2017; Witchley et al., 2013). Patterning molecule expression gradients are rapidly rescaled after amputation, facilitating de novo progenitor specification in a new appropriate location. For example, eye progenitors are not specified in the tail during homeostasis. However, anterior patterning molecules are upregulated in the anterior of tail fragments after amputation, facilitating de novo expression of eye progenitors (Gurley et al., 2010; Lapan and Reddien, 2011, 2012; Petersen and Reddien, 2009). Regional patterning molecule expression therefore spatially restricts neoblast specification during homeostasis and regeneration, affecting overall production of specific tissues. Whether the same patterning molecules also contribute to relative rates of progenitor specification within a given location is not clear.

Tissue-specific progenitor numbers are also modulated under physiological conditions such as regeneration (Figure 8). For example, during homeostasis, *ovo*$^{+}$ eye progenitors are present in small numbers in the head. Decapitation results in dramatic amplification of eye progenitor numbers in the anterior of the remaining body, facilitating rapid eye regeneration (Lapan and Reddien, 2011, 2012). Similarly, pharynx removal induces amplification of *FoxA*$^{+}$ pharynx progenitors, facilitating pharynx regeneration (Adler et al., 2014). These findings raise the possibility that tissues might limit the specification of their own progenitors through a chalone-like autoregulatory feedback loop (Adler and Sánchez Alvarado, 2015; Adler et al., 2014; Mangel et al., 2016; Nishimura et al., 2011; Ziller-Sengel, 1967) but several questions remain regarding this

hypothesis. For example, pharynx removal increased *FoxA*$^{+}$ progenitors, but the responses of non-pharynx progenitors following pharynx resection have not been examined (Adler et al., 2014), so the specificity of progenitor amplification in this context is unclear. Decapitation removes the eyes and results in amplification of eye progenitors (Lapan and Reddien, 2011, 2012), yet also likely results in amplification of progenitors for the many neural cell types that require regeneration after such an injury. Whether eye removal alone also induces eye progenitor amplification has not been tested, but this would be predicted for a system depending on autoregulatory feedback loops for individual tissues. Thus, it is currently unclear whether progenitor amplification is a result of general regional neoblast proliferation near wounds, or if progenitor amplification is controlled specifically by the presence or absence of individual differentiated tissues. Distinguishing between these possibilities is crucial to understanding how proportional tissue size control is achieved in planarians, and an experimental undertaking of this question is presented in Chapter 2.

Regulation of cell death

The regulation of cell death plays a complementary role to neoblast proliferation and specific tissue production in the control of planarian tissue proportion. Similar to neoblast proliferation, cell death is dynamically modulated in response to feeding, starvation, wounding, and tissue absence. However, considerably less is known about cell death, as robust tools for observing its occurrence in specific cell types and altering its progression have not been established in planarians. Direct analysis of apoptotic cell death has been performed at a non-tissue-specific body-wide or regional level using TUNEL (terminal

deoxynucleotidyl transferase-mediated dUTP nick end labeling) (Pellettieri et al., 2010). The contribution of cell death to tissue size control is also evident based on the fact that tissues decrease in size and cell number during degrowth and regeneration, providing an indirect indicator of cell death.

Starvation induces proportional degrowth of tissues (Baguñà and Romero, 1981; Oviedo et al., 2003), which results from cell death occurring at a rate that exceeds cell production. Given that neoblast mitoses return to baseline within 2 weeks post feeding (Baguñà, 1974, 1976), roughly coinciding with the onset of measurable degrowth (Oviedo et al., 2003), a static rate of cell death that is greater than tissue production at baseline mitotic rates but less than tissue production during feeding-induced proliferation would be sufficient to explain growth and degrowth. Nevertheless, TUNEL indicates that starvation induces progressively increasing rates of apoptosis (Pellettieri et al., 2010). The outcome of progressively increasing death rates paired with long-term static neoblast proliferation should be progressively accelerated degrowth. However, degrowth proceeds at a constant rate at the organismal (Baguñà and Romero, 1981; Bowen et al., 1976) and tissue-specific level (Oviedo et al., 2003), and may even decelerate in very small animals (Baguñà and Romero, 1981). Therefore, additional studies are needed to clarify the balance between tissue production and cell death during growth and degrowth in planarians.

The apoptotic response to wounding has been elegantly characterized by whole-mount TUNEL (Pellettieri et al., 2010). The dynamics of apoptosis show intriguing parallels with those of mitosis following amputation; an early wave of apoptosis is observed near the wound site at 4 hours, followed by a second, body-wide increase at 72

hours that gradually subsides by 1-2 weeks post amputation (Figure 7A) (Pellettieri et al., 2010; Wenemoser and Reddien, 2010), and wound-induced mitosis and apoptosis show strikingly similar dynamics when examined in parallel (Hill and Petersen, 2015). Similar to mitosis, the early apoptotic response is induced by incisions that do not result in significant tissue removal. Whether the 72-hour global response is also induced by incisions was not reported, but it is likely reduced or absent based on the fact that global apoptosis at 72 hours varies as a function of the amount of removed tissue (Pellettieri et al., 2010). An interesting difference is that whereas the early and late apoptotic responses are local to the wound and global, respectively, the opposite is seen with early and late mitotic responses, which are global and localized to the wound, respectively (Figure 7A).

Amputation-induced apoptosis is not simply a passive response to general stress, since wound-induced *follistatin* expression is required for the 72-hour apoptotic response (Gaviño et al., 2013). As in other organisms (Dhanasekaran and Reddy, 2008), the JNK signaling pathway has been implicated in apoptosis in planarians, and *jnk* RNAi is reported to inhibit apoptosis after wounding and slow degrowth of differentiated tissues during starvation (Almuedo-Castillo et al., 2014). However, these findings are complicated by the role of JNK signaling in neoblast proliferation (Almuedo-Castillo et al., 2014; Wagner et al., 2012), and conflicting reports about requirements for JNK signaling in apoptosis (Almuedo-Castillo et al., 2014; Tejada-Romero et al., 2015). TOR signaling, which is required for both regeneration and feeding-induced growth, also seems to affect cell death, as *tor* RNAi is reported to increase apoptosis in homeostatic and starved animals (Peiris et al., 2012; Tu et al., 2012). Besides these early clues into the

general regulation of apoptosis in planarians, little is known about the signals that initiate the apoptotic response to wounding.

The role of cell death in planarian regeneration

Cell death is critical for degrowth of tissues that become disproportionately large as a result of injury. For example, a decapitated head will have a disproportionately large brain for the size of the animal that will be regenerated, and the elimination of brain cells is necessary for degrowth to a size proportionate to the new tissue fragment (Figure 6A). The initiating signals that promote cell death in response to wounding or disproportion are unknown. Furthermore, whether individual tissues such as a suddenly oversized brain actually sense disproportionality, or if death induced by tissue removal occurs indiscriminately in tissues regardless of their disproportion after wounding is not known. The development of methods for comparing apoptotic rates among different tissues after wounding will be necessary for further investigating this question.

Given the similar dynamics of apoptosis and neoblast proliferation, it is possible that apoptotic cells might induce compensatory proliferation in surrounding neoblasts, or provide other feedback signals critical for regeneration, as has been shown for other regenerative systems discussed above. The proliferation of neoblasts and regeneration of missing tissues occurs even in the absence of food, yet some source of energy and material must fuel de novo tissue growth (Morgan, 1901). Phagocytosis of apoptotic cells in degrowing tissues could ultimately provide the energy and material necessary for the growth of others. Despite these intriguing possibilities, a method for specifically

inhibiting apoptosis in planarians has not been reported, so a causal role for cell death in the proliferative response to wounding has not been experimentally demonstrated.

CONCLUSION

Diverse molecular and cellular strategies of feedback control contribute to proportion maintenance and restoration in metazoans. Planarians are remarkable in their ability to maintain and restore tissue proportion after limitless injuries, implying robust feedback mechanisms. Alterations in the production and death of tissues in response to injury have been well-characterized, but how injury or disproportion actually induces these changes is still poorly understood. Furthermore, whether feedback is implemented on a tissue-specific level is unknown, as a signal linking the current size or proportion of a specific tissue to its own production or death has not been identified. The specificity of the wound response to tissue-specific size perturbations has also not been sufficiently characterized.

The work presented in this thesis addresses the problem of tissue specificity in regeneration, primarily using the planarian eye lineage. In Chapter 2, we show that although eye cell production can be increased in response to large head injuries, eye absence is not sufficient or necessary to induce this response. Extension of these findings to additional tissues demonstrates a striking lack of specificity in tissue production after wounding. Together, these findings argue that the production of eye cells (and potentially differentiated planarian tissues in general) by neoblasts is not regulated by a tissue-specific negative feedback mechanism. In Chapter 3, I discuss the implications of these findings for planarian regeneration in general, and attempt to reconcile how a system with such strikingly non-specific tissue production gives rise to the robust tissue-specific growth and degrowth observed after limitless injuries in planarians.

A

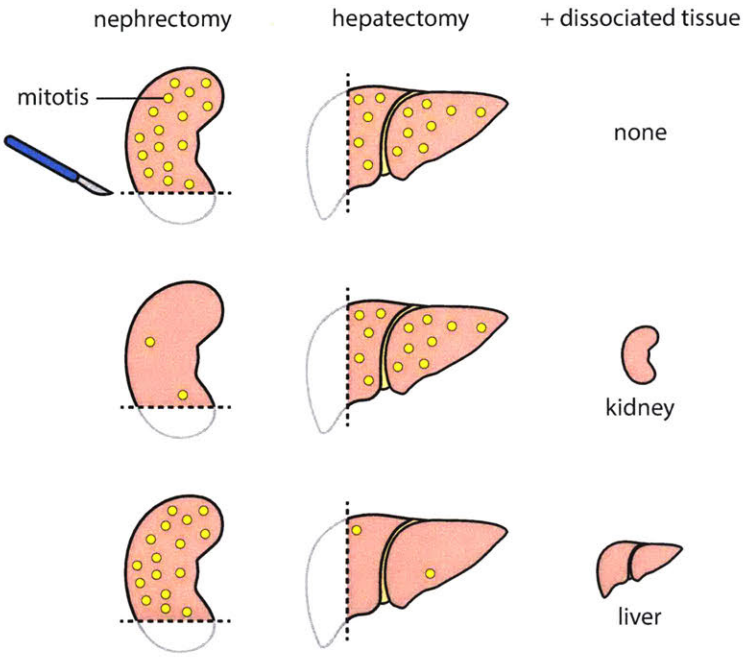
nephrectomy
hepatectomy
+ dissociated tissue
mitotis
none
kidney
liver

B

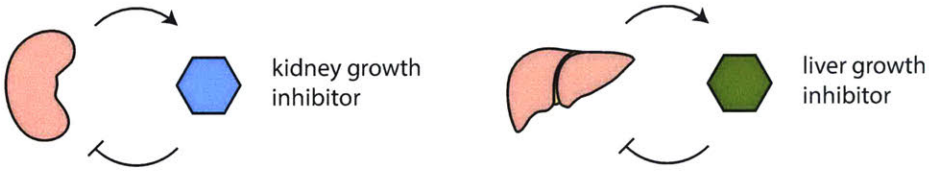
kidney growth inhibitor
liver growth inhibitor

Figure 1. Autoregulation of tissue growth and the chalone hypothesis

(A) Partial nephrectomy or hepatectomy induces a mitotic response in the kidney or liver, respectively (top). Administration of dissociated cells of the kidney (middle) or liver (bottom) specifically inhibits the mitotic response in the corresponding organ.

(B) The chalone model posits that each tissue produces a secreted molecule specifically inhibiting its own growth.

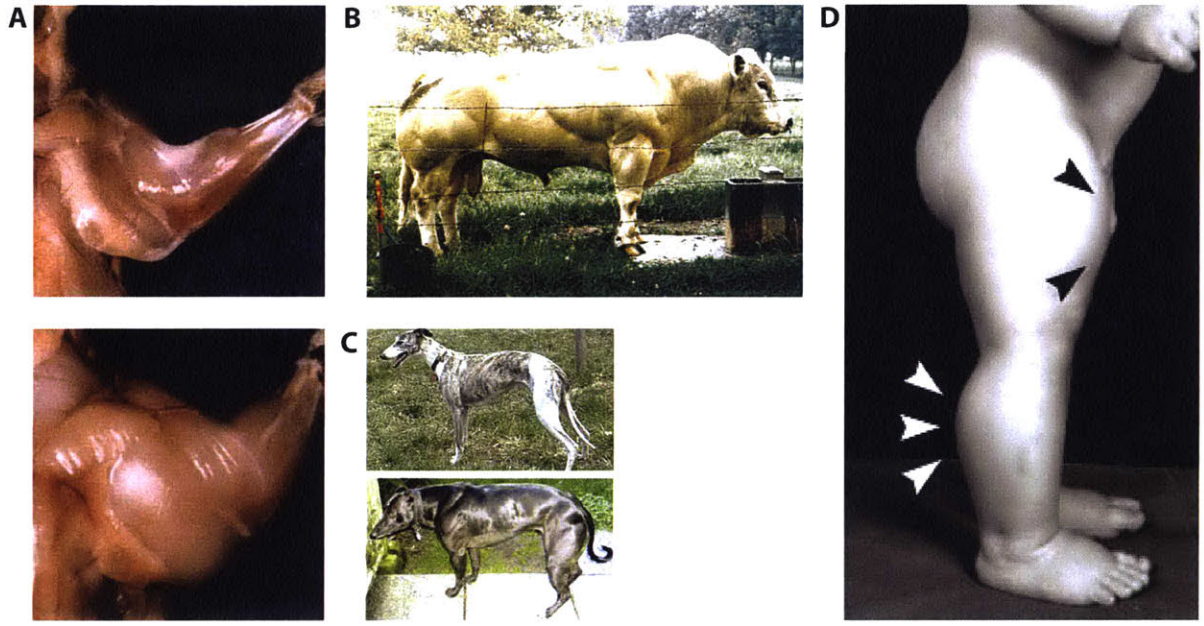
A
B
C
D

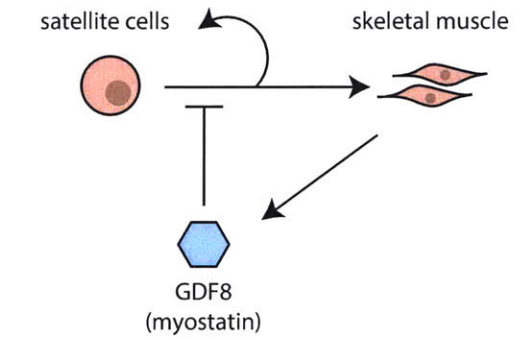
E
satellite cells
skeletal muscle
GDF8
(myostatin)

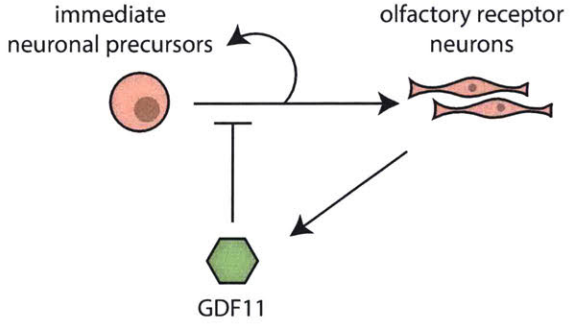
F
immediate
neuronal precursors
olfactory receptor
neurons
GDF11

Figure 2. Autoregulation of tissue growth by TGF-β

(A) Upper limb skeletal muscle in wild-type (top) and homozygous *myostatin* null mutant mice (bottom). *myostatin* null mutants have increased muscle mass. Reproduced with permission (McPherron et al., 1997), Copyright © Nature Publishing Group.

(B) A Belgian Blue bull with "double-muscling" phenotype resulting from a homozygous loss-of-function *myostatin* mutation. Reproduced with permission (McPherron and Lee, 1997), Copyright © National Academy of Sciences.

(C) Wild-type whippet dog breed (left) and "bully" whippet homozygous for *myostatin* mutant allele containing a premature stop codon (right). Reproduced from Mosher et al., 2007.

(D) 7 month-old human with homozygous loss-of-function *myostatin* mutation. Arrowheads indicate abnormally protruding muscles in thigh and calf. Reproduced with permission (Schuelke et al., 2004), Copyright © Massachusetts Medical Society.

(E) Cellular control of skeletal muscle mass by GDF8/myostatin. Skeletal muscles produce myostatin, which inhibits proliferation and differentiation of satellite cells.

(F) Cellular control of neurogenesis in the olfactory epithelium (OE) by GDF11. Olfactory receptor neurons (ORNs) secrete GDF11, which inhibits proliferation and differentiation of immediate neuronal precursors (INPs).

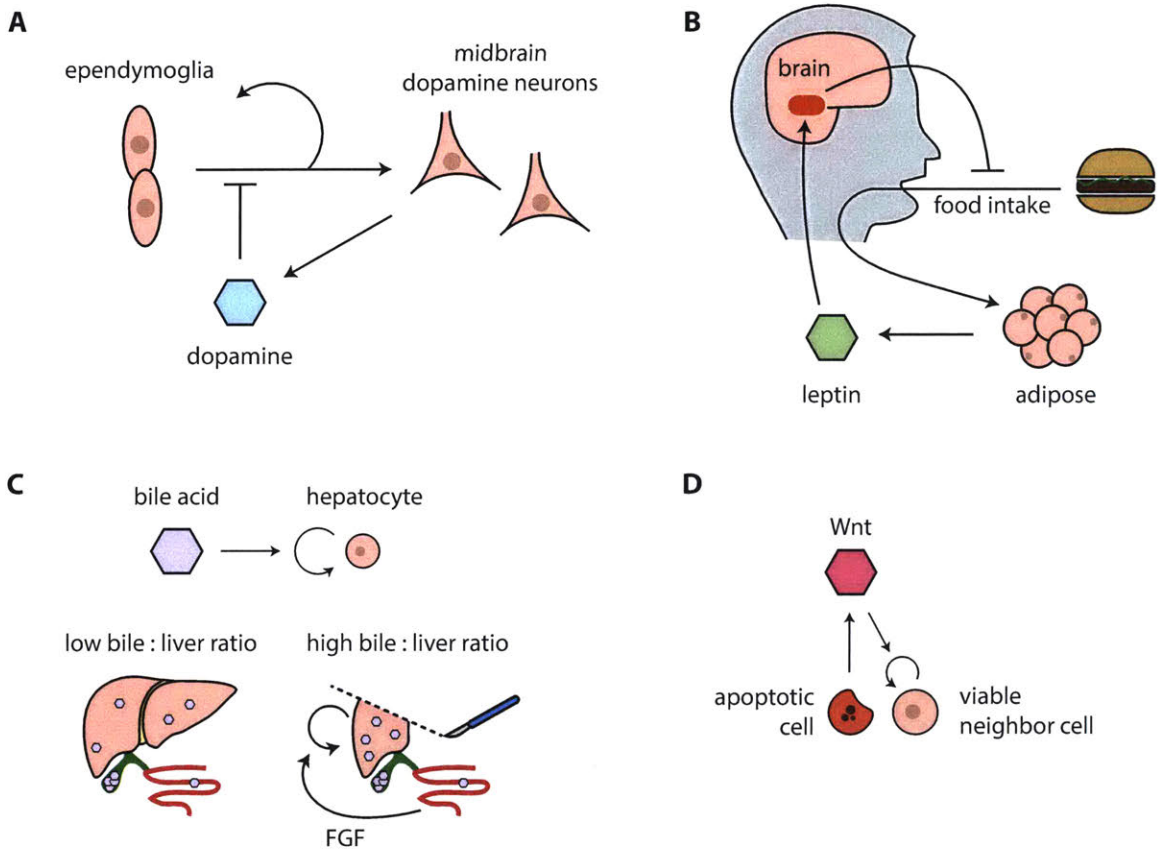
A
ependymoglia
midbrain
dopamine neurons
dopamine
B
brain
food intake
leptin
adipose
C
bile acid
hepatocyte
low bile : liver ratio
high bile : liver ratio
FGF
D
Wnt
apoptotic
cell
viable
neighbor cell

Figure 3. Diverse mechanisms of tissue size feedback control

(A) Dopamine inhibits proliferation and differentiation of ependymoglia stem cells into dopaminergic midbrain neurons in the adult salamander.

(B) Adipose tissue secretes the hormone leptin, which signals through neurons in the hypothalamus to decrease food intake behavior.

(C) Hepatectomy increases bile acid : liver mass ratio, stimulating hepatocyte proliferation. Bile acid also stimulates intestine-derived FGF production to promote liver regeneration.

(D) Apoptotic cells secrete mitogens such as Wnt to induce proliferation in neighboring cells.

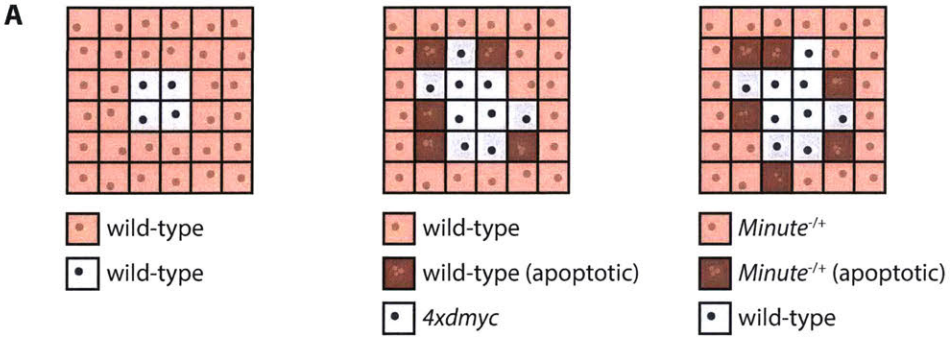
A
wild-type
wild-type
wild-type
wild-type (apoptotic)
4xdmyc
Minute-/+
Minute-/+ (apoptotic)
wild-type

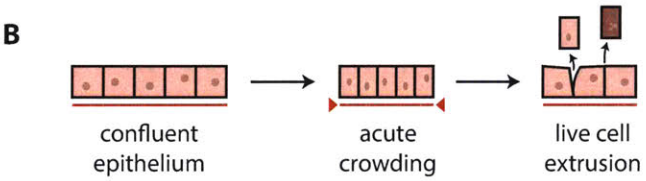
B
confluent epithelium
acute crowding
live cell extrusion

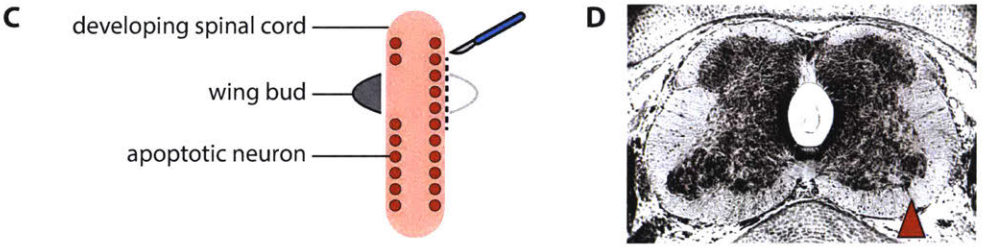
C
developing spinal cord
wing bud
apoptotic neuron
D

Figure 4. Cell death limits tissue size

(A) *Drosophila* wing imaginal disc epithelium cells (pink) surrounding clones (grey) of indicated phenotypes. Cells that grow more rapidly than neighboring cells expand at the expense of neighboring cells that undergo apoptosis (dark red). *4xdmyc* cells grow fast, *Minute*$^{-/+}$ cells grow slow, in comparison to wild-type cells.

(B) Epithelial cells grow to confluence (left) on a stretched elastic surface (red line). Acute crowding of epithelial cells (center) induces active live cell extrusion to restore appropriate cellular density (right). Extruded cells subsequently undergo apoptosis.

(C) Apoptosis in the developing chick spinal cord is spared from segments innervating the wing bud. Wing bud extirpation extends apoptosis to the normally spared segments on the operated side.

(D) Hematoxylin-stained cross-section of fifteenth spinal segment corresponding to wing bud. Red arrowhead indicates atrophied ventral horn on side of extirpated wing bud. The corresponding dorsal root ganglion is also atrophied (not shown). Reproduced with permission (Hamburger, 1934),

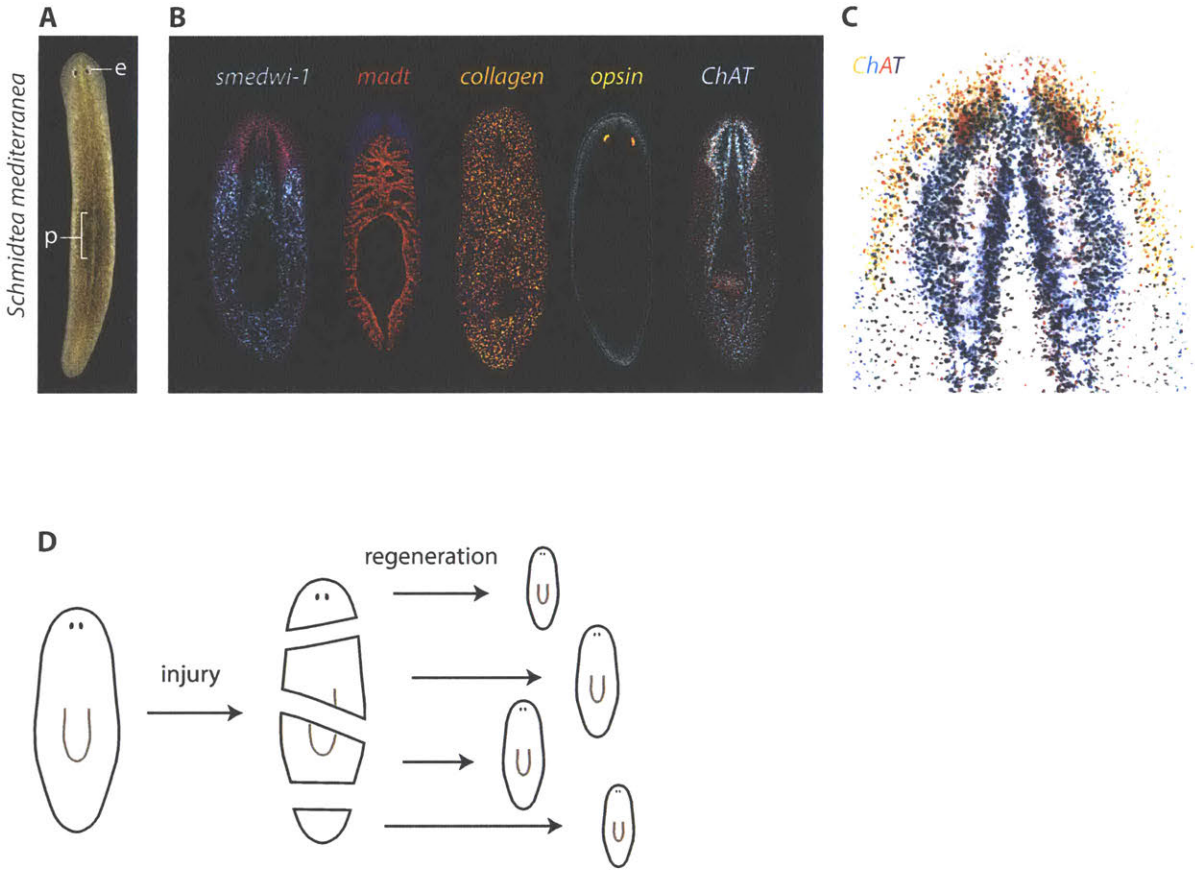
A
B
C
Schmidtea mediterranea
e
p
smedwi-1
madt
collagen
opsin
ChAT
ChAT
D
injury
regeneration

Figure 5. Planarian anatomy and regeneration

(A) Live image of an adult planarian flatworm of the species *Schmidtea mediterranea*. Dorsal view, anterior up. Eyes (e) and location of pharynx (p) are visible in live animals.

(B) Whole-mount fluorescence in situ hybridization (FISH) for probes in indicated colors on contrasting DAPI background. Left to right: *smedwi-1*$^{+}$ neoblasts, *madt*$^{+}$ intestine, *collagen*$^{+}$ muscle, *opsin*$^{+}$ photoreceptor neurons, *ChAT*$^{+}$ central nervous system.

(C) FISH for *ChAT* in head, with optical sections pseudocolored according to z-axis, displaying ventral nerve cords (purple), cephalic ganglia (blue), dorsal photoreceptor neurons (red) and peripheral head rim neurons (orange).

(D) Planarians regenerate complex proportional anatomy after diverse injuries. The current example shows the result of regeneration in the absence of food, with proportion restoration occurring without net organismal growth. Thus, each regenerate is smaller than the original intact animal.

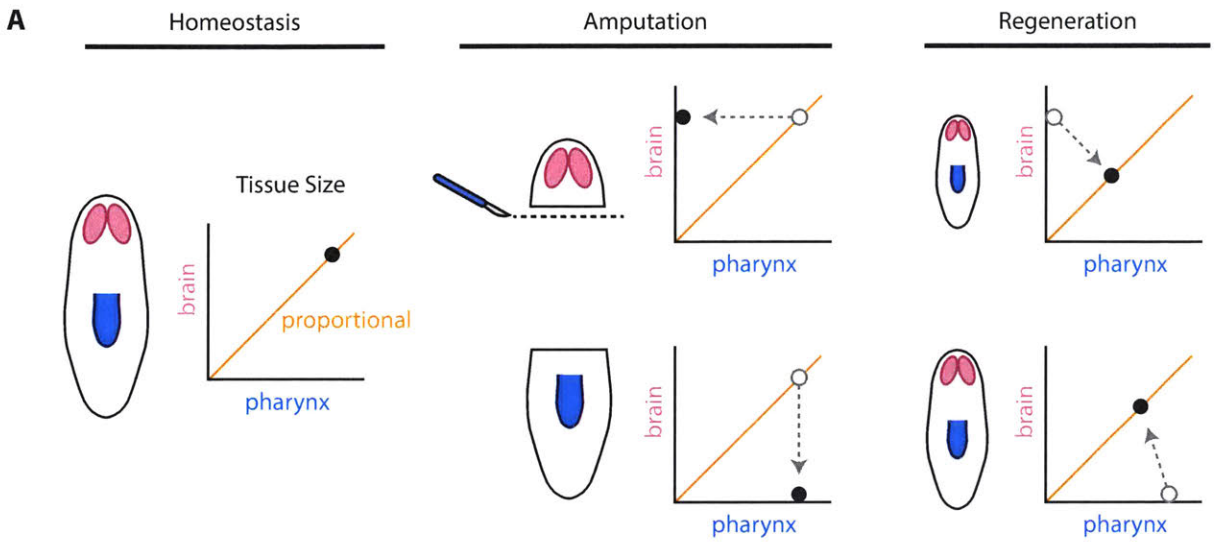
A
Homeostasis
Amputation
Regeneration
Tissue Size
brain
proportional
pharynx
brain
pharynx
brain
pharynx
brain
pharynx
brain
pharynx

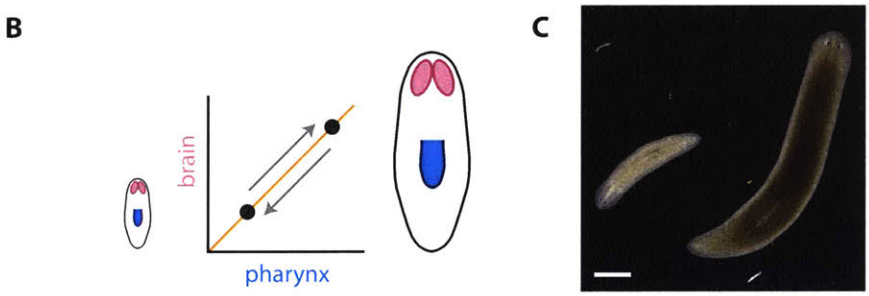
B
brain
pharynx
C

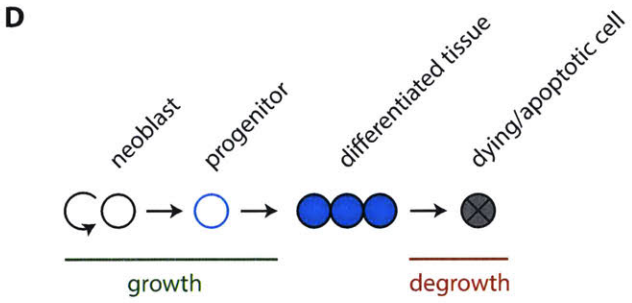
D
neoblast
progenitor
differentiated tissue
dying/apoptotic cell
growth
degrowth

Figure 6. Maintenance and restoration of tissue proportion in planarians

(A) Homeostatic planarian (left) with proportional brain size : pharynx size ratio. Graph indicates sizes of brain and pharynx, with orange line representing proportionality. Head amputation (center) results in two disproportionate fragments with no pharynx (top) or no brain (bottom). Regeneration (right) results in restoration of proportion, which involves coordinated growth and degrowth of the brain and pharynx.

(B) Planarians maintain proportionality during growth and degrowth resulting from feeding and starvation, respectively.

(C) Live adult *S. mediterranea* animals vary in size. Scale bar, 200 μm.

(D) Processes affecting differentiated tissue growth and degrowth in planarians. Neoblasts proliferate and are specified into lineage-specific progenitors, which incorporate into existing or regenerating post-mitotic differentiated tissues to promote growth. Differentiated tissues undergo cell death / apoptosis to promote degrowth.

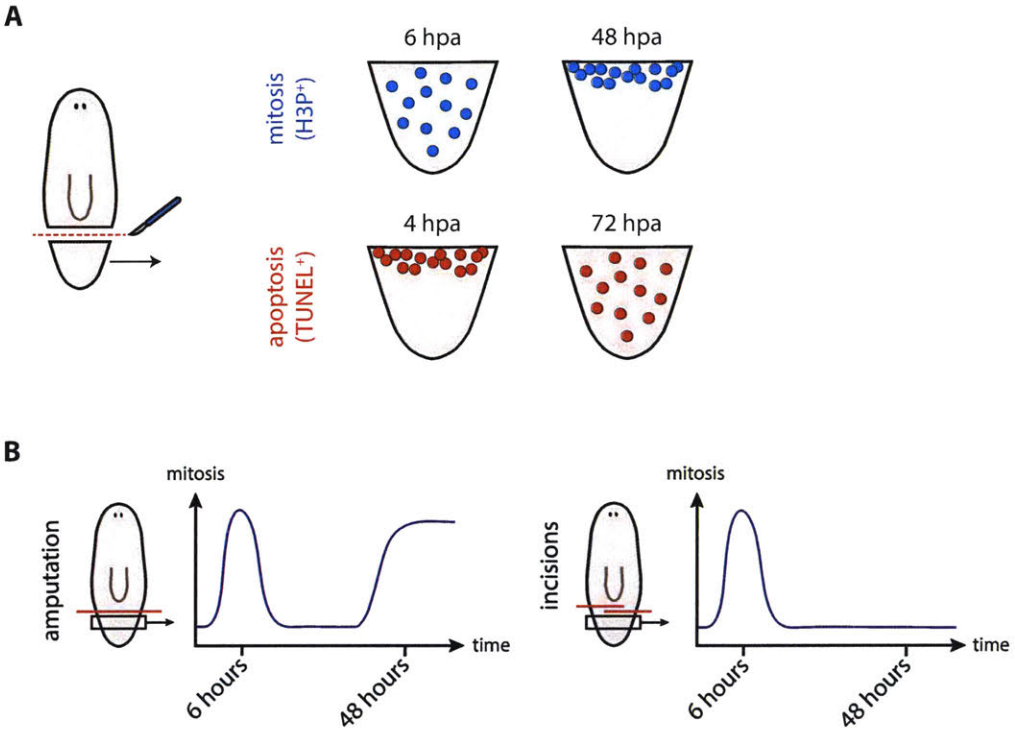
A
6 hpa
48 hpa
mitosis
(H3P+)
4 hpa
72 hpa
apoptosis
(TUNEL+)
B
mitosis
amputation
time
6 hours
48 hours
mitosis
incisions
time
6 hours
48 hours

Figure 7. Mitotic and apoptotic responses to wounding

(A) Mitosis (blue) and apoptosis (red) in amputated tails. Mitosis is increased globally at 6 hours post amputation (hpa), and locally at the wound site at 48 hpa. Apoptosis is increased at the wound site at 4 hpa, and globally at 72 hpa.

(B) Mitotic density over time near wound face in amputated tails (left) and tails with non-amputating incisions (right). Only amputation results in sustained mitosis starting at 48 hpa.

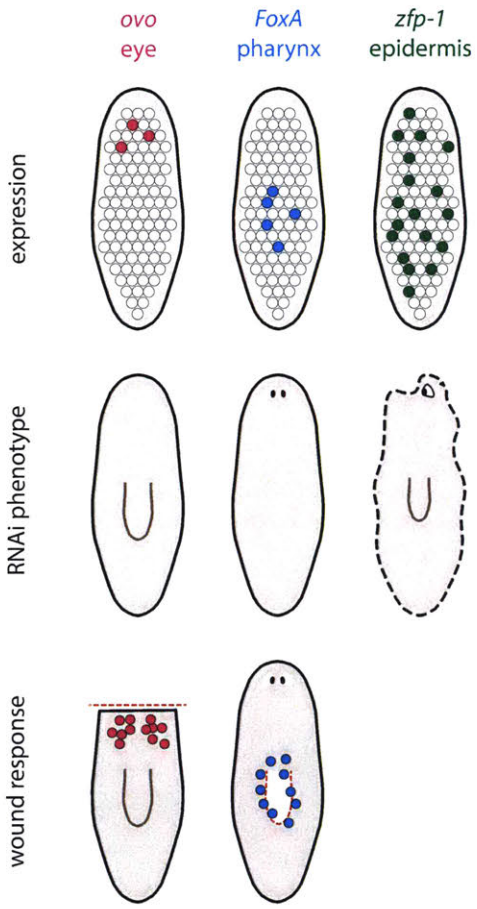
ovo
eye
FoxA
pharynx
zfp-1
epidermis
expression
RNAi phenotype
wound response

Figure 8. Progenitor distribution and behavior underlies homeostatic tissue size and regeneration

Transcription factor expression (italics) marks progenitors for indicated tissues. Top row indicates homeostatic progenitor distribution. White circles represent neoblasts, colored circles represent neoblasts expressing lineage-specific transcription factors. Middle row indicates morphological result of RNAi of indicated transcription factor, leading to eye absence (left), pharynx absence (center), or loss of epidermal integrity (right). Bottom row shows amplified tissue progenitor numbers after removal of corresponding differentiated tissue.

REFERENCES

Adler, C.E., and Sánchez Alvarado, A. (2015). Types or states? Cellular dynamics and regenerative potential. Trends Cell Biol. *25*, 687-96.

Adler, C.E., Seidel, C.W., McKinney, S.A., and Sánchez Alvarado, A. (2014). Selective amputation of the pharynx identifies a FoxA-dependent regeneration program in planaria. eLife *3*, e02238.

Almuedo-Castillo, M., Crespo-Yanez, X., Seebeck, F., Bartscherer, K., Salò, E., and Adell, T. (2014). JNK controls the onset of mitosis in planarian stem cells and triggers apoptotic cell death required for regeneration and remodeling. PLOS Genet. *10*, e1004400.

Aurora, A.B., Porrello, E.R., Tan, W., Mahmoud, A.I., Hill, J.A., Bassel-Duby, R., Sadek, H.A., and Olson, E.N. (2014). Macrophages are required for neonatal heart regeneration. J. Clin. Invest. *124*, 1382-92.

Baguñà, J. (1974). Dramatic mitotic response in planarians after feeding, and a hypothesis for the control mechanism. J. Exp. Zool. *190*, 117-22.

Baguñà, J. (1976). Mitosis in the intact and regenerating planarian *Dugesia mediterranea* n.sp. I. Mitotic studies during growth, feeding and starvation. J. Exp. Zool. *195*, 53-64.

Baguñà, J., and Romero, R. (1981). Quantitative analysis of cell types during growth, degrowth and regeneration in the planarians *Dugesia mediterranea* and *Dugesia tigrina*. Hydrobiologia *84*, 181-94.

Baguñà, J., Saló, E., and Auladell, C. (1989). Regeneration and pattern formation in planarians III. Evidence that neoblasts are totipotent stem cells and the source of blastema cells. Development *107*, 77-86.

Berg, D.A., Kirkham, M., Wang, H., Frisén, J., and Simon, A. (2011). Dopamine controls neurogenesis in the adult salamander midbrain in homeostasis and during regeneration of dopamine neurons. Cell Stem Cell *8*, 426-33.

Bonar, N.A., and Petersen, C.P. (2017). Integrin suppresses neurogenesis and regulates brain tissue assembly in planarian regeneration. Development *144*, 784-94.

Bowen, E.D., Ryder, T.A., and Dark, C. (1976). The effects of starvation on the planarian worm *Polycelis tenuis* Iijima. Cell Tissue Res. *169*, 193-209.

Bullough, W.S. (1962). The control of mitotic activity in adult mammalian tissues. Biol. Rev. Camb. Philos. Soc. *37*, 307-42.

Bullough, W.S., and Laurence, E.B. (1960). The control of epidermal mitotic activity in the mouse. Proc. R. Soc. B *151*, 517-36.

Calof, A.L., Bonnin, A., Crocker, C., Kawauchi, S., Murray, R.C., Shou, J., and Wu, H.H. (2002). Progenitor cells of the olfactory receptor neuron lineage. Microsc. Res. Tech. *58*, 176-88.

Chen, C.C., Wang, L., Plikus, M.V., Jiang, T.X., Murray, P.J., Ramos, R., Guerrero-Juarez, C.F., Hughes, M.W., Lee, O.K., Shi, S., *et al.* (2015). Organ-level quorum sensing directs regeneration in hair stem cell populations. Cell *161*, 277-90.

Chera, S., Ghila, L., Dobretz, K., Wenger, Y., Bauer, C., Buzgariu, W., Martinou, J.C., and Galliot, B. (2009). Apoptotic cells provide an unexpected source of Wnt3 signaling to drive *Hydra* head regeneration. Dev. Cell *17*, 279-89.

Chiang, J.Y. (2013). Bile acid metabolism and signaling. Compr. Physiol. *3*, 1191-212.

Clop, A., Marcq, F., Takeda, H., Pirottin, D., Tordoir, X., Bibe, B., Bouix, J., Caiment, F., Elsen, J.M., Eychenne, F., *et al.* (2006). A mutation creating a potential illegitimate microRNA target site in the myostatin gene affects muscularity in sheep. Nat. Genet. *38*, 813-8.

Cohen, S. (1960). Purification of a nerve-growth promoting protein from the mouse salivary gland and Its neuro-cytotoxic antiserum. Proc. Natl. Acad. Sci. U.S.A. *46*, 302-11.

Cohen, S., and Levi-Montalcini, R. (1956). A nerve growth-stimulating factor isolated from snake venom. Proc. Natl. Acad. Sci. U.S.A. *42*, 571-4.

Coleman, D.L. (1973). Effects of parabiosis of obese with diabetes and normal mice. Diabetologia *9*, 294-8.

Cordeiro, J.V., and Jacinto, A. (2013). The role of transcription-independent damage signals in the initiation of epithelial wound healing. Nat. Rev. Mol. Cell Biol. *14*, 249-62.

Cowles, M.W., Brown, D.D., Nisperos, S.V., Stanley, B.N., Pearson, B.J., and Zayas, R.M. (2013). Genome-wide analysis of the bHLH gene family in planarians identifies factors required for adult neurogenesis and neuronal regeneration. Development *140*, 4691-702.

Currie, K.W., and Pearson, B.J. (2013). Transcription factors *lhx1/5-1* and *pitx* are required for the maintenance and regeneration of serotonergic neurons in planarians. Development *140*, 3577-88.

de la Cova, C., Abril, M., Bellosta, P., Gallant, P., and Johnston, L.A. (2004). *Drosophila* Myc regulates organ size by inducing cell competition. Cell *117*, 107-16.

Deng, B., Wehling-Henricks, M., Villalta, S.A., Wang, Y., and Tidball, J.G. (2012). IL-10 triggers changes in macrophage phenotype that promote muscle growth and regeneration. J. Immunol. *189*, 3669-80.

Dhanasekaran, D.N., and Reddy, E.P. (2008). JNK signaling in apoptosis. Oncogene *27*, 6245-51.

Dubois, F. (1949). Contribution a l'étude de la migration des cellules de régénération chez les *Planaires dulcicoles*. Bull. Biol. Fr. Belg. *83*, 213-83.

Eisenhoffer, G.T., Loftus, P.D., Yoshigi, M., Otsuna, H., Chien, C.B., Morcos, P.A., and Rosenblatt, J. (2012). Crowding induces live cell extrusion to maintain homeostatic cell numbers in epithelia. Nature *484*, 546-9.

Elgjo, K., and Reichelt, K.L. (2004). Chalones: from aqueous extracts to oligopeptides. Cell Cycle *3*, 1208-11.

Forsthoefel, D.J., Park, A.E., and Newmark, P.A. (2011). Stem cell-based growth, regeneration, and remodeling of the planarian intestine. Dev. Biol. *356*, 445-59.

Friedman, J.M., and Halaas, J.L. (1998). Leptin and the regulation of body weight in mammals. Nature *395*, 763-70.

Gamer, L.W., Nove, J., and Rosen, V. (2003). Return of the chalones. Dev. Cell *4*, 143-4.

Gauron, C., Rampon, C., Bouzaffour, M., Ipendey, E., Teillon, J., Volovitch, M., and Vriz, S. (2013). Sustained production of ROS triggers compensatory proliferation and is required for regeneration to proceed. Sci. Rep. *3*, 2084.

Gaviño, M.A., Wenemoser, D., Wang, I.E., and Reddien, P.W. (2013). Tissue absence initiates regeneration through Follistatin-mediated inhibition of Activin signaling. eLife *2*, e00247.

Gokoffski, K.K., Wu, H.H., Beites, C.L., Kim, J., Kim, E.J., Matzuk, M.M., Johnson, J.E., Lander, A.D., and Calof, A.L. (2011). Activin and GDF11 collaborate in feedback control of neuroepithelial stem cell proliferation and fate. Development *138*, 4131-42.

Grobet, L., Martin, L.J., Poncelet, D., Pirottin, D., Brouwers, B., Riquet, J., Schoeberlein, A., Dunner, S., Ménissier, F., Massabanda, J., *et al.* (1997). A deletion in the bovine myostatin gene causes the double-muscled phenotype in cattle. Nat. Genet. *17*, 71-4.

Grobet, L., Poncelet, D., Royo, L.J., Brouwers, B., Pirottin, D., Michaux, C., Ménissier, F., Zanotti, M., Dunner, S., and Georges, M. (1998). Molecular definition of an allelic series of mutations disrupting the myostatin function and causing double-muscling in cattle. Mamm. Genome *9*, 210-3.

Gudipaty, S.A., Lindblom, J., Loftus, P.D., Redd, M.J., Edes, K., Davey, C.F., Krishnegowda, V., and Rosenblatt, J. (2017). Mechanical stretch triggers rapid epithelial cell division through Piezo1. Nature *543*, 118-21.

Guedelhoefer, O.C.I., and Sánchez Alvarado, A. (2012). Amputation induces stem cell mobilization to sites of injury during planarian regeneration. Development *139*, 3510-20.

Gurley, K.A., Elliott, S.A., Simakov, O., Schmidt, H.A., Holstein, T.W., and Sánchez Alvarado, A. (2010). Expression of secreted Wnt pathway components reveals unexpected complexity of the planarian amputation response. Dev. Biol. *347*, 24-39.

Gurley, K.A., Rink, J.C., and Sánchez Alvarado, A. (2008). β-catenin defines head versus tail identity during planarian regeneration and homeostasis. Science *319*, 323-7.

Hamburger, V. (1934). The effects of wing bud extirpation on the development of the central nervous system in chick embryos. J. Exp. Zool. *68*, 449-94.

Hamburger, V., and Levi-Montalcini, R. (1949). Proliferation, differentiation and degeneration in the spinal ganglia of the chick embryo under normal and experimental conditions. J. Exp. Zool. *111*, 457-501.

Haynie, J.L., and Bryant, P.J. (1977). The effects of X-rays on the proliferation dynamics of cells in the imaginal wing disc of *Drosophila melanogaster*. Wilehm Roux Arch. Dev. Biol. *183*, 85-100.

Heredia, J.E., Mukundan, L., Chen, F.M., Mueller, A.A., Deo, R.C., Locksley, R.M., Rando, T.A., and Chawla, A. (2013). Type 2 innate signals stimulate fibro/adipogenic progenitors to facilitate muscle regeneration. Cell *153*, 376-88.

Hill, E.M., and Petersen, C.P. (2015). Wnt/Notum spatial feedback inhibition controls neoblast differentiation to regulate reversible growth of the planarian brain. Development *142*, 4217-29.

Huang, W., Ma, K., Zhang, J., Qatanani, M., Cuvillier, J., Liu, J., Dong, B., Huang, X., and Moore, D.D. (2006). Nuclear receptor-dependent bile acid signaling is required for normal liver regeneration. Science *312*, 233-6.

Huh, J.R., Guo, M., and Hay, B.A. (2004). Compensatory proliferation induced by cell death in the *Drosophila* wing disc requires activity of the apical cell death caspase Dronc in a nonapoptotic role. Curr. Biol. *14*, 1262-6.

Huttenlocher, A., and Horwitz, A.R. (2011). Integrins in cell migration. Cold Spring Harb. Perspect. Biol. *3*, a005074.

Ingalls, A.M., Dickie, M.M., and Snell, G.D. (1950). Obese, a new mutation in the house mouse. J. Hered. *41*, 317-8.

Kam, I., Lynch, S., Svanas, G., Todo, S., Polimeno, L., Francavilla, A., Penkrot, R.J., Takaya, S., Ericzon, B.G., Starzl, T.E., *et al.* (1987). Evidence that host size determines liver size: studies in dogs receiving orthotopic liver transplants. Hepatology *7*, 362-6.

Kambadur, R., Sharma, M., Smith, T.P., and Bass, J.J. (1997). Mutations in *myostatin (GDF8)* in double-muscled Belgian Blue and Piedmontese cattle. Genome Res. *7*, 910-6.

Kennedy, G.C. (1953). The role of depot fat in the hypothalamic control of food intake in the rat. Proc. R. Soc. B *140*, 578-96.

Lapan, S.W., and Reddien, P.W. (2011). *dlx* and *sp6-9* control optic cup regeneration in a prototypic eye. PLOS Genet. *7*, e1002226.

Lapan, S.W., and Reddien, P.W. (2012). Transcriptome analysis of the planarian eye identifies *ovo* as a specific regulator of eye regeneration. Cell Rep. *2*, 294-307.

Lee, S.J. (2004). Regulation of muscle mass by myostatin. Annu. Rev. Cell Dev. Bio. *20*, 61-86.

Lee, S.J. (2008). Genetic analysis of the role of proteolysis in the activation of latent myostatin. PLOS One *3*, e1628.

Lee, S.J., and McPherron, A.C. (2001). Regulation of myostatin activity and muscle growth. Proc. Natl. Acad. Sci. U.S.A. *98*, 9306-11.

Lee, S.J., Reed, L.A., Davies, M.V., Girgenrath, S., Goad, M.E., Tomkinson, K.N., Wright, J.F., Barker, C., Ehrmantraut, G., Holmstrom, J., *et al.* (2005). Regulation of muscle growth by multiple ligands signaling through activin type II receptors. Proc. Natl. Acad. Sci. U.S.A. *102*, 18117-22.

Levi-Montalcini, R. (1987). The nerve growth factor 35 years later. Science *237*, 1154-62.

Li, F., Huang, Q., Chen, J., Peng, Y., Roop, D.R., Bedford, J.S., and Li, C.Y. (2010). Apoptotic cells activate the "phoenix rising" pathway to promote wound healing and tissue regeneration. Sci. Signal. *3*, ra13.

Lindemans, C.A., Calafiore, M., Mertelsmann, A.M., O'Connor, M.H., Dudakov, J.A., Jenq, R.R., Velardi, E., Young, L.F., Smith, O.M., Lawrence, G., *et al.* (2015). Interleukin-22 promotes intestinal-stem-cell-mediated epithelial regeneration. Nature *528*, 560-4.

Mangel, M., Bonsall, M.B., and Aboobaker, A. (2016). Feedback control in planarian stem cell systems. BMC Syst. Biol. *10*, 17.

Marinari, E., Mehonic, A., Curran, S., Gale, J., Duke, T., and Baum, B. (2012). Live-cell delamination counterbalances epithelial growth to limit tissue overcrowding. Nature *484*, 542-5.

März, M., Seebeck, F., and Bartscherer, K. (2013). A Pitx transcription factor controls the establishment and maintenance of the serotonergic lineage in planarians. Development *140*, 4499-509.

Matulionis, D.H. (1975). Ultrastructural study of mouse olfactory epithelium following destruction by $ZnSO_4$ and its subsequent regeneration. Am. J. Anat. *142*, 67-89.

Matzuk, M.M., Lu, N., Vogel, H., Sellheyer, K., Roop, D.R., and Bradley, A. (1995). Multiple defects and perinatal death in mice deficient in follistatin. Nature *374*, 360-3.

McCroskery, S., Thomas, M., Maxwell, L., Sharma, M., and Kambadur, R. (2003). Myostatin negatively regulates satellite cell activation and self-renewal. J. Cell Biol. *162*, 1135-47.

McPherron, A.C., Lawler, A.M., and Lee, S.J. (1997). Regulation of skeletal muscle mass in mice by a new TGF-β superfamily member. Nature *387*, 83-90.

McPherron, A.C., and Lee, S.J. (1997). Double muscling in cattle due to mutations in the myostatin gene. Proc. Natl. Acad. Sci. U.S.A. *94*, 12457-61.

Moolten, F.L., and Bucher, N.L. (1967). Regeneration of rat liver: transfer of humoral agent by cross circulation. Science *158*, 272-4.

Morata, G., and Ripoll, P. (1975). Minutes: mutants of *Drosophila* autonomously affecting cell division rate. Dev. Biol. *42*, 211-21.

Moreno, E., and Basler, K. (2004). dMyc transforms cells into super-competitors. Cell *117*, 117-29.

Morgan, T.H. (1898). Experimental studies of the regeneration of *Planaria maculata*. Arch. Entw. Mech. Org. *7*, 364-97.

Morgan, T.H. (1901). Growth and Regeneration in *Planaria lugubris*. Arch. Entw. Mech. Org. *13*, 179-212.

Mosher, D.S., Quignon, P., Bustamante, C.D., Sutter, N.B., Mellersh, C.S., Parker, H.G., and Ostrander, E.A. (2007). A mutation in the myostatin gene increases muscle mass and enhances racing performance in heterozygote dogs. PLOS Genet. *3*, e79.

Mumm, J.S., Shou, J., and Calof, A.L. (1996). Colony-forming progenitors from mouse olfactory epithelium: evidence for feedback regulation of neuron production. Proc. Natl. Acad. Sci. U.S.A. *93*, 11167-72.

Nakashima, M., Toyono, T., Akamine, A., and Joyner, A. (1999). Expression of growth/differentiation factor 11, a new member of the BMP/TGF-β superfamily during mouse embryogenesis. Mech. Dev. *80*, 185-9.

Newmark, P., and Sánchez Alvarado, A. (2000). Bromodeoxyuridine specifically labels the regenerative stem cells of planarians. Dev. Biol. *220*, 142-53.

Nishimura, K., Inoue, T., Yoshimoto, K., Taniguchi, T., Kitamura, Y., and Agata, K. (2011). Regeneration of dopaminergic neurons after 6-hydroxydopamine-induced lesion in planarian brain. J. Neurochem. *119*, 1217-31.

Oppenheim, R.W. (1991). Cell death during development of the nervous system. Annu. Rev. Neurosci. *14*, 453-501.

Oviedo, N.J., Newmark, P.A., and Sánchez Alvarado, A. (2003). Allometric scaling and proportion regulation in the freshwater planarian Schmidtea mediterranea. Dev. Dynam. *226*, 326-33.

Paravicini, U., Stoeckel, K., and Thoenen, H. (1975). Biological importance of retrograde axonal transport of nerve growth factor in adrenergic neurons. Brain Res. *84*, 279-91.

Park, H., and Poo, M.M. (2013). Neurotrophin regulation of neural circuit development and function. Nat. Rev. Neurosci. *14*, 7-23.

Paukovits, W.R., and Laerum, O.D. (1982). Isolation and synthesis of a hemoregulatory peptide. Z. Naturforsch. C *37*, 1297-300.

Peiris, T.H., Weckerle, F., Ozamoto, E., Ramirez, D., Davidian, D., García-Ojeda, M.E., and Oviedo, N.J. (2012). TOR signaling regulates planarian stem cells and controls localized and organismal growth. J. Cell Sci. *125*, 1657-65.

Pellettieri, J., Fitzgerald, P., Watanabe, S., Mancuso, J., Green, D.R., and Sánchez Alvarado, A. (2010). Cell death and tissue remodeling in planarian regeneration. Dev. Biol. *338*, 76-85.

Pérez-Garijo, A., Martin, F.A., and Morata, G. (2004). Caspase inhibition during apoptosis causes abnormal signalling and developmental aberrations in *Drosophila*. Development *131*, 5591-8.

Petersen, C.P., and Reddien, P.W. (2008). *Smed-βcatenin-1* is required for anteroposterior blastema polarity in planarian regeneration. Science *319*, 327-30.

Petersen, C.P., and Reddien, P.W. (2009). A wound-induced Wnt expression program controls planarian regeneration polarity. Proc. Natl. Acad. Sci. U.S.A. *106*, 17061-6.

Reddien, P.W. (2011). Constitutive gene expression and the specification of tissue identity in adult planarian biology. Trends Genet. *27*, 277-85.

Reddien, P.W., Bermange, A.L., Murfitt, K.J., Jennings, J.R., and Sánchez Alvarado, A. (2005a). Identification of genes needed for regeneration, stem cell function, and tissue homeostasis by systematic gene perturbation in planaria. Dev. Cell *8*, 635-49.

Reddien, P.W., Oviedo, N.J., Jennings, J.R., Jenkin, J.C., and Sánchez Alvarado, A. (2005b). SMEDWI-2 is a PIWI-like protein that regulates planarian stem cells. Science *310*, 1327-30.

Reddien, P.W., and Sánchez Alvarado, A. (2004). Fundamentals of planarian regeneration. Annu. Rev. Cell Dev. Bio. *20*, 725-57.

Rhiner, C., Lopez-Gay, J.M., Soldini, D., Casas-Tinto, S., Martin, F.A., Lombardia, L., and Moreno, E. (2010). Flower forms an extracellular code that reveals the fitness of a cell to its neighbors in *Drosophila*. Dev. Cell *18*, 985-98.

Roberts-Galbraith, R.H., and Newmark, P.A. (2013). Follistatin antagonizes Activin signaling and acts with Notum to direct planarian head regeneration. Proc. Natl. Acad. Sci. U.S.A. *110*, 1363-8.

Ryoo, H.D., Gorenc, T., and Steller, H. (2004). Apoptotic cells can induce compensatory cell proliferation through the JNK and the Wingless signaling pathways. Dev. Cell *7*, 491-501.

Saetren, H. (1956). A principle of auto-regulation of growth. Production of organ specific mitose-inhibitors in kidney and liver. Exp. Cell Res. *11*, 229-32.

Schuelke, M., Wagner, K.R., Stolz, L.E., Hübner, C., Riebel, T., Kömen, W., Braun, T., Tobin, J.F., and Lee, S.J. (2004). Myostatin mutation associated with gross muscle hypertrophy in a child. N. Engl. J. Med. *350*, 2682-8.

Schwartz Levey, M., Chikaraishi, D.M., and Kauer, J.S. (1991). Characterization of potential precursor populations in the mouse olfactory epithelium using immunocytochemistry and autoradiography. J. Neurosci. *11*, 3556-64.

Schwob, J.E., Szumowski, K.E., and Stasky, A.A. (1992). Olfactory sensory neurons are trophically dependent on the olfactory bulb for their prolonged survival. J. Neurosci. *12*, 3896-919.

Scimone, M.L., Cote, L.E., Rogers, T., and Reddien, P.W. (2016). Two FGFRL-Wnt circuits organize the planarian anteroposterior axis. eLife *5*, e12845.

Scimone, M.L., Kravarik, K.M., Lapan, S.W., and Reddien, P.W. (2014a). Neoblast specialization in regeneration of the planarian *Schmidtea mediterranea*. Stem Cell Rep. *3*, 339-52.

Scimone, M.L., Lapan, S.W., and Reddien, P.W. (2014b). A *forkhead* transcription factor is wound-induced at the planarian midline and required for anterior pole regeneration. PLOS Genet. *10*, e1003999.

Scimone, M.L., Srivastava, M., Bell, G.W., and Reddien, P.W. (2011). A regulatory program for excretory system regeneration in planarians. Development *138*, 4387-98.

Seebeck, F., März, M., Meyer, A.W., Reuter, H., Vogg, M.C., Stehling, M., Mildner, K., Zeuschner, D., Rabert, F., and Bartscherer, K. (2017). Integrins are required for tissue organization and restriction of neurogenesis in regenerating planarians. Development *144*, 795-807.

Shou, J., Murray, R.C., Rim, P.C., and Calof, A.L. (2000). Opposing effects of bone morphogenetic proteins on neuron production and survival in the olfactory receptor neuron lineage. Development *127*, 5403-13.

Shou, J., Rim, P.C., and Calof, A.L. (1999). BMPs inhibit neurogenesis by a mechanism involving degradation of a transcription factor. Nat. Neurosci. *2*, 339-45.

Shraiman, B.I. (2005). Mechanical feedback as a possible regulator of tissue growth. Proc. Natl. Acad. Sci. U.S.A. *102*, 3318-23.

Simms, H.S., and Stillman, N.P. (1937). Substances affecting adult tissue in vitro II. A growth inhibitor in adult tissue. J. Gen. Physiol. *20*, 621-9.

Stückemann, T., Cleland, J.P., Werner, S., Thi-Kim Vu, H., Bayersdorf, R., Liu, S.Y., Friedrich, B., Jülicher, F., and Rink, J.C. (2017). Antagonistic self-organizing patterning systems control maintenance and regeneration of the anteroposterior axis in planarians. Dev. Cell *40*, 248-63.

Tartaglia, L.A., Dembski, M., Weng, X., Deng, N., Culpepper, J., Devos, R., Richards, G.J., Campfield, L.A., Clark, F.T., Deeds, J., *et al.* (1995). Identification and expression cloning of a leptin receptor, OB-R. Cell *83*, 1263-71.

Tejada-Romero, B., Carter, J.M., Mihaylova, Y., Neumann, B., and Aboobaker, A.A. (2015). JNK signalling is necessary for a Wnt- and stem cell-dependent regeneration programme. Development *142*, 2413-24.

Thi-Kim Vu, H., Rink, J.C., McKinney, S.A., McClain, M., Lakshmanaperumal, N., Alexander, R., and Sánchez Alvarado, A. (2015). Stem cells and fluid flow drive cyst formation in an invertebrate excretory organ. eLife *4*, e07405.

Thomas, M., Langley, B., Berry, C., Sharma, M., Kirk, S., Bass, J., and Kambadur, R. (2000). Myostatin, a negative regulator of muscle growth, functions by inhibiting myoblast proliferation. J. Biol. Chem. *275*, 40235-43.

Tseng, A.S., Adams, D.S., Qiu, D., Koustubhan, P., and Levin, M. (2007). Apoptosis is required during early stages of tail regeneration in *Xenopus laevis*. Dev. Biol. *301*, 62-9.

Tu, K.C., Pearson, B.J., and Sánchez Alvarado, A. (2012). TORC1 is required to balance cell proliferation and cell death in planarians. Dev. Biol. *365*, 458-69.

van Wolfswinkel, J.C., Wagner, D.E., and Reddien, P.W. (2014). Single-cell analysis reveals functionally distinct classes within the planarian stem cell compartment. Cell Stem Cell *15*, 326-39.

Vásquez-Doorman, C., and Petersen, C.P. (2016). The NuRD complex component *p66* suppresses photoreceptor neuron regeneration in planarians. Regeneration *3*, 168-78.

Vénéreau, E., Ceriotti, C., and Bianchi, M.E. (2015). DAMPs from cell death to new life. Front. Immunol. *6*, 422.

Vincent, J.P., Fletcher, A.G., and Baena-Lopez, L.A. (2013). Mechanisms and mechanics of cell competition in epithelia. Nat. Rev. Mol. Cell Biol. *14*, 581-91.

Vriz, S., Reiter, S., and Galliot, B. (2014). Cell death: a program to regenerate. Curr. Top. Dev. Biol. *108*, 121-51.

Wagner, D.E., Ho, J.J., and Reddien, P.W. (2012). Genetic regulators of a pluripotent adult stem cell system in planarians identified by RNAi and clonal analysis. Cell Stem Cell *10*, 299-311.

Wagner, D.E., Wang, I.E., and Reddien, P.W. (2011). Clonogenic neoblasts are pluripotent adult stem cells that underlie planarian regeneration. Science *332*, 811-6.

Weiss, P., and Kavanau, J.L. (1957). A model of growth and growth control in mathematical terms. J. Gen. Physiol. *41*, 1-47.

Wenemoser, D., Lapan, S.W., Wilkinson, A.W., Bell, G.W., and Reddien, P.W. (2012). A molecular wound response program associated with regeneration initiation in planarians. Genes Dev. *26*, 988-1002.

Wenemoser, D., and Reddien, P.W. (2010). Planarian regeneration involves distinct stem cell responses to wounds and tissue absence. Dev. Biol. *344*, 979-91.

Witchley, J.N., Mayer, M., Wagner, D.E., Owen, J.H., and Reddien, P.W. (2013). Muscle cells provide instructions for planarian regeneration. Cell Rep. *4*, 633-41.

Wu, H.H., Ivkovic, S., Murray, R.C., Jaramillo, S., Lyons, K.M., Johnson, J.E., and Calof, A.L. (2003). Autoregulation of neurogenesis by GDF11. Neuron *37*, 197-207.

Wurtzel, O., Cote, L.E., Poirier, A., Satija, R., Regev, A., and Reddien, P.W. (2015). A generic and cell-type-specific wound response precedes regeneration in planarians. Dev. Cell *35*, 632-45.

Wurtzel, O., Oderberg, I.M., and Reddien, P.W. (2017). Planarian epidermal stem cells respond to positional cues to promote cell-type diversity. Dev. Cell *40*, 491-504.

Wynn, T.A., and Vannella, K.M. (2016). Macrophages in tissue repair, regeneration, and fibrosis. Immunity *44*, 450-62.

Yun, M.H., Davaapil, H., and Brockes, J.P. (2015). Recurrent turnover of senescent cells during regeneration of a complex structure. eLife *4*, e05505.

Zhang, L., Wang, Y.D., Chen, W.D., Wang, X., Lou, G., Liu, N., Lin, M., Forman, B.M., and Huang, W. (2012a). Promotion of liver regeneration/repair by farnesoid X receptor in both liver and intestine in mice. Hepatology *56*, 2336-43.

Zhang, M.Z., Yao, B., Yang, S., Jiang, L., Wang, S., Fan, X., Yin, H., Wong, K., Miyazawa, T., Chen, J., *et al.* (2012b). CSF-1 signaling mediates recovery from acute kidney injury. J. Clin. Invest. *122*, 4519-32.

Zhang, Y., Proenca, R., Maffei, M., Barone, M., Leopold, L., and Friedman, J.M. (1994). Positional cloning of the mouse *obese* gene and its human homologue. Nature *372*, 425-32.

Ziller-Sengel, C. (1967). [Investigation of the inhibition of the regeneration of the planarian pharynx. I. Evidence of an auto-inhibiting factor found in the regenerating pharynx]. J. Embryol. Exp. Morphol. *18*, 91-105.

CHAPTER 2

Eye absence does not regulate planarian stem cells during eye regeneration

Samuel A. LoCascio,[1,2,4] Sylvain W. Lapan,[1,3,4] and Peter W. Reddien[1,3,4]

[1]Whitehead Institute for Biomedical Research, 455 Main Street, Cambridge, MA 02142

[2]Department of Brain and Cognitive Sciences, Massachusetts Institute of Technology (MIT), 77 Massachusetts Avenue, Cambridge, MA 02139

[3]Department of Biology, MIT

[4]Howard Hughes Medical Institute

Published as:

LoCascio, S.A., Lapan, S.W., and Reddien, P.W. (2017). Eye absence does not regulate planarian stem cells during eye regeneration. Dev. Cell *40*, 381-91.

SUMMARY

Dividing cells called neoblasts contain pluripotent stem cells and drive planarian flatworm regeneration from diverse injuries. A long-standing question is whether neoblasts directly sense and respond to the identity of missing tissues during regeneration. We used the eye to investigate this question. Surprisingly, eye removal was neither sufficient nor necessary for neoblasts to increase eye progenitor production. Neoblasts normally increase eye progenitor production following decapitation, facilitating regeneration. Eye removal alone, however, did not induce this response. Eye regeneration following eye-specific resection resulted from homeostatic rates of eye progenitor production and less cell death in the regenerating eye. Conversely, large head injuries that left eyes intact increased eye progenitor production. Large injuries also non-specifically increased progenitor production for multiple uninjured tissues. We propose a model for eye regeneration in which eye tissue production by planarian stem cells is not directly regulated by the presence or absence of the eye itself.

INTRODUCTION

Regeneration is the replacement of body parts lost to injury, such as organs or appendages, and occurs throughout the animal kingdom (Poss, 2010; Sánchez Alvarado, 2000; Tanaka and Reddien, 2011). How animals respond to the absence of specific tissues following injury to bring about their precise replacement is a central but poorly understood problem in regeneration biology.

Planarians are free-living flatworms that can regenerate from almost any injury, making them a powerful model for the study of animal regeneration (Reddien and Sánchez Alvarado, 2004). Underlying this regenerative ability is a proliferative population of cells called neoblasts that contain pluripotent stem cells (Baguñà et al., 1989; Wagner et al., 2011). Neoblasts constitute the only dividing adult somatic planarian cells and are required for the regeneration and homeostatic maintenance of all differentiated tissues. A remarkable aspect of planarian regeneration is that it is tissue specific; whether an injury removes an entire section of the body, or specifically ablates a single tissue of virtually any type, the animal replaces precisely those tissues that were lost (Adler et al., 2014; Nishimura et al., 2011; Reddien and Sánchez Alvarado, 2004). One hypothesis to explain this highly specific nature of planarian regeneration is that neoblasts sense the presence and absence of specific tissues after injury, modifying their output in accordance with the identity of missing tissues (Adler and Sánchez Alvarado, 2015; Mangel et al., 2016; Nishimura et al., 2011). However, whether neoblast output is directly regulated by the presence or absence of the specific tissues to be regenerated is unclear.

Planarian eyes present an ideal venue to investigate the mechanistic basis of tissue-specific regeneration in vivo. The paired planarian eyes, which can be formed de novo after head amputation, are simple organs composed of pigmented optic cup cells and photoreceptor neurons (PRNs) that connect to a bilobed brain. The eyes are discretely located, visible in live animals, and dispensable for viability, making them good targets for specific surgical manipulation. Molecular characterization has identified tissue-specific markers for eye cell types and provided tools for the visualization of eye progenitors during regeneration (Lapan and Reddien, 2011, 2012; Sánchez Alvarado and Newmark, 1999). Previously, we found that head amputation leads to the formation of a large number of specialized neoblasts expressing eye-associated transcription factors. These eye-specialized neoblasts give rise to progenitors that migrate anteriorly, progressively differentiate, and coalesce to form the regenerated eyes (Lapan and Reddien, 2011, 2012). The potential for inducing tissue-specific injuries combined with the ability to observe the cellular stages of eye regeneration presented a unique opportunity to investigate the mechanistic basis of tissue-specific regeneration.

To directly test the hypothesis that neoblasts are regulated by the presence or absence of eye tissue, we examined eye progenitor responses to tissue-specific eye resection and to various large injuries that either removed the eyes or left the eyes uninjured. Surprisingly, our data demonstrate that stem cell-based eye progenitor production is not regulated by the presence or absence of the eye itself. Specific removal of the eye did not affect eye progenitor production. Instead, less cell death occurred in regenerating eyes, allowing them to grow in size despite no specific increase in the rate of eye progenitor production. Such a passive process could fuel regeneration from a myriad

of injuries removing different cell types. Eye absence was also not necessary for increased eye progenitor formation. Increased eye progenitor formation was induced whenever large injuries triggered general neoblast proliferation in the body position where eye progenitor specification occurs, regardless of the presence or absence of the eyes. Large injuries also non-specifically increased the production of uninjured pharynx and ventral nerve cord tissue. We propose a ''target-blind'' progenitor model for planarian eye regeneration, which could apply to many other regenerative contexts, in which stem cells do not respond to the presence or absence of the specific tissue to be regenerated.

RESULTS

Planarian eyes exhibit tissue-specific regeneration

How regeneration occurs following removal of specific tissues is poorly understood (Figure 1A). To address this problem, we developed tissue-specific surgical manipulations to partially or fully resect one or both of the planarian eyes (Figures 1B–1G and S1A–S1C). In all cases the injured or absent eye returned, representing the regeneration of an entire organ following its specific removal (Figures 1B–1G). We therefore utilized these tissue-specific surgical strategies in combination with various large injuries to seek the mechanistic basis of tissue-specific regeneration.

Eye absence is not sufficient to increase eye progenitor production

Previously, we found that head amputation leads to increased neoblast-derived eye progenitor numbers (eye progenitor amplification), facilitating eye regeneration (Figure 2A) (Lapan and Reddien, 2011, 2012). If eye progenitor amplification following decapitation involves neoblasts responding to eye absence, then eye removal alone should also induce eye progenitor amplification. We therefore assessed whether eye resection was sufficient to increase eye progenitor numbers above basal levels found in uninjured animals.

As expected, 3 days after injury, eye progenitor numbers were increased in response to decapitation. Surprisingly, however, eye progenitor numbers were not increased after eye resection (Figures 2B and 2C), despite the fact that eyes regenerated following this injury (Figure 1E). We also quantified eye progenitors every day for 1

week following injury. This time window allows substantial regeneration, including of a functional head and eyes, with animals capable of feeding and negative phototaxis. Eye-resected animals did not show elevated progenitor numbers at any of the eight time points quantified, whereas decapitated animals exhibited elevated progenitor numbers from day 3 to day 7 (Figure 2D). Quantification with a semi-automated computer protocol yielded similar results (Figures S1D–S1H). *ovo* RNAi animals did not regenerate eyes following eye resection, indicating that the amplification of an *ovo*$^{-}$ progenitor population does not contribute to eye regeneration in this context (Figure S1I). We conclude that eye absence alone is not sufficient to induce eye progenitor amplification.

Eye absence is not sufficient to induce a tissue-specific increase in progenitor incorporation

Although eye resection did not increase eye progenitor numbers, a tissue-specific increase in eye progenitor incorporation could in principle drive regeneration in this context. For instance, eye progenitors might only survive and incorporate into eyes that are disproportionately small or absent. More generally, if neoblasts respond to eye absence in a tissue-specific manner, then an eye-specific increase in progenitor incorporation should occur following eye resection. To assess progenitor incorporation rate, we utilized bromodeoxyuridine (BrdU) to label neoblasts (Newmark and Sánchez Alvarado, 2000) and quantified the number of BrdU^{+}/*opsin*$^{+}$ PRNs 6 days later. Whereas decapitation resulted in an increased rate of new PRN formation from neoblasts, eye resection alone did not (Figures 3A and 3B).

To exclude the possibility that we failed to observe an increase in PRN incorporation following eye resection because of the specific timing of our experiment, we systematically varied the timing of BrdU delivery and animal fixation with respect to surgery in uninjured, eye-resected, and decapitated animals (Figure 3C). In most cases decapitated animals had significantly more BrdU$^+$/*opsin*$^+$ cells than did uninjured animals. Conversely, in most cases no difference between eye-resected animals and uninjured controls was observed. A modest increase in PRN incorporation was observed in eye-resected animals only for the day 0–6 and day 1–7 delivery-fixation intervals. To determine whether this effect was specifically a consequence of eye absence, we resected a similar amount of tissue from a region lateral to the eyes and used the day 1–7 delivery-fixation interval to assess PRN incorporation. Tissue resection lateral to the eye resulted in a similar increase in PRN incorporation (Figure 3D). These data suggest that this modest, transient increase in progenitor incorporation is a generic consequence of injury-induced proliferation, rather than eye absence. This is consistent with a global wave of mitosis previously described to occur in planarians following any small injury (Baguñà, 1976; Wenemoser and Reddien, 2010). Tissue-specific regeneration also occurred in the case of single eye removal, enabling paired comparisons of regenerating and non-regenerating eyes within the same individuals (Figure 1F). Uninjured and regenerating eyes had similar incorporation rates regardless of the delivery-fixation interval (Figures 3E and S2).

We also used perdurance of the neoblast protein SMEDWI-1 (Guo et al., 2006; Reddien et al., 2005; Scimone et al., 2010) as a marker of newly differentiated PRNs, providing a second direct readout of progenitor incorporation rate into the eye. Whereas

animals regenerating from decapitation showed elevated numbers of SMEDWI-1^{+}/*opsin*$^{+}$ PRNs, animals regenerating from eye resection did not (Figures 3F and 3G). We conclude that tissue-specific eye regeneration, following eye resection, is accomplished in the absence of a tissue-specific neoblast response.

Regenerating eyes exhibit less cell death than uninjured eyes

How are the eyes specifically regenerated following eye resection if their absence is not sensed by neoblasts, and there is no specific alteration in their progenitor production or incorporation rates? For instance, in animals with only one resected eye, the intact eye and the regenerating eye have the same rate of progenitor incorporation (Figures 1F and 3E). Thus, how does growth occur only on the injured side? Because the size of a tissue remains constant when cell production and cell death are in equilibrium, alteration in either process can affect tissue size. Therefore, if the rate of eye progenitor incorporation remains constant following eye resection, then the rate of cell loss in regenerating eyes (defined as total cell loss events per eye per unit time) must be lower in the regenerating eye in order to facilitate net growth. To test this prediction, we sought to compare rates of cell loss in uninjured and regenerating eyes (Figure 4A). Animals underwent right eye resection, leaving left eyes uninjured. Right eyes were allowed to partially regenerate for 8 days. Animals were then irradiated with 6,000 rad, a procedure that specifically and rapidly eliminates neoblasts (Figure 4A) (Dubois, 1949) and neoblast-derived eye progenitors (Lapan and Reddien, 2011), but has no detectable effect on differentiated planarian tissues (Guo et al., 2006; Reddien et al., 2005; Wagner et al., 2012; Wagner et al., 2011). Because neoblasts are the only dividing planarian cells and the sole source of

new differentiated tissue (Baguñà et al., 1989; Newmark and Sánchez Alvarado, 2000), subsequent alterations in the number of eye cells could be attributed to eye cell loss. We therefore predicted that the right eyes, which were regenerating at the time of irradiation, would decrease in size more slowly than the uninjured left eyes. To quantify eye size, we counted the total number of PRNs per eye (Figure S3A). As predicted, uninjured left eyes significantly decreased in size from day 3 to day 10 post irradiation (Figures 4B and 4C). Uninjured eyes also decreased in size following irradiation when the contralateral eye was not injured, indicating that this effect was not a consequence of contralateral eye absence (Figure S3B). In contrast to the uninjured left eyes, regenerating right eyes did not significantly decrease in size, indicating that less cell loss occurred in the regenerating eye during this interval (Figures 4B and 4C). Consistent with these observations, the intra-animal PRN number difference between uninjured and regenerating eyes was decreased from day 3 to day 10 post irradiation (Figure S3C). The ratio of PRNs in the regenerating to uninjured eye was increased over this time interval, also demonstrating proportionally less cell loss in the regenerating eye (Figure 4D). We also used fluorescence in situ hybridization (FISH) combined with whole-mount TUNEL (terminal deoxynucleotidyl transferase-mediated dUTP nick end labeling) (Pellettieri et al., 2010) to observe apoptotic cell death events in intact and regenerating PRNs (Figures 4E and S3D). Apoptosis accounts for a small fraction of the lifetime of a cell, making TUNEL$^+$/*opsin*$^+$ PRNs rare. We therefore analyzed >350 eyes that were uninjured or regenerating from eye resection. A greater proportion of uninjured eyes contained TUNEL$^+$/*opsin*$^+$ PRNs than did regenerating eyes (Figure 4F). Taken together, our data indicate that regenerating eyes specifically exhibit a decrease in the rate of cell death (cell

death events per eye per unit time), facilitating net growth without a specific increase in eye progenitor incorporation.

A passive model for tissue-specific eye regeneration

Based on these findings, we propose a simple, passive model for tissue-specific eye regeneration (Figure 5A), in which the rate of eye cell production by progenitors remains constant. Following eye resection, there are initially zero cells available for cell death, allowing any addition of new cells to result in net growth. In the following days, fewer cells are available for cell death than during homeostasis, with no old PRNs present. Net growth thus continues because the rate of cell death is less than the rate of incorporation, as a passive consequence of the emergent properties of a regenerating eye. As sufficient numbers of PRNs accumulate and age, the rate of cell death per eye once again matches the rate of incorporation events per eye, resulting in homeostatic eye size. This model allows tissue-specific eye regeneration to occur while not requiring neoblasts to specifically interpret or respond to the absence of the eye.

Consistent with this passive model, the rate of eye degrowth following irradiation was similar to the rate of growth following eye resection, indicating that both incorporation and cell death occur at appreciable rates during homeostasis (Figure S4A). Furthermore, unlike the case for regenerating eyes described above, partially resected eyes (Figure 1G) decreased in size at a rate comparable with larger, uninjured eyes following irradiation (Figures S4B and S4C). This is consistent with cell age contributing to PRN death because unlike regenerating eyes, partially resected eyes are not exclusively composed of young cells. The result also indicates that an active size-sensing

mechanism is unable to suppress death in partially resected eyes. Our passive model for tissue-specific eye regeneration also predicts that eyes regenerate following resection, but slowly. Indeed, eye-resected animals regenerated eyes more slowly than did decapitated animals, despite the fact that decapitated animals were significantly smaller than their eye-resected counterparts because of surgery and had to regenerate not only the eyes but also all other cell types of an entire head (Figures 5B, 5C, S5A, and S5B).

Eye progenitor amplification is associated with wounds that induce proliferation in the location of eye progenitor specification

Our data indicate that eye progenitor amplification is not a consequence of eye removal. We therefore sought to explore how large injuries induce eye progenitor amplification if eye absence is not regulating this process. Tail removal did not increase eye progenitor numbers in uninjured heads (Figure 6A), indicating that the response does not simply occur after any wound removing a large amount of tissue. Anterior incisions made in the same location as decapitation, but that did not remove the head, also failed to significantly increase eye progenitors (Figure 6A), indicating that eye progenitor amplification requires anterior wounds that remove tissue. Injuries removing substantial tissue (such as amputation) differ from wounds that do not remove tissue (such as incisions) in multiple ways. Importantly, amputations but not incisions elicit a sustained increase in neoblast proliferation that is localized near the wound site (Wenemoser and Reddien, 2010). Accordingly, decapitation increased proliferation in the pre-pharyngeal region (assessed with phosphorylated histone H3 [H3P] immunofluorescence), whereas eye resection, tail amputation, and anterior incisions did not (Figure 6B). Specification of

eye progenitors occurs in a spatially restricted manner within the head and pre-pharyngeal region (Lapan and Reddien, 2011, 2012). We therefore hypothesized that eye progenitor amplification occurs as a consequence of injury-induced proliferation in the body position where eye progenitors are specified, rather than as a consequence of eye absence.

To explore this possibility, we assessed neoblast proliferation and eye progenitor amplification in the pre-pharyngeal region following wounds that removed progressively increasing amounts of anterior tissue. Animals were left uninjured or underwent transverse amputation just anterior to the eyes, transverse amputation just posterior to the eyes, or full decapitation (Figure 6C). Neoblast proliferation in the pre-pharyngeal region increased proportionately with the amount of anterior tissue removed (Figure 6D) and eye progenitor amplification also occurred, closely paralleling the degree of neoblast proliferation (Figure 6E). Importantly, the difference in eye progenitor numbers between pre-eye and post-eye amputations was very small, despite the fact that former injury type left the eyes intact while the latter completely removed them. The fact that eye progenitor numbers increased following amputation of the anterior head tip, an injury that did not remove eyes or eye progenitors, also demonstrates that eye absence is not required for increased eye progenitor production (Figures 6E and S6A).

Amputated body fragments, such as tails, initially lack the region where eye progenitors are specified, yet they produce large numbers of eye progenitors de novo and regenerate eyes. Positional information is required for maintenance of the planarian adult body plan and proper regeneration (Reddien, 2011). Regional expression gradients of patterning molecules (such as Wnt, BMP, and FGFRL/*ndl*) exist in planarian body wall

muscle (Scimone et al., 2016; Witchley et al., 2013), and the pattern of expression of these molecules is restored early in the process of regeneration. In tails, anterior patterning molecules reappear by 48 hours post amputation (Figure 6F) (Gurley et al., 2010; Petersen and Reddien, 2009), coinciding with increased neoblast proliferation (Figure 6H) (Wenemoser and Reddien, 2010) and the location of de novo eye progenitor amplification (Figure 6I). Therefore, similar to the case of decapitated animals, eye progenitor amplification in tail fragments involves significant tissue removal and induction of sustained neoblast proliferation in a region coinciding with the location of eye progenitor specification (the anterior-facing wound expressing head patterning molecules). We propose that it is not the absence of eyes promoting eye progenitor amplification in either case.

Eye absence is not required for eye progenitor amplification

We utilized additional injuries to further test predictions of the hypothesis that eye progenitor amplification caused by large wounds is not a consequence of eye absence itself. We resected large lateral flanks in the pre-pharyngeal region while leaving the eyes uninjured (Figures 7A and 7B). Similarly to decapitation, lateral flank resection induced a missing tissue response involving a large increase in neoblast proliferation in the location of eye progenitor specification. These flank injuries caused amplification of eye progenitors (Figures 7C–7E). Flank resection also increased the incorporation rate of eye progenitors into uninjured eyes (Figure 7F). We conclude that increased eye progenitor production and acceleration of eye progenitor incorporation into the eye do not require eye absence.

Identical flank resection injuries in the tail, where eye progenitors are not normally specified, increased neoblast proliferation locally, while not inducing proliferation in the pre-pharyngeal region (Figures S6B–S6D). Accordingly, eye progenitors were not amplified after flank resection in the tail (Figures S6E and S6F). Eye progenitor amplification is therefore not a general consequence of flank resection injury at any location. To rule out the possibility that pre-pharyngeal flank resection was simply interpreted as a decapitation injury, with the tissue posterior to the flank wounds mounting a head regeneration response, we analyzed the expression of anterior positional markers *sFRP-1* and *ndl-2* following flank resection (Figure S6G). We did not observe *sFRP-1* expression at the posterior boundary of the flank wound by 36 hours post surgery. Flank resection also did not induce expansion of the *ndl-2* expression domain, a gene that is expressed in muscle of the pre-pharyngeal region (Scimone et al., 2016). These results suggest that flank resection is not interpreted as a decapitation injury. This is further supported by the fact that eye progenitors were not amplified in the tail after posterior flank resection (Figure S6F). Together, our data indicate that large injuries that induce proliferation in the location of eye progenitor specification result in eye progenitor amplification, regardless of the presence or absence of the eye.

Anterior flank resection accelerates eye regeneration

It is known that wounds resulting in significant tissue loss induce a process called morphallaxis, whereby overabundant tissues shrink to a size appropriate for the new size of the animal (Morgan, 1898). Therefore, flank resection cannot lead to robust overgrowth of intact eyes. We tested the impact of eye progenitor amplification caused

by flank resection in the context of regeneration. Animals underwent eye resection alone or eye resection combined with flank resection. One week later, animals that underwent both eye and flank resection had more PRNs than did animals that underwent eye resection alone (Figure 7G). We conclude that flank resection accelerated the rate of eye regeneration.

Increased progenitor incorporation into the ventral nerve cords and pharynx does not require specific tissue removal

Other than the eye, the pharynx is the most accessible planarian organ for complete and specific surgical resection (Adler et al., 2014). Whereas pharynx removal increases pharynx progenitor production, the pharynx is much larger than the eyes (Figure S7A) and its removal results in significant neoblast proliferation in the location of pharynx progenitor specification (Figures S7B–S7E) (Adler et al., 2014). Because pharynx removal elevates local neoblast proliferation, we predicted that it would also lead to the amplification of non-pharynx progenitors that are specified in a nearby region but that correspond to uninjured tissues. Indeed, pharynx resection led to increased incorporation of BrdU-labeled progenitors into the uninjured ventral nerve cords (VNCs) anterior to the pharynx, and also increased the incidence of newly differentiated SMEDWI-1^{+}/*ChAT*$^{+}$ VNC neurons (Figures 7H, S7F, and S7G). This result demonstrates that the response to tissue-specific pharynx resection is not restricted to pharynx progenitors. It also demonstrates that similar to the case of the eye, removal of the VNCs is not required for increased VNC tissue production.

We also wondered whether large injuries that do not remove the pharynx, but that induce proliferation in the region of pharynx progenitor specification, would lead to increased pharynx progenitor incorporation. Para-pharyngeal flank resection increased proliferation near the pharynx, where pharynx progenitor specification occurs (Figures S7H–S7K). This surgery increased incorporation of BrdU-labeled neoblast-derived cells into the intact pharynx, including more newly incorporated BrdU-labeled *ChAT*$^{+}$ neurons in the distal tip of the pharynx (Figures 7I, 7J, and S7L). These observations support a generalizable model for progenitor amplification in which large wounds that cause sustained proliferation amplify nearby progenitor types regardless of the presence or absence of their target tissue.

DISCUSSION

How animals detect absent tissues and specifically regenerate them from diverse, unpredictable injuries is one of the great mysteries of biology. We used the planarian eye to dissect the mechanistic basis of tissue-specific regeneration in a model organ. We found that eye removal failed to specifically alter eye cell production, indicating that the eyes do not suppress their own formation by neoblasts (Figure 8). Instead, constant progenitor production and incorporation, together with a tissue-specific decrease in the rate of cell death per eye, led to specific regeneration (Figure 5A). This passive mode of tissue-specific regeneration obviates the need for a complex tissue-specific sensing strategy by neoblasts for multiple tissues.

A similar process could allow neoblasts to fuel tissue-specific regeneration from an unlimited set of small injuries, in principle for many cell types, without sensing the identity of missing tissues. Experiments indicate that robust homeostatic tissue production exists for multiple other cell types, including the epidermis and various neural populations (Cowles et al., 2013; Newmark and Sánchez Alvarado, 2000; van Wolfswinkel et al., 2014). Furthermore, specialized neoblasts, like those for the eyes, have been identified for many planarian tissues, such as the protonephridia, epidermis, intestine, pharynx, and various neuron classes (Adler et al., 2014; Cowles et al., 2013; Currie and Pearson, 2013; März et al., 2013; Scimone et al., 2014; Scimone et al., 2011; van Wolfswinkel et al., 2014). Future development of tools for the specific ablation of additional tissues and quantification of their progenitors will allow assessment of the generality of our model. However, the simplicity of our passive model for tissue-specific

regeneration suggests that it may explain diverse regenerative contexts in planarians and other organisms as well, particularly in cases where tissues display high turnover rates.

Our data support a model in which a decreased cell death rate emerges as a passive consequence of regenerating eyes containing fewer and younger PRNs. A regenerating eye has fewer cells available to undergo death than a homeostatic eye, which would allow net growth even if PRN cell death were purely stochastic. Indeed, our TUNEL results indicate that some death occurs even in regenerating eyes. Nonetheless, the ratio of PRNs in regenerating versus uninjured eyes was increased following irradiation, indicating a decrease in the rate of cell loss beyond what would be expected if death were a purely stochastic process. This could be mediated by the fact that regenerating eyes, by definition, contain exclusively young PRNs. We also considered whether an active size-sensing mechanism contributed to the decreased rate of death. In contrast to regenerating eyes, partially resected eyes exhibited cell loss similar to that in uninjured eyes, inconsistent with active suppression of death occurring in smaller eyes in this context. Partially resected eyes contained a mixture of young and old cells, consistent with PRN age contributing to death in homeostatic and partially resected eyes, but not regenerating eyes. In principle cell death regulation could have an active role in constraining the maximum relative size of eyes and other organs, but this is not a necessary prediction. It will therefore be of interest to continue to investigate mechanisms of cell death regulation to further understand how tissue proportions are reached.

We found that eye progenitor amplification could be accelerated when large injuries coincided with the location of eye progenitor specification (Figure 8). Because eye progenitor specification occurs in a location separate from the eyes themselves, we

were able to decouple this cause of eye progenitor amplification from neoblasts sensing and responding directly to a feedback signal from the presence or absence of the eyes themselves. Flank resections that did not remove the eyes, but that removed tissue and increased neoblast proliferation in the location where eye progenitors are specified, induced eye progenitor amplification and increased progenitor incorporation into the eyes. We extended this finding to additional tissues, demonstrating that increased progenitor incorporation into the pharynx or VNCs does not require the removal of these tissues. We cannot exclude that tissue-specific negative feedback regulation from the pharynx or VNCs might also contribute to regulation of neoblast-derived progenitor numbers. However, our findings support a model that explains how progenitor amplification for the eyes, pharynx, and VNCs can occur without requiring removal of such tissues.

How might a large wound in the location of progenitor specification trigger progenitor amplification? Neoblasts exhibit a general response to any wound involving substantial missing tissue that includes sustained proliferation and accumulation at the wound site (Wenemoser and Reddien, 2010). One simple scenario is that in a region where positional information is appropriate for the specification of a particular progenitor type (e.g., the eye), neoblast proliferation and accumulation simply creates more opportunities for differentiation/cell fate decisions to occur. Our finding that eye progenitor production in the pre-pharyngeal region closely reflects the degree of general neoblast proliferation is consistent with this hypothesis. Although stem cell progeny are reported to regulate stem cells in various contexts (Hsu and Fuchs, 2012), we observed that anterior wounds that did not remove the eyes or eye progenitors also increased eye

progenitor numbers, suggesting that negative feedback by eye progenitors themselves also does not explain eye progenitor behavior. Furthermore, the pharynx itself does not contain VNC progenitors, yet its removal increased incorporation of progenitors into the VNCs. It will be important in future work to determine how large wounds and positional information communicate with and affect neoblast biology to give rise to progenitor amplification. However, our work indicates that progenitor amplification is not simply a result of neoblasts interpreting and responding to the exact identity of missing tissue. We propose that a target-blind mode of progenitor amplification could explain how progenitors are amplified, with neoblasts being regulated by coarse positional information and general wounding signals rather than the presence or absence of the specific target tissues to be regenerated.

Our findings suggest that the specificity of tissue production during regeneration is inherently imprecise. Increased production of cells in uninjured tissue regions have been observed in BrdU incorporation experiments elsewhere, for example in the planarian gut, where neoblasts differentiate and incorporate into both regenerating and pre-existing intestinal branches after injury (Forsthoefel et al., 2011). In this context, incorporation into non-regenerating tissues may play a role in intestinal branch remodeling. In the axolotl brain, resection of the dorsal pallium increased production of neurons in more rostral, uninjured regions (Amamoto et al., 2016). Hair plucking experiments in mice revealed non-specific regenerative responses in adjacent un-plucked follicles (Chen et al., 2015). These findings highlight the importance of considering non-tissue-specific feedback mechanisms for explaining how animals sense and respond to injury.

CONCLUSION

We found that constant eye progenitor production and less cell death allow planarian eyes to passively regenerate without the need for a tissue-specific sensing strategy by neoblasts. Eye progenitors are amplified when large injuries induce proliferation in a location where eye progenitors are specified, but this process is not influenced by the presence or absence of the eye itself. We conclude that the eye does not regulate production of its own progenitors during eye regeneration. Our work identifies a mode of regeneration whereby progenitor specification is target blind – not directly regulated by the presence or absence of the specific target tissue to be regenerated.

MATERIALS AND METHODS

Experimental subject

Asexual *S. mediterranea* clonal strain CIW4 animals (Sánchez Alvarado et al., 2002), starved 1-2 weeks, were used for all experiments.

Fluorescence in situ hybridization

Animals were killed in 5% NAC in 1x PBS before fixation in 4% formaldehyde in PBSTx (1x PBS containing 0.1% Triton X-100), then stored in methanol at -20°C until subsequent steps. Animals were bleached in 1x SSC solution containing 5% deionized formamide and 1.2% hydrogen peroxide for 1.5 hours while exposed to light. Animals were treated with 2 mg/ml proteinase K in PBSTx with 0.1% SDS, then hybridized with RNA probes diluted 1:800 in a solution of 50% formamide, 5x SSC, 1 mg/ml yeast RNA, 1% Tween-20 and 5% dextran sulfate at 56°C overnight. Animals were blocked for 1-2 hours prior to labeling overnight at 4°C with anti-DIG-POD (1:1500, Roche #11207733910), anti-FITC-POD (1:2000, Roche #11426346910), or anti-DNP-HRP (1:100, Perkin-Elmer #FP1129) in blocking solutions of PBSTx containing 5% heat inactivated horse serum and 5% 10x casein solution (Sigma) for anti-DIG-POD, 10% 10x casein solution for anti-FITC-POD, and 5% horse serum and 5% western blocking reagent (Roche) for anti-DNP-HRP. For tyramide development, animals were placed for 10 minutes in borate buffer (0.1M boric acid, 2M NaCl, pH 8.5), followed by 10 minutes in borate buffer containing rhodamine (1:1000) or fluorescein (1:1500) tyramide and 0.0003% hydrogen peroxide. Prior to antibody labeling for a second probe, peroxidase

inactivation was performed in 1% sodium azide overnight at 4°C. Animals were stained in a solution of 1mg/ml DAPI (Sigma) prior to mounting on slides. FISH protocol was adapted from previous work (King and Newmark, 2013; Pearson et al., 2009; Scimone et al., 2016).

BrdU immunofluorescence

Prior to BrdU immunostaining, FISH was performed as described above, with the following exceptions: bleaching was performed overnight in methanol containing 6% hydrogen peroxide, and tyramide development was performed by placing animals in PBSTi (PBSTx containing 10 mM imidazole) for 30 minutes, then PBSTi containing rhodamine tyramide for 30 minutes, then PBSTi containing tyramide and 0.0002% hydrogen peroxide for 45 minutes. After FISH steps, animals were placed in 2N HCl with 0.5% Triton X-100 for 45 minutes, followed by 0.1M sodium borate for 3 minutes and rinsed in PBSTx. Animals were placed in blocking solution (1x PBS containing 0.3% Triton-X 100, 5mM thymidine, 0.6% BSA, 5% western blocking reagent (Roche)) for 1-2 hours, then labeled with mouse anti-BrdU (1:300, Becton Dickinson #347580) in blocking solution overnight at 4°C. After PBSTx washes and blocking as described above, samples were labeled with goat anti-mouse-HRP secondary antibody (1:200, Invitrogen #G-21040) in block overnight at 4°C. Samples were then developed with fluorescein tyramide in PBSTi containing hydrogen peroxide as described above, and stained with DAPI prior to mounting. BrdU immunofluorescence protocol was adapted from previous work (Newmark and Sánchez Alvarado, 2000; van Wolfswinkel et al., 2014).

H3P immunofluorescence

Animals were killed in 2% HCl and placed on ice for 30 seconds, then transferred to Carnoy's fixative (60% ethanol, 30% chloroform, 10% glacial acetic acid) for 5 minutes at room temperature then 2 hours on ice. Bleaching was performed as for BrdU immunofluorescence, followed by treatment with 2 mg/ml proteinase K in PBSTx with 0.1% SDS. Animals were blocked 1-2 hours in PBSTx containing 10% horse serum, then labeled with anti-H3P (1:100, Millipore #04-817) in block overnight at 4°C. After PBSTx washes and blocking as described above, samples were labeled with goat anti-rabbit-HRP secondary antibody (1:100, Invitrogen #G-21234) in block overnight at 4°C. Samples were developed with rhodamine tyramide in PBSTi containing hydrogen peroxide as described for BrdU immunofluorescence, and stained with DAPI prior to mounting. H3P immunofluorescence protocol was adapted from previous work (Newmark and Sánchez Alvarado, 2000; Wenemoser and Reddien, 2010).

TUNEL

All FISH steps were performed as described above using *opsin* probe developed with fluorescein tyramide prior to TUNEL. TUNEL was performed using reagents from ApopTag Red In Situ Apoptosis Detection Kit (Millipore, #S7165). Animals were transferred to droplets on eight-well patterned microscope slides (Tekdon, Slide ID# 8-82) in PBSTx and a micropipette was used to replace PBSTx with 30 ml ApopTag equilibration buffer. Slides were incubated at room temperature for 30 minutes. Equilibration buffer was replaced with 30 ml 3 parts ApopTag TdT enzyme mix, 7 parts ApopTag reaction buffer, and slide was sealed and incubated in a dark humid chamber

overnight at 37°C. Stop/wash buffer was used to transfer animals back to in situ baskets, which were incubated 5 minutes at 37°C. Animals were transferred to room temperature, washed thoroughly with PBSTx, and incubated one hour in a blocking solution of PBSTx containing 5% horse serum and 5% western blocking reagent (Roche). Animals were again transferred to droplets on eight-well patterned microscope slides, blocking solution was replaced with 30 ml of 1 part blocking solution (described above), 1 part ApopTag anti-digoxigenin rhodamine conjugate, and slides were incubated in dark sealed humid chamber at 4°C overnight. Animals were washed in PBSTx and counterstained in a solution of 1mg/ml DAPI (Sigma) in 1x PBS containing 0.1% Triton-X 100 (PBSTx) before mounting. TUNEL protocol was adapted from previous work (Pellettieri et al., 2010).

Image acquisition and quantification

Live images were acquired using a Zeiss Discovery V8 stereomicroscope with an AxioCam HRc camera. Fluorescence image acquisition was performed using a Zeiss LSM 700 confocal microscope. Image J software (Fiji) (Schindelin et al., 2012) or ZEN digital imaging software (Zeiss) was used for processing and quantification of all images. *ovo*$^{+}$ eye progenitor quantification was performed on maximum intensity projections (MIPs) of optical sections using blind manual counting or a semi-automated computer protocol as described in Figure S1. *ovo*$^{+}$, *opsin*$^{+}$, TUNEL^{+}/*opsin*$^{+}$, BrdU^{+}/*opsin*$^{+}$, BrdU^{+}/*ChAT*$^{+}$, SMEDWI-1^{+}/*opsin*$^{+}$, SMEDWI-1^{+}/*ChAT*$^{+}$, BrdU^{+} pharynx, and H3P^{+} cells were quantified blind in files with randomized numerical names by examining optical sections of overlayed fluorescence channels in pre-defined regions of animals as

indicated in figures. H3P counting was performed on MIPs for Figures 7D, S6C, S6D, and S7K. For PRN counting, individual eyes were cropped and left eye images were flipped horizontally so that all images appeared as right eyes (or vice versa) for blind quantification, with no indication of experimental condition.

For automated eye progenitor identification (Figure S1), the following steps were performed identically for all files in Fiji: optical section stacks were converted to 8-bit, and maximum intensity projections were generated. The processing tool ''Find Edges'' was applied. Threshold was applied, with minimum and maximum set at 100 and 255, respectively. The ''Analyze Particles'' tool was used to highlight eye progenitors and add them to the ROI manager for counting.

BrdU delivery

BrdU (Sigma #B5002) was administered by soaking for two hours, or by injecting into the pre-pharyngeal region (Figures 7I and S7L), a solution of 1x Montjuic salts containing 25mg/ml BrdU and 3% DMSO. Following administration, animals were rinsed thoroughly with 1x Montjuic salts, then transitioned to 5g/l Instant Ocean until fixation.

Irradiation

Animals were irradiated using a dual Gammacell-40 ^{137}cesium source to deliver 6,000 rad.

RNAi

dsRNA was synthesized by in vitro transcription (Promega) from PCR-generated templates with flanking T7 promoters, ethanol precipitated, resuspended in water and annealed, and diluted in liver for delivery by feeding (Petersen and Reddien, 2008; Rouhana et al., 2013). Animals were fed 10, 8, 6, 4, and 2 days prior to eye resection with *ovo* or *Caenorhabditis elegans unc-22* (control) (Benian et al., 1989) dsRNA.

Surgical procedures

Animals were placed on moist filter paper on a cold block in order to limit movement, and a microsurgery blade was used to remove desired tissues. Pharynx resection was performed by surgical extraction through a small longitudinal dorsal incision. Chemical amputation by exposure to sodium azide was avoided because of its metabolic effects that cause global suppression of mitotic activity (Adler et al., 2014).

Statistical analysis

All statistical analyses were performed in GraphPad Prism software. Statistical tests, significance, data points, error bars, and other information relevant to figures are described and explained in corresponding legends.

ACKNOWLEDGEMENTS

We thank Dan Wagner and Josien van Wolfswinkel for BrdU, FISH, IF, and TUNEL advice, Kendyll Martin for technical assistance, and Kutay Deniz Atabay and members of the Reddien laboratory for comments and discussion. We acknowledge NIH (R01GM080639) support. S.A.L. received government support under FA9550-11-C-0028, awarded by the Department of Defense, Air Force Office of Scientific Research, National Defense Science and Engineering Graduate (NDSEG) Fellowship, 32 CFR 168a. P.W.R. is an Investigator of the Howard Hughes Medical Institute and an associate member of the Broad Institute of Harvard and MIT.

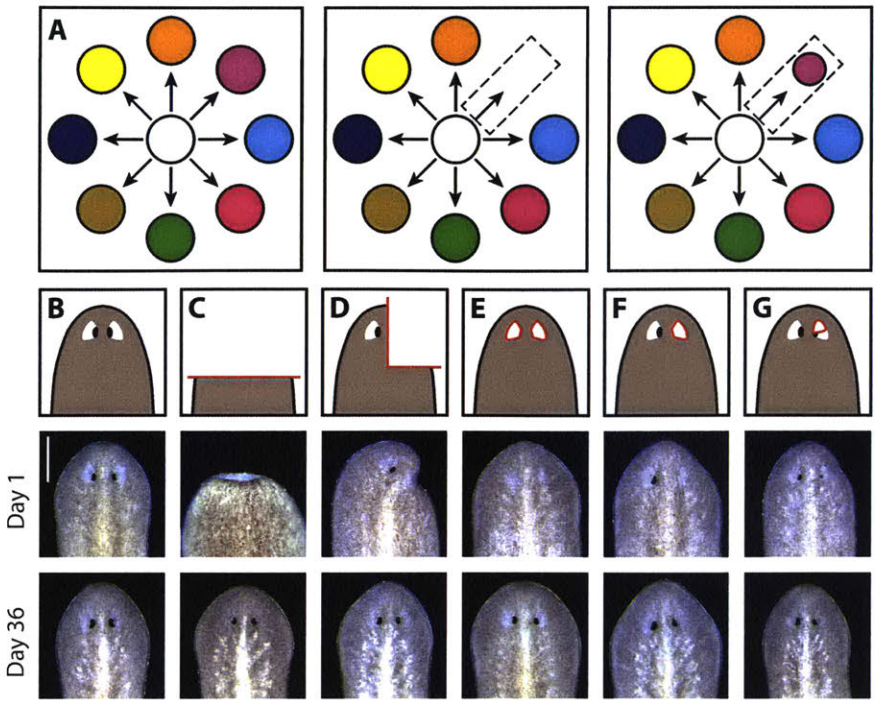
A
B
C
D
E
F
G
Day 1
Day 36

Figure 1. Planarian eyes exhibit tissue-specific regeneration

(A) Schematic of tissue-specific regeneration. White circle represents the neoblast population and colored circles represent distinct differentiated tissues. Neoblasts produce differentiated tissue types (left). Tissue-specific injury (center) is followed by tissue-specific regeneration (right).

(B–G) Cartoons (top) and live images 1 day (center) and 36 days (bottom) after no injury (B), decapitation (C), half decapitation (D), bilateral eye resection (E), right eye resection (F), and partial right eye resection (G). Scale bar, 200 μm. See also Figures S1A–S1C.

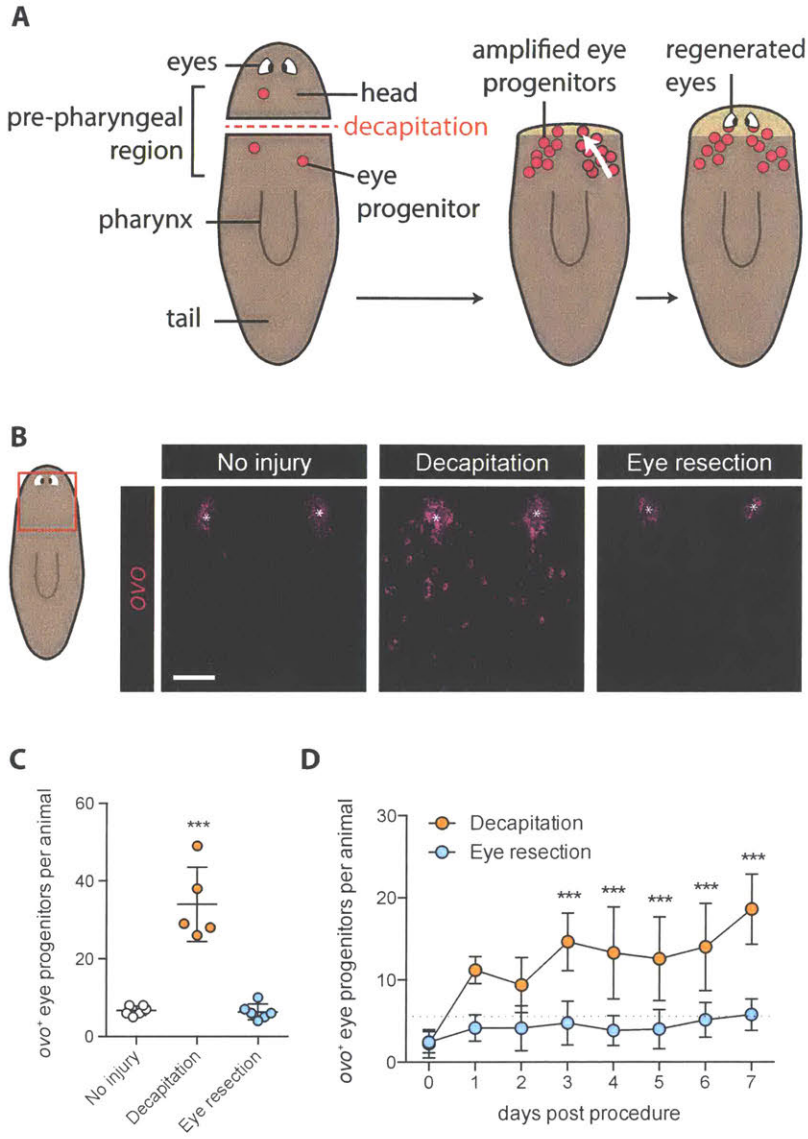
A
eyes
head
pre-pharyngeal region
decapitation
eye progenitor
pharynx
tail
amplified eye progenitors
regenerated eyes
B
No injury
Decapitation
Eye resection
ovo
C
ovo+ eye progenitors per animal
60
40
20
0
***
No injury
Decapitation
Eye resection
D
ovo+ eye progenitors per animal
30
20
10
0
Decapitation
Eye resection
***
0
1
2
3
4
5
6
7
days post procedure

Figure 2. Eye absence is not sufficient to induce eye progenitor amplification

(A) Schematic of eye regeneration following decapitation. Decapitation (left) leads to amplification of *ovo*$^{+}$ eye progenitors (center), which migrate anteriorly (white arrow) and coalesce to form regenerating eyes (right).

(B) Fluorescence in situ hybridization (FISH) with *ovo* RNA probe, 3 days after indicated surgeries. Maximum-intensity projections. Red box on cartoon indicates displayed region. Asterisks mark presumptive eyes, identifiable as coalesced *ovo*$^{+}$ cells anterior to progenitors. Scale bar, 50 μm.

(C and D) *ovo*$^{+}$ eye progenitor numbers 3 days (C) and 0 to 7 days (D) post surgery. Data presented as mean ± SD. Dots reflect eye progenitor numbers for individual animals for (C) and means for (D). In (D), dotted line reflects mean of uninjured animals on day 0. Decapitation but not eye resection resulted in significantly elevated eye progenitor numbers in comparison with uninjured controls. $n \geq 4$ animals per condition. Statistical significance assessed with respect to uninjured animals by one-way ANOVA (***$p<0.001$). See also Figures S1D–S1I.

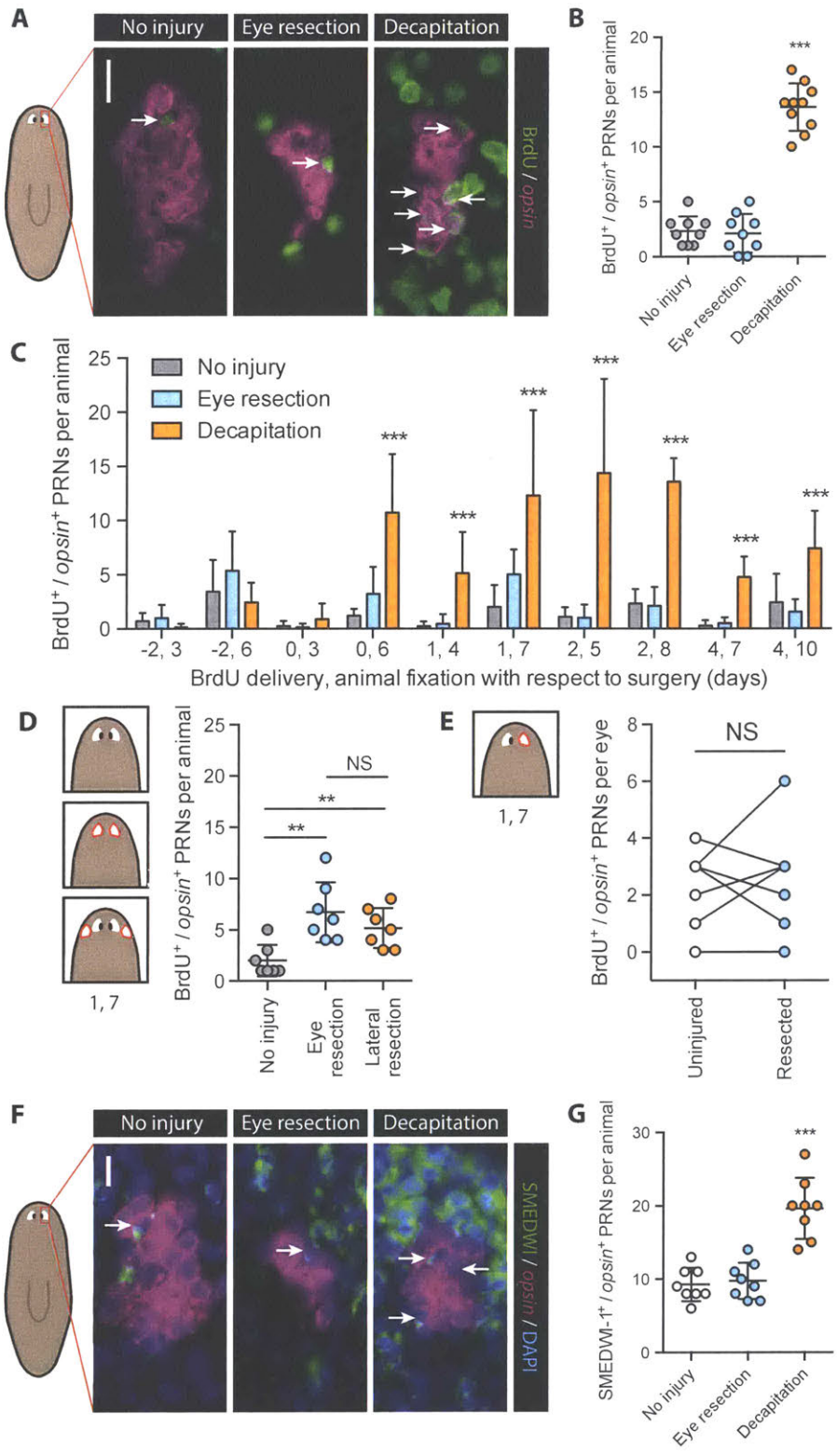
A
No injury
Eye resection
Decapitation
BrdU / opsin
B
BrdU+ / opsin+ PRNs per animal
***
No injury
Eye resection
Decapitation
C
BrdU+ / opsin+ PRNs per animal
No injury
Eye resection
Decapitation
-2, 3
-2, 6
0, 3
0, 6
1, 4
1, 7
2, 5
2, 8
4, 7
4, 10
BrdU delivery, animal fixation with respect to surgery (days)
D
1, 7
BrdU+ / opsin+ PRNs per animal
NS
**
**
No injury
Eye resection
Lateral resection
E
1, 7
BrdU+ / opsin+ PRNs per eye
NS
Uninjured
Resected
F
No injury
Eye resection
Decapitation
SMEDWI / opsin / DAPI
G
SMEDWI-1+ / opsin+ PRNs per animal
***
No injury
Eye resection
Decapitation

Figure 3. Increased eye progenitor incorporation does not contribute to eye-specific regeneration

(A) BrdU immunofluorescence (IF) together with FISH for *opsin*. Arrows indicate $BrdU^+$/$opsin^+$ PRNs. Scale bar, 10 μm.

(B–E) $BrdU^+$/$opsin^+$ PRNs per animal or per eye after surgeries indicated in text or cartoons. (B) BrdU delivery on day 2, animal fixation on day 8. Decapitated but not eye-resected animals had significantly more $BrdU^+$ PRNs than uninjured animals. (C) BrdU delivery-fixation intervals denoted on x axis as day of delivery, day of fixation. Asterisks indicate significant increase above uninjured condition for given interval. Interval data for days 2–8 is also shown in (B). PRN incorporation is higher in eye-resected animals than in uninjured controls for day 0–6 ($p=0.0235$) and day 1–7 ($p=0.0120$) intervals by Student's t test. $n\geq5$ animals per condition. (D) BrdU delivery on day 1, fixation on day 7. n=7 animals per condition. (E) BrdU delivery on day 1, fixation on day 7. n=7 animals. See also Figure S2. Data presented as mean ± SD. Dots represent values from individual animals. In (B) and (C), statistical significance was assessed by one-way ANOVA comparing eye-resected and decapitated animals with uninjured animals for same interval, in (D) by Student's t test, and in (E) by paired Student's t test: $^{**}p<0.01$, $^{***}p<0.001$; NS, not significant.

(F) SMEDWI-1 IF with FISH for *opsin* and DAPI labeling 5 days after indicated surgeries. Arrows indicate SMEDWI-1^+/$opsin^+$ cells. Scale bar, 10 μm. (G) SMEDWI-1^+/$opsin^+$ PRNs per animal 5 days after indicated surgeries. n=8 animals per condition. $^{***}p<0.001$.

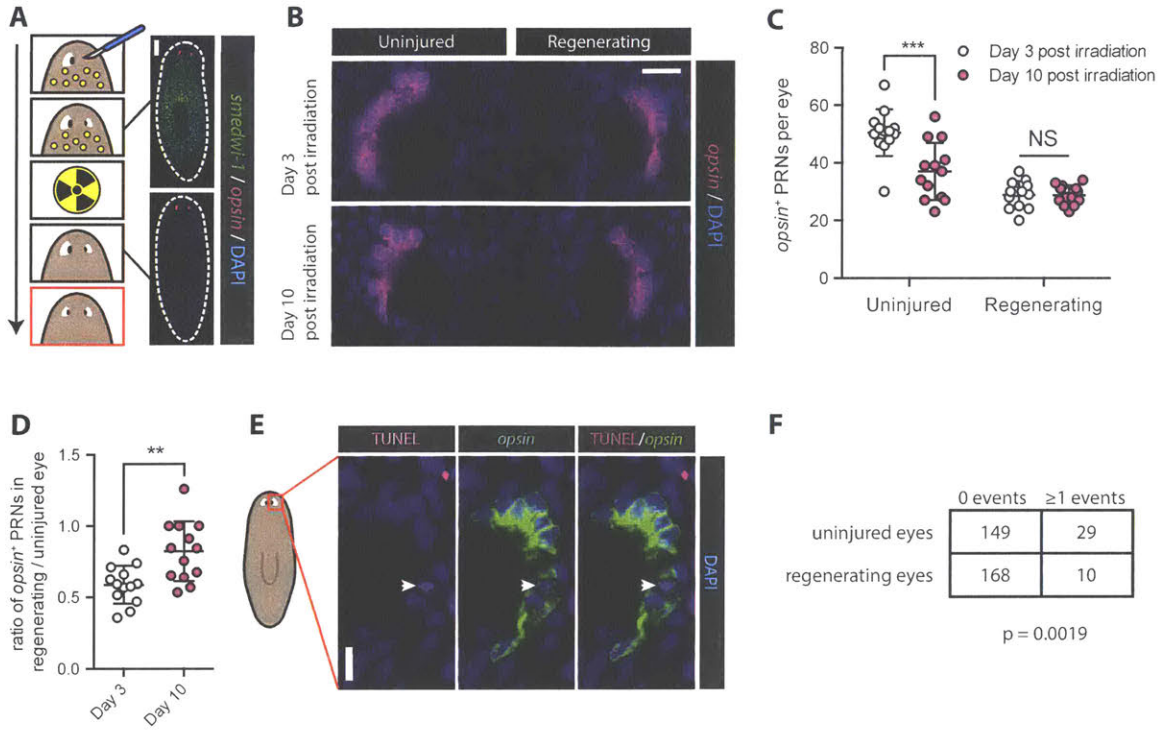
A
smedwi-1 / opsin / DAPI
B
Uninjured
Regenerating
Day 3 post irradiation
Day 10 post irradiation
opsin / DAPI
C
opsin+ PRNs per eye
***
Day 3 post irradiation
Day 10 post irradiation
NS
Uninjured
Regenerating
D
ratio of opsin+ PRNs in regenerating / uninjured eye
**
Day 3
Day 10
E
TUNEL
opsin
TUNEL/opsin
DAPI
F
0 events
≥1 events
uninjured eyes
149
29
regenerating eyes
168
10
p = 0.0019

Figure 4. Regenerating eyes exhibit less cell death than uninjured eyes

(A) Experimental schematic and prediction for comparing PRN loss in uninjured and regenerating eyes after neoblast ablation by irradiation (6,000 rad). Arrow represents time and yellow circles represent neoblasts. Bottom panel (red outline) is predicted outcome if there is less cell death in the regenerating eye. Panels on the right display FISH for *smedwi-1* and *opsin* with DAPI labeling, pre irradiation and 3 days post irradiation. *smedwi-1*$^+$ neoblasts are absent 3 days post irradiation. Dashed white line denotes animal boundary. Scale bar, 200 μm.

(B) Representative *opsin* FISH with DAPI labeling, 3 and 10 days post irradiation. Scale bar, 20 μm.

(C) Total PRNs per eye, 3 and 10 days post irradiation. Decreased PRN number was detected in uninjured but not regenerating eyes. Data presented as mean ± SD. Dots represent PRN counts for individual eyes. Statistical significance assessed by Student's t test (***$p<0.001$). See also Figures S3A–S3C.

(D) Intra-animal ratio of PRNs in regenerating/intact eyes increased from day 3 to day 10 post irradiation. Data presented as mean ± SD. Dots represent ratios from individual animals. Statistical significance assessed by Student's t test (**$p<0.01$).

(E) Combined TUNEL and FISH for *opsin* with DAPI labeling in an uninjured eye. Arrowheads indicate TUNEL$^+$/*opsin*$^+$ PRN. Scale bar, 10 μm.

(F) Table indicating number of uninjured or regenerating eyes 10 days post surgery that contained either 0 or ≥1 TUNEL$^+$/*opsin*$^+$ PRNs. A greater proportion of uninjured eyes than regenerating eyes contained TUNEL$^+$/*opsin*$^+$ PRNs. Statistical significance assessed by Fisher's exact test ($p=0.0019$).

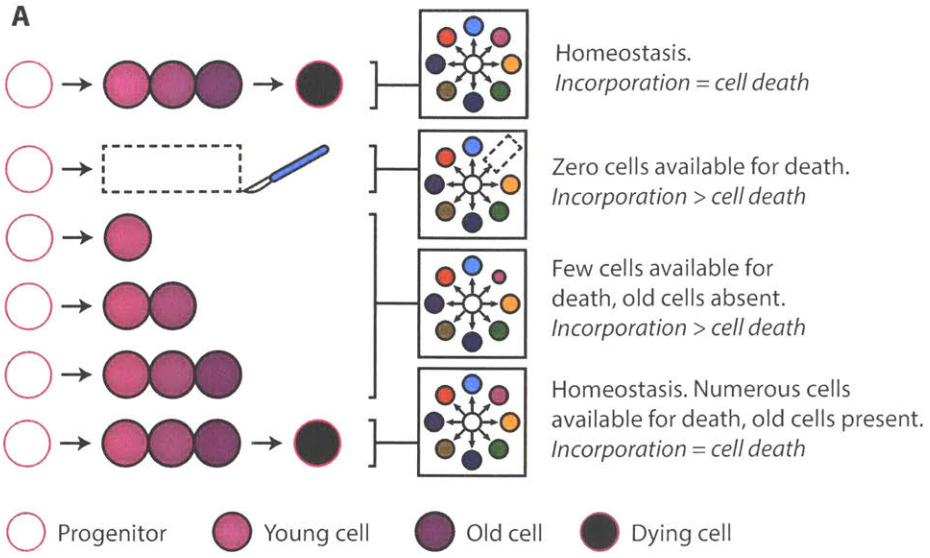
A
Homeostasis.
Incorporation = cell death
Zero cells available for death.
Incorporation > cell death
Few cells available for
death, old cells absent.
Incorporation > cell death
Homeostasis. Numerous cells
available for death, old cells present.
Incorporation = cell death
Progenitor
Young cell
Old cell
Dying cell

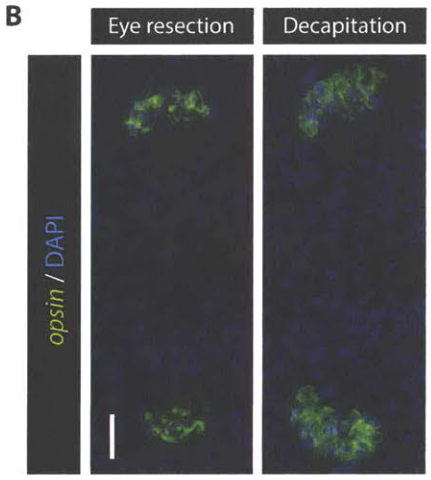
B
Eye resection
Decapitation
opsin / DAPI

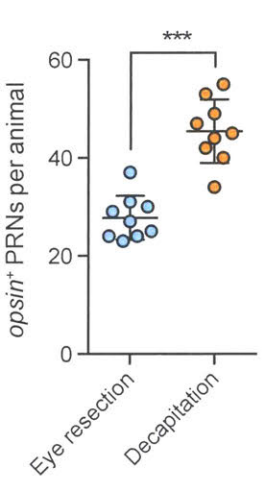
C
***
60
40
20
0
opsin+ PRNs per animal
Eye resection
Decapitation

Figure 5. A passive model for tissue-specific eye regeneration

(A) A passive model for tissue-specific eye regeneration with constant progenitor incorporation. Timeline moves from top to bottom. For right panels, the white circle represents neoblasts and colored circles represent distinct differentiated tissues, as in Figure 1A.

(B) Maximum-intensity projections of FISH for *opsin* with DAPI labeling, 7 days after eye resection or decapitation. Anterior facing left. Scale bar, 20 μm.

(C) Total PRNs per animal 7 days post surgery. Decapitated animals had more PRNs than eye-resected animals. Data presented as mean ± SD. Dots represent PRN counts from individual animals. Statistical significance assessed by Student's t test (***$p<0.001$).

See also Figures S4 and S5.

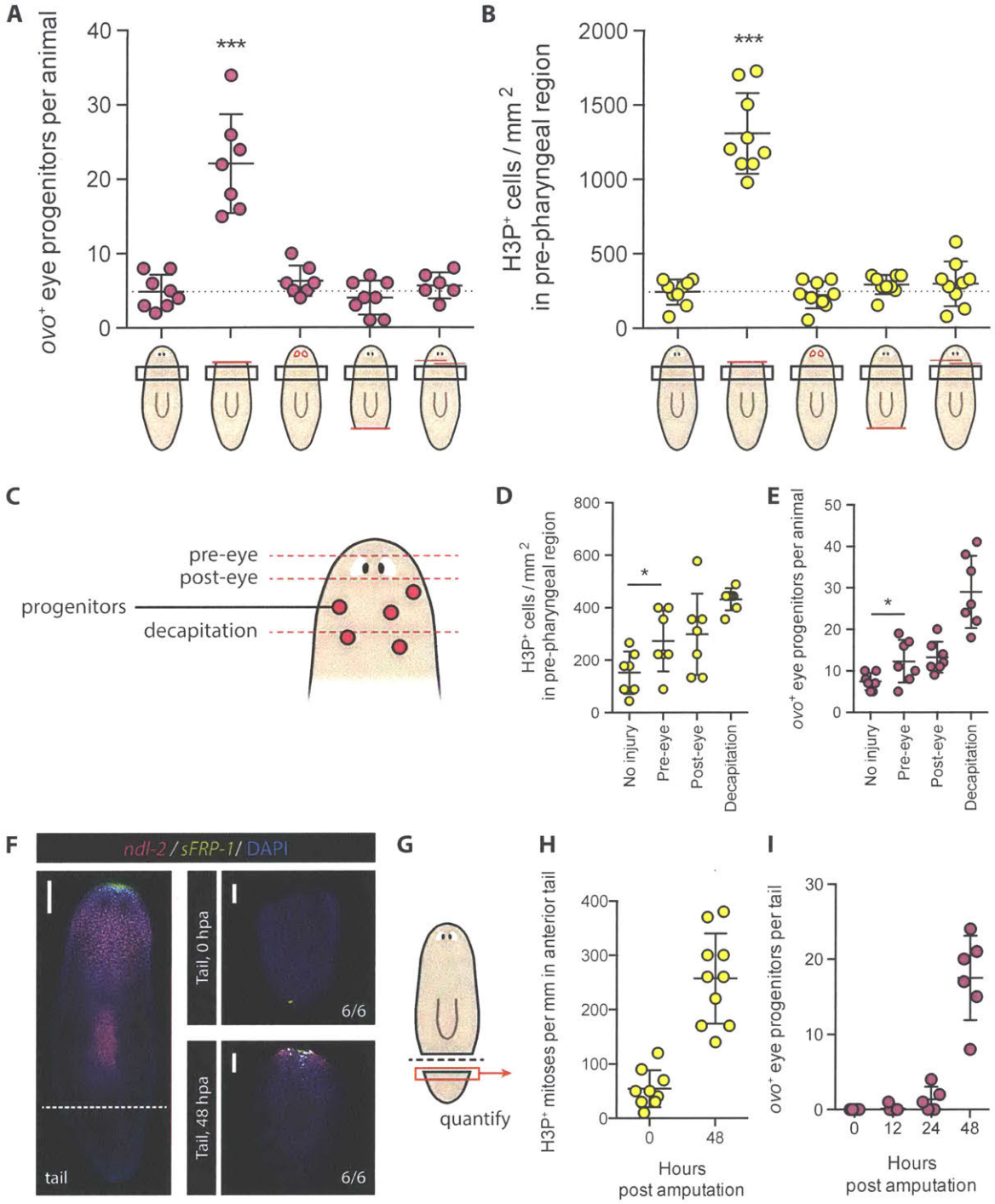
A
ovo+ eye progenitors per animal
***
B
H3P+ cells / mm 2 in pre-pharyngeal region
***
C
pre-eye
post-eye
progenitors
decapitation
D
H3P+ cells / mm 2 in pre-pharyngeal region
*
No injury
Pre-eye
Post-eye
Decapitation
E
ovo+ eye progenitors per animal
*
No injury
Pre-eye
Post-eye
Decapitation
F
ndl-2 / sFRP-1 / DAPI
tail
Tail, 0 hpa
6/6
Tail, 48 hpa
6/6
G
quantify
H
H3P+ mitoses per mm in anterior tail
Hours post amputation
I
ovo+ eye progenitors per tail
Hours post amputation

Figure 6. Eye progenitor amplification is associated with wounds that induce proliferation in the location of eye progenitor specification

(A and B) *ovo*$^{+}$ eye progenitors per animal 4 days post surgery (A) and H3P^{+} mitotic cells per mm^{2} in pre-pharyngeal region 2 days post surgery (B). Cartoons depict surgeries with red lines, from left to right: no surgery, decapitation, eye resection, tail amputation, anterior incisions. Black boxes represent quantification area. Only decapitation led to elevated eye progenitor numbers and increased density of mitotic cells. Data presented as mean ± SD. Dotted lines indicate mean of uninjured animals. Dots represent values from individual animals. Significance assessed with respect to uninjured animals by one-way ANOVA (***$p<0.001$).

(C) Cartoon depicting amputation planes (dashed red lines) for surgeries in (D) and (E).

(D and E) H3P^{+} mitotic cells per mm^{2} (D) and *ovo*$^{+}$ eye progenitors per animal (E) in pre-pharyngeal region following indicated surgeries. Data presented as mean ± SD. Dots represent values from individual animals. Pre-eye amputation increased mitotic density and eye progenitor numbers, as assessed by Student's t test (*$p<0.05$). See also Figure S6A.

(F) Maximum-intensity projection of FISH for *ndl-2* and *sFRP-1* with DAPI labeling in uninjured animal (left) and amputated tails (right), 0 and 48 hr post amputation (hpa). Dotted line indicates amputation plane. *ndl-2* and *sFRP-1* are restored in amputated tails by 48 hpa. Numbers in bottom right of tail insets indicate that 6 of 6 animals displayed the expression patterns shown. Scale bars, 100 μm.

(G) Cartoon indicating region quantified in amputated tails for (H) and (I).

(H and I) H3P^{+} mitotic cells per mm in anterior of tail (H) and *ovo*$^{+}$ cells per tail (I), at indicated hours post amputation. Data presented as mean ± SD. Dots represent values from individual tails.

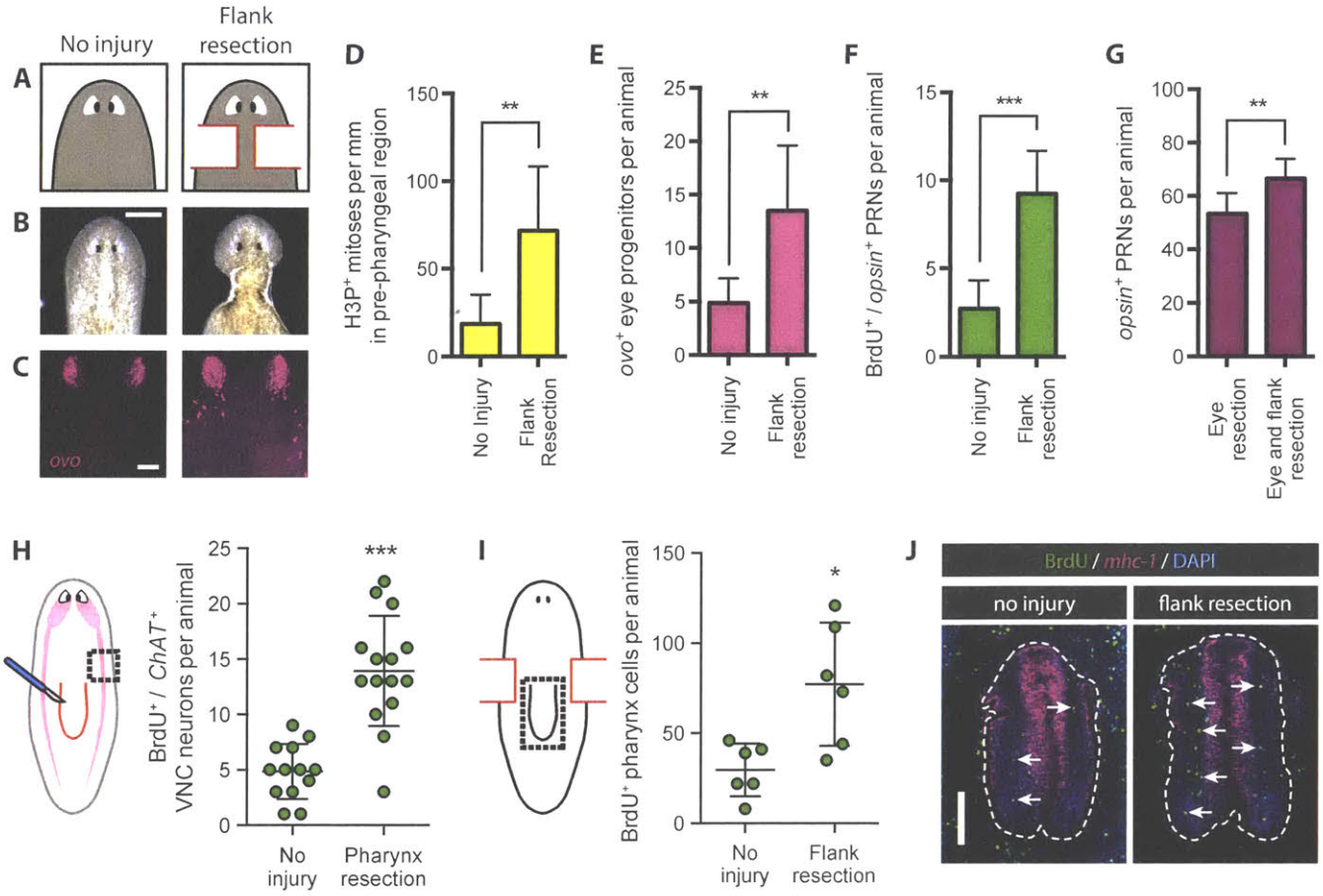
No injury
Flank resection
A
B
C
ovo
D
H3P+ mitoses per mm in pre-pharyngeal region
No Injury
Flank Resection
E
ovo+ eye progenitors per animal
No injury
Flank resection
F
BrdU+ / opsin+ PRNs per animal
No injury
Flank resection
G
opsin+ PRNs per animal
Eye resection
Eye and flank resection
H
BrdU+ / ChAT+ VNC neurons per animal
No injury
Pharynx resection
I
BrdU+ pharynx cells per animal
No injury
Flank resection
J
BrdU / mhc-1 / DAPI
no injury
flank resection

Figure 7. Specific tissue absence is not required for progenitor amplification

(A–C) Uninjured animals (left) and animals that underwent pre-pharyngeal lateral flank resection (right). (A) Cartoon depictions. (B) Live images. Scale bar, 200 μm. (C) FISH for *ovo*. Scale bar, 50 μm.

(D–G) Pre-pharyngeal flank resection increases eye tissue production. (D) $H3P^+$ mitotic cells per mm in pre-pharyngeal region, 48 hr post surgery. (E) ovo^+ eye progenitors per animal 4 days post surgery. (F) $BrdU^+/opsin^+$ PRNs per animal, BrdU pulse-fixation interval days 1–7. (G) PRNs per animal 1 week after eye resection alone or eye and flank resection. Data presented as mean ± SD. Statistical significance assessed using Student's t tests (**p<0.01, ***p<0.001). n≥7 animals per condition. See also Figure S6.

(H and I) Cartoons indicate location of tissue resection (red lines) and quantification areas (dotted black lines). For (J), pink area represents brain and ventral nerve cords (VNCs). Graphs display number of $BrdU^+/ChAT^+$ VNC neurons (H) or $BrdU^+$ cells in pharynx as assessed by *mhc-1* staining (I) per animal following no injury or indicated surgery. BrdU pulse-fixation interval days 1–7 (H) and days 1–4 (I). Data presented as mean ± SD. Dots represent quantified values from individual animals. Statistical significance assessed by Student's t test (*p<0.05, ***p<0.001). See also Figure S7.

(J) IF for BrdU with FISH for *mhc-1* and DAPI labeling in pharynges of animals following no injury or flank resection. Dashed white lines outline pharynx. Arrows indicate examples of $BrdU^+$ cells inside pharynx. Scale bar, 100 μm.

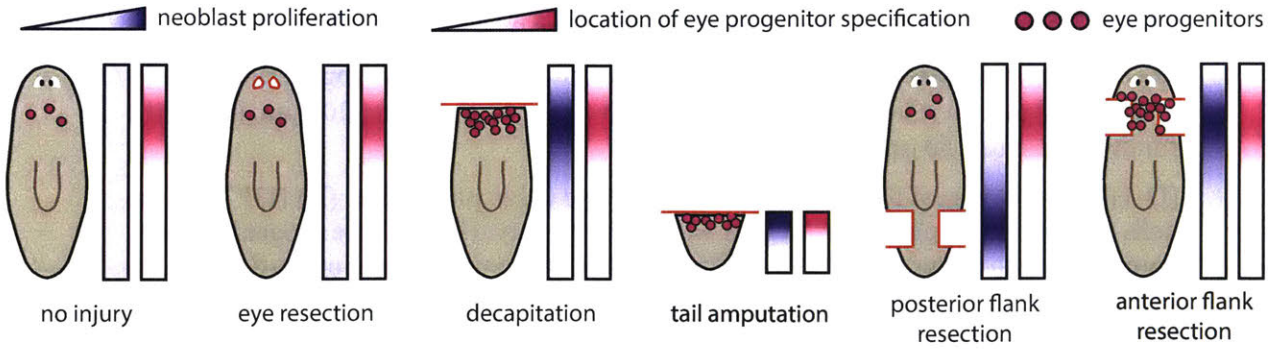
neoblast proliferation
location of eye progenitor specification
eye progenitors
no injury
eye resection
decapitation
tail amputation
posterior flank resection
anterior flank resection

Figure 8. A target-blind model for eye progenitor amplification

Summary of conditions leading to eye progenitor amplification. Red lines indicate surgical procedures and pink dots represent eye progenitors. For each surgery, blue gradient rectangles represent regional neoblast proliferation (dark is increased), and pink gradient rectangles represent location of eye progenitor specification. Eye progenitors are amplified when neoblast proliferation coincides with location of eye progenitor specification. Eye absence was not sufficient or necessary for eye progenitor amplification.

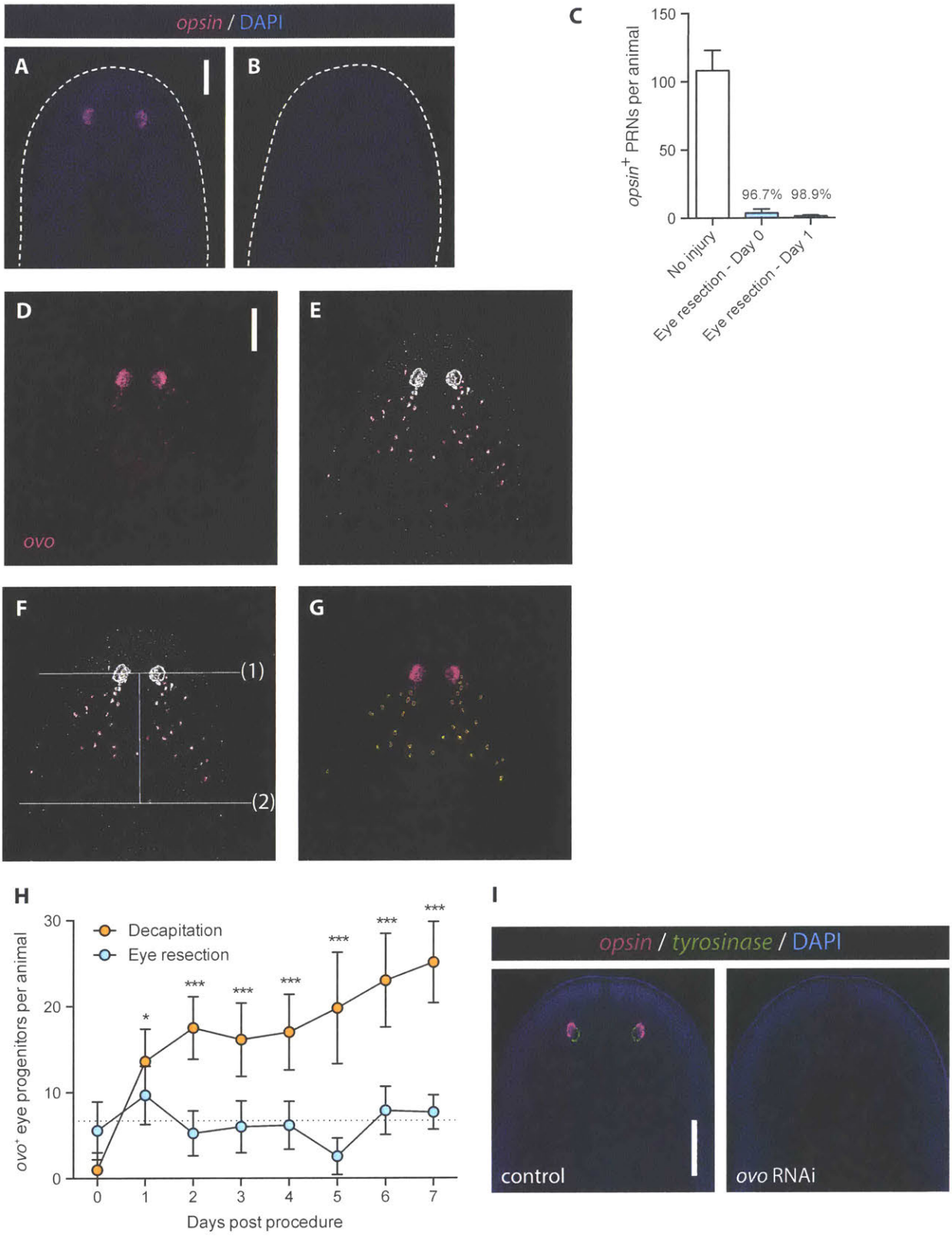
opsin / DAPI
A
B
C
150
100
50
0
opsin+ PRNs per animal
96.7%
98.9%
No injury
Eye resection - Day 0
Eye resection - Day 1
D
ovo
E
F
(1)
(2)
G
H
30
20
10
0
ovo+ eye progenitors per animal
Decapitation
Eye resection
*
***
***
***
***
***
0
1
2
3
4
5
6
7
Days post procedure
I
opsin / tyrosinase / DAPI
control
ovo RNAi

Figure S1. Eye resection controls and semi-automated eye progenitor counting

Related to Figures 1 and 2

(A and B) FISH for *opsin* with DAPI labeling in uninjured animals (A) and eye-resected animals (B) 1 day post surgery demonstrates PRN removal. Dashed white line indicates animal boundary. Scale bar, 100 μm.

(C) PRNs per animal in uninjured and eye-resected animals, 0 and 1 day post surgery. n≥6 animals per condition. Data presented as mean ± SD. Percentages indicate % PRN removal (mean number of PRNs per animal after resection / mean number of PRNs per animal in intact animals x 100). Day 0 and day 1 eye resection data are also shown in Figure S5 regeneration timecourse.

(D-G) Semi-automated progenitor counting procedure. (D) Representative maximum intensity projection from z-stack of FISH for *ovo* in decapitated animal seven days post surgery. Scale bar, 100μm. (E) Appearance of image after processing algorithm. Computer-identified eye progenitors are outlined in magenta. (F) Lines indicate area of progenitor counting, defined as the area between a line running through the eyes (1) and a parallel line 300 μm posterior to the first (2). Events touching the line are counted, events completely outside lines or completely inside eye are not counted. (G) All counted progenitor outlines (yellow) overlayed on original maximum intensity projection.

(H) *ovo*$^{+}$ eye progenitor numbers 0 to 7 days post surgery, as quantified by semi-automated progenitor counting. Data presented as mean ± SD. Dotted line represents mean of uninjured animals on Day 0. Decapitation but not eye resection results in significantly elevated eye progenitor numbers in comparison to uninjured controls. Statistical significance assessed with respect to uninjured animals by one-way ANOVA (*$p<0.05$, ***$p<0.001$).

(I) FISH for *opsin* and *tyrosinase* with DAPI labeling in eye-resected animals 1 week post surgery under control RNAi and *ovo* RNAi conditions. Control RNAi animals regenerated normal eyes containing *tyrosinase*$^{+}$ pigmented optic cup cells and *opsin*$^{+}$ PRNs (10 of 10 animals). *ovo* RNAi animals failed to regenerate eyes (10 of 10 animals had ≤ 3 PRNs, 6 of 10 had 0 PRNs). Scale bar, 200 μm.

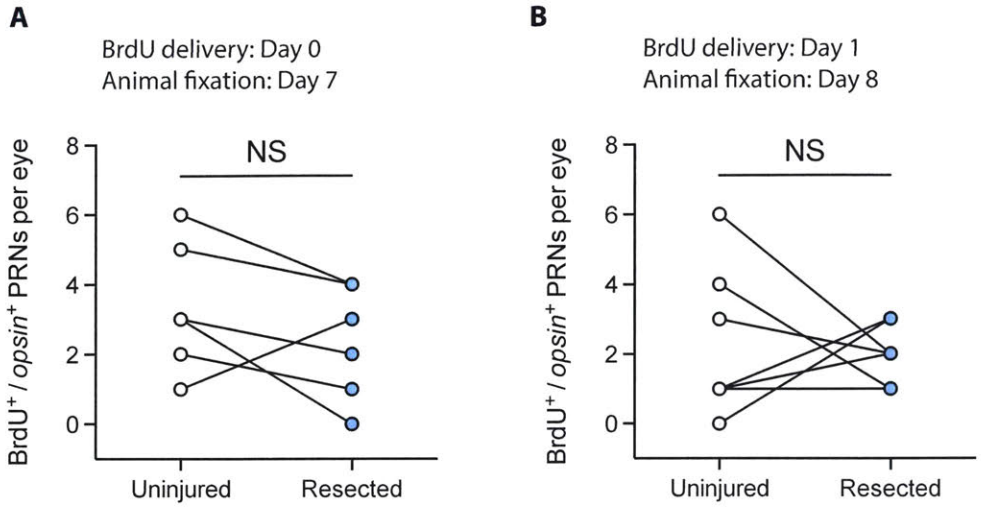
A
BrdU delivery: Day 0
Animal fixation: Day 7
BrdU+ / opsin+ PRNs per eye
8
6
4
2
0
NS
Uninjured
Resected
B
BrdU delivery: Day 1
Animal fixation: Day 8
BrdU+ / opsin+ PRNs per eye
8
6
4
2
0
NS
Uninjured
Resected

Figure S2. Additional single eye resection BrdU incorporation experiments

Related to Figure 3

(A and B) BrdU$^+$/*opsin*$^+$ PRNs per eye after single eye resection. (A) BrdU delivery day 0, animal fixation day 7. n=7 animals. (B) BrdU delivery day 1, animal fixation day 8. n=8 animals. Statistical significance assessed by paired Student's t-tests (NS, not significant).

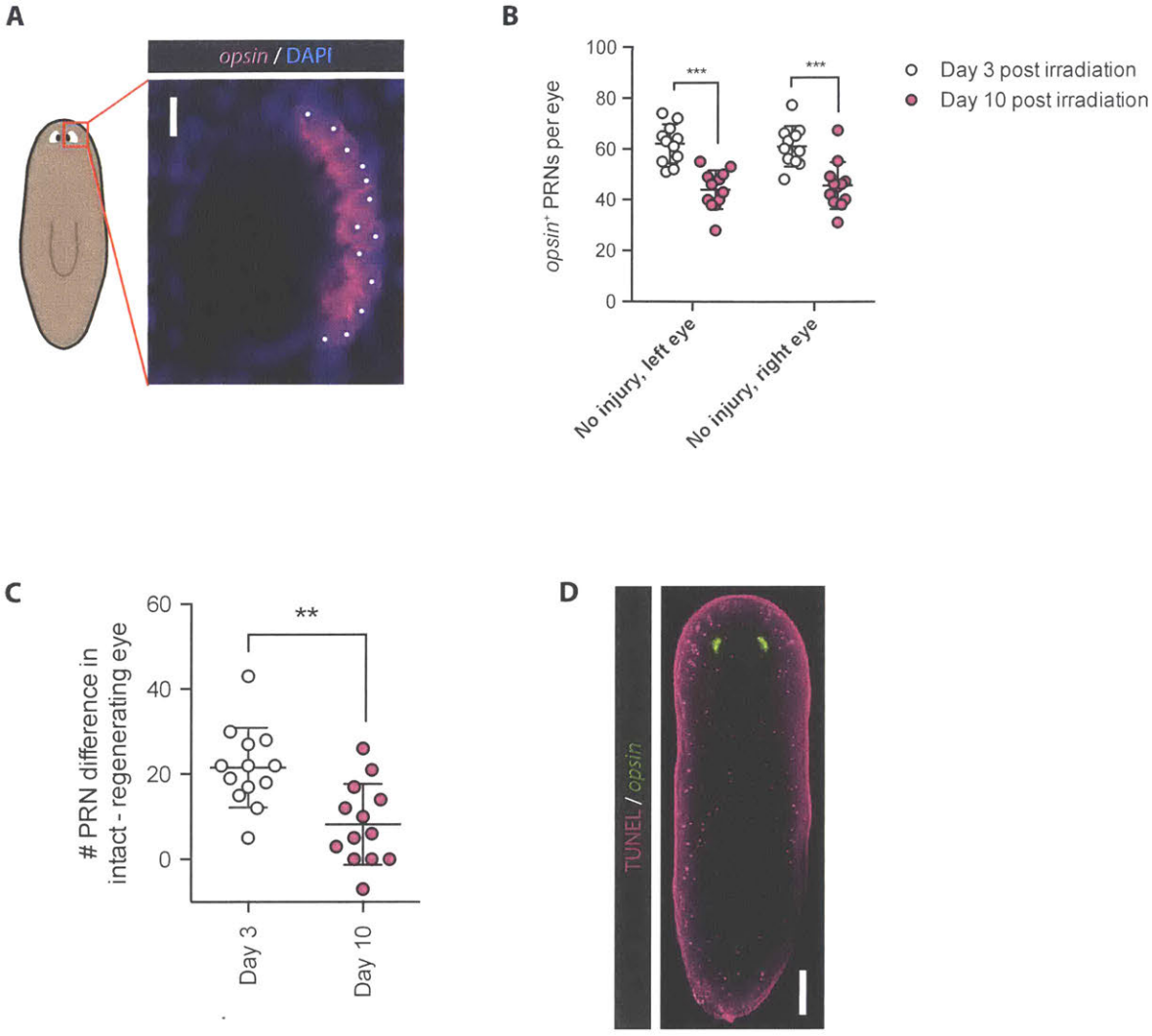
A
opsin / DAPI
B
opsin+ PRNs per eye
100
80
60
40
20
0
***
***
No injury, left eye
No injury, right eye
Day 3 post irradiation
Day 10 post irradiation
C
PRN difference in intact - regenerating eye
60
40
20
0
**
Day 3
Day 10
D
TUNEL / opsin

Figure S3. Cell loss controls and combined TUNEL and FISH for opsin

Related to Figure 4

(A) Example of PRN counting in a single eye. FISH for *opsin* with DAPI labeling. Single confocal optical section, showing individual PRNs marked with white spots. All PRN counting was performed blind to condition. Scale bar, 10 μm.

(B) PRNs per eye, 3 and 10 days post irradiation in uninjured animals. Data presented as mean ± SD. Dots represent PRN counts for individual eyes. Statistical significance assessed by Student's t test (***$p<0.001$).

(C) Intra-animal difference in PRN number (uninjured – regenerating), decreases from Day 3 to Day 10 post-irradiation. Data presented as mean ± SD. Dots represent differences from individual animals. Statistical significance assessed by paired Student's t test (**$p<0.01$).

(D) Combined TUNEL and FISH for *opsin*. Maximum intensity projection. Scale bar, 100 μm.

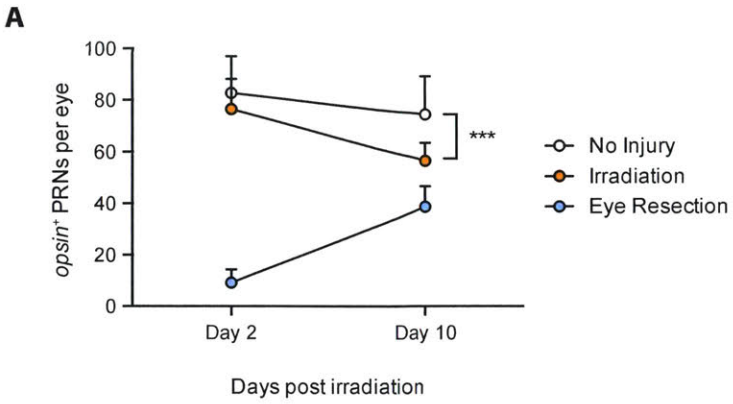
A
100
80
60
40
20
0
opsin+ PRNs per eye
***
No Injury
Irradiation
Eye Resection
Day 2
Day 10
Days post irradiation

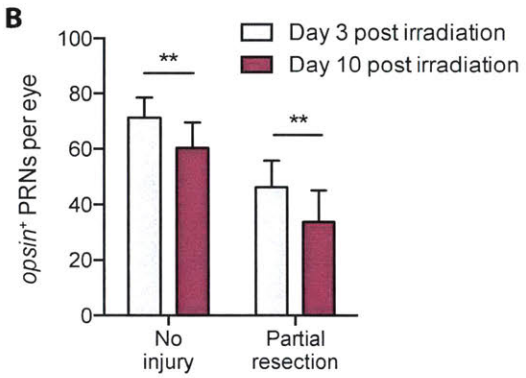
B
Day 3 post irradiation
Day 10 post irradiation
100
80
60
40
20
0
opsin+ PRNs per eye
**
**
No injury
Partial resection

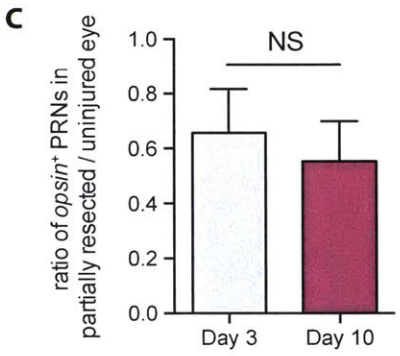
C
NS
1.0
0.8
0.6
0.4
0.2
0.0
ratio of opsin+ PRNs in partially resected / uninjured eye
Day 3
Day 10

Figure S4. Dynamics of eye growth and de-growth are consistent with a passive model for tissue-specific eye regeneration

Related to Figures 4 and 5

(A) PRNs per eye day 2 and day 10 after indicated manipulation. Data presented as mean ± SD. Significance assessed by Student's t-test (***$p<0.001$). $n\geq10$ animals per condition.

(B and C) Uninjured and partially resected eyes undergo cell loss at similar rates. (B) PRNs per eye Day 3 and Day 10 post irradiation for indicated surgeries. (C) Intra-animal ratio of PRNs in regenerating/intact eyes remained constant from day 3 to day 10 post irradiation. Data presented as mean ± SD. Significance assessed by Student's t-test (**$p<0.01$); NS, not significant. $n=12$ animals per time point.

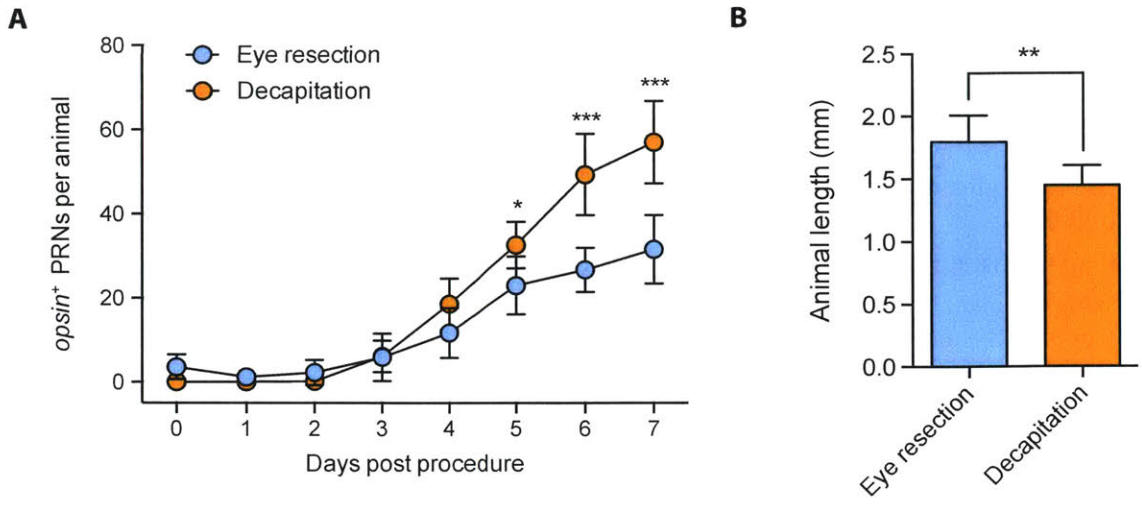
A
B
Eye resection
Decapitation
opsin+ PRNs per animal
Days post procedure
Animal length (mm)
Eye resection
Decapitation
*
**
***

Figure S5. Eye-resected animals regenerate eyes more slowly than decapitated animals

Related to Figure 5

(A) PRN regeneration timecourse following decapitation or eye resection. PRNs per animal day 0 to day 7 post procedure are shown. Decapitated animals have a significantly greater number of PRNs than eye-resected animals at 5, 6 and 7 days post procedure. Animals are same as used for eye progenitor counting in Figure 2D. Day 0 and day 1 eye resection data is also shown in Figure S1C. Data presented as mean ± SD. Statistical significance assessed by Student's t-test (*$p<0.05$, ***$p<0.001$). $n\geq4$ animals per condition.

(B) Animal length seven days post surgery. Decapitated animals are significantly shorter than eye-resected animals. Data presented as mean ± SD. Statistical significance assessed by Student's t-test (**$p<0.01$). $n\geq9$ animals per condition.

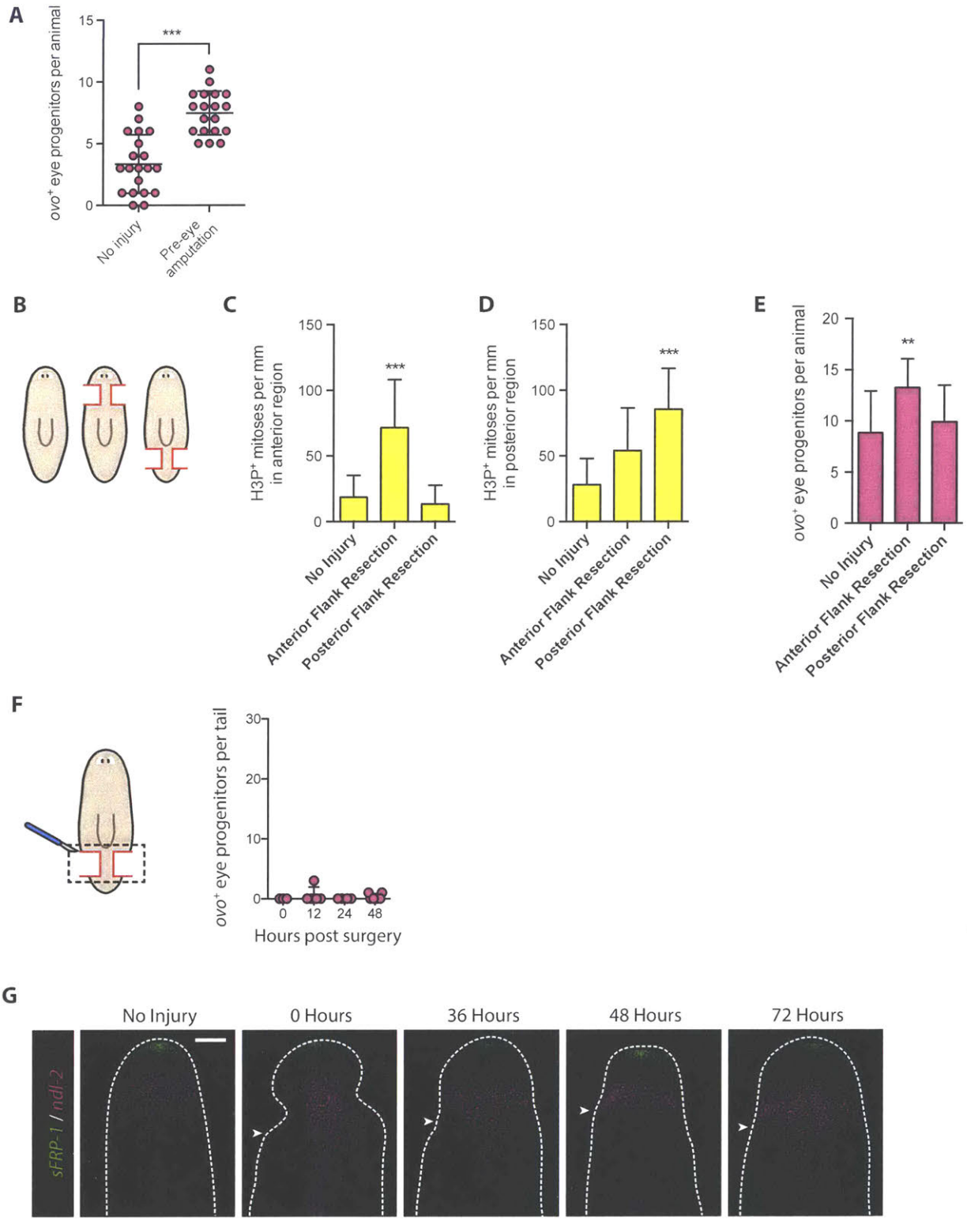
A
ovo+ eye progenitors per animal
15
10
5
0
***
No injury
Pre-eye amputation
B
C
H3P+ mitoses per mm in anterior region
150
100
50
0
***
No Injury
Anterior Flank Resection
Posterior Flank Resection
D
H3P+ mitoses per mm in posterior region
150
100
50
0
***
No Injury
Anterior Flank Resection
Posterior Flank Resection
E
ovo+ eye progenitors per animal
20
15
10
5
0
**
No Injury
Anterior Flank Resection
Posterior Flank Resection
F
ovo+ eye progenitors per tail
30
20
10
0
0
12
24
48
Hours post surgery
G
No Injury
0 Hours
36 Hours
48 Hours
72 Hours
sFRP-1 / ndl-2

Figure S6. Eye progenitor amplification is associated with wounds that induce proliferation in the location of eye progenitor specification

Related to Figures 6 and 7

(A) Independent experiment determining the effect of pre-eye amputation on eye progenitor numbers. *ovo*$^{+}$ eye progenitors per animal 4 days after no injury and pre-eye amputation, as depicted in Figure 6C. Pre-eye amputation induces significant increase in eye progenitor numbers. Data presented as mean ± SD. Dots represent values from individual animals. Statistical significance assessed by Student's t-test (***$p<0.001$).

(B) Cartoon depiction of uninjured animal (left), anterior flank resection (center), and posterior flank resection (right).

(C and D) H3P^{+} cells per mm in anterior (C) and posterior (D) regions 48 hours after surgeries indicated in (B). Data from (C) is also displayed in Figure 7D. Data presented as mean ± SD. Statistical significance assessed with respect to uninjured animals by one-way ANOVA (***$p<0.001$). $n\geq9$ animals per condition.

(E) *ovo*$^{+}$ eye progenitors per animal 4 days after surgeries depicted in (B). Data presented as mean ± SD. Significance assessed with respect to uninjured animals by one-way ANOVA (**$p<0.01$). $n\geq11$ animals per condition.

(F) *ovo*$^{+}$ eye progenitors per tail 0, 12, 24, and 48 hr post flank resection. Cartoon depicts surgery (red lines) and area quantified (dotted black lines). Posterior flank resection does not amplify *ovo*$^{+}$ eye progenitors in the tail. Dots represent values from individual animals. $n\geq3$ animals per time point.

(G) FISH for *sFRP-1* and *ndl-2* in anterior of uninjured and anterior flank-resected animals 0, 36, 48, and 72 hr post surgery. Dashed white line denotes animal boundary. Arrowheads indicate posterior boundary of flank resections. *sFRP-1* expression was not detected at the posterior boundary of flank resection. *ndl-2* was not posteriorly expanded after flank resection. $n\geq5$ animals per condition. Scale bar, 200 μm.

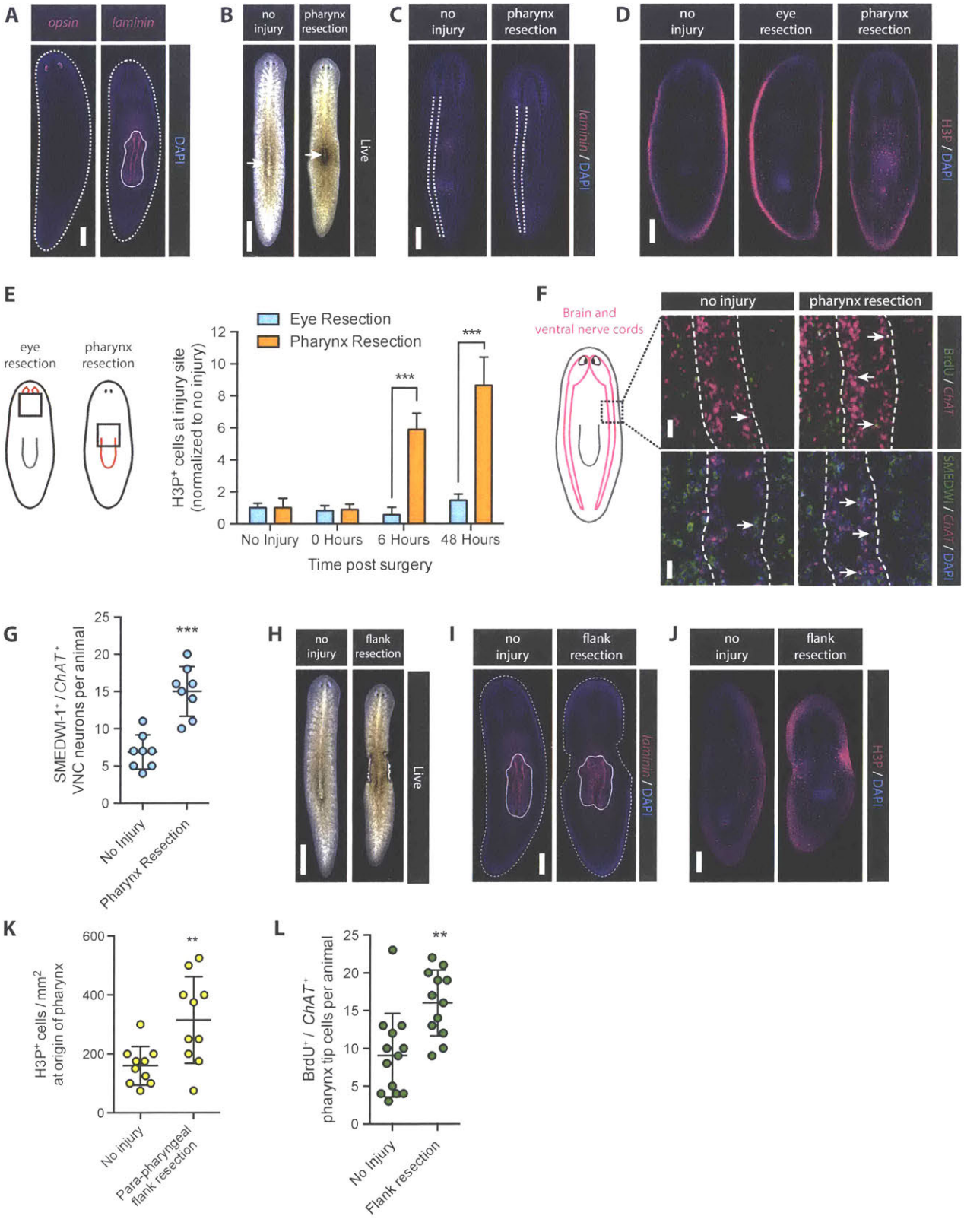
A
opsin
laminin
DAPI
B
no injury
pharynx resection
Live
C
no injury
pharynx resection
laminin / DAPI
D
no injury
eye resection
pharynx resection
H3P / DAPI
E
eye resection
pharynx resection
Eye Resection
Pharynx Resection
H3P+ cells at injury site (normalized to no injury)
***
***
No Injury
0 Hours
6 Hours
48 Hours
Time post surgery
F
Brain and ventral nerve cords
no injury
pharynx resection
BrdU / ChAT
SMEDWI / ChAT / DAPI
G
SMEDWI-1+ / ChAT+ VNC neurons per animal
***
No Injury
Pharynx Resection
H
no injury
flank resection
Live
I
no injury
flank resection
laminin / DAPI
J
no injury
flank resection
H3P / DAPI
K
H3P+ cells / mm2 at origin of pharynx
**
No injury
Para-pharyngeal flank resection
L
BrdU+ / ChAT+ pharynx tip cells per animal
**
No Injury
Flank resection

Figure S7. Increased progenitor incorporation into the ventral nerve cords and pharynx does not require specific tissue removal

Related to Figure 7

(A) FISH for *opsin* or *laminin* with DAPI labeling. *laminin* marks pharynx tissue. Dashed lines indicate animal boundaries, solid lines indicate borders of PRNs or pharynx. Scale bar, 200 μm. The pharynx is much larger than the eyes.

(B) Live images of the same animal immediately before (left) and after (right) dorsal surgical pharynx resection. Arrow indicates location of pharynx (left) or location of dorsal incision through which pharynx was excised (right). Scale bar, 1 mm.

(C) FISH for *laminin* with DAPI labeling after no injury and dorsal surgical pharynx resection. Dashed white lines indicate left ventral nerve cord (VNC). Scale bar, 200 μm. Surgery removes pharynx and leaves VNCs continuous and intact.

(D) IF for H3P with DAPI labeling in uninjured, eye-resected and pharynx-resected animals 48 hours post surgery. Scale bar, 200 μm. Pharynx-resected but not eye-resected animals display increased mitotic activity near the site of tissue removal.

(E) Cartoons depict surgeries (red lines) and location of quantification (black boxes) for eye- and pharynx-resected animals. Graph indicates mitotic density at indicated times post surgery, normalized to mean of uninjured animals. Pharynx but not eye resection induces sustained local neoblast proliferation. Data presented as mean ± SD. Significance assessed by Student's t-test (***$p<0.001$).

(F) IF for BrdU with FISH for *ChAT* (top insets) and IF for SMEDWI-1 with FISH for *ChAT* and DAPI labeling (bottom insets) after no injury or pharynx resection. Dashed white lines indicate VNC boundaries. Arrows indicate BrdU$^+$/*ChAT*$^+$ or SMEDWI-1$^+$/*ChAT*$^+$ VNC cells. Scale bars, 20 μm.

(G) SMEDWI-1$^+$/*ChAT*$^+$ VNC neurons per animal 4 days after no injury or pharynx resection. Quantification performed in VNC just anterior to pharynx. Data presented as mean ± SD. Dots represent values from individual animals. Significance assessed by Student's t-test (***$p<0.001$).

(H) Live images of the same animal immediately before (left) and after (right) para-pharyngeal flank resection. Scale bar, 1 mm.

(I) FISH for *laminin* with DAPI labeling in animals fixed immediately after no injury or para-pharyngeal flank resection. Dashed white lines indicate animal boundaries, solid white lines outline pharynges. Scale bar, 200 μm. Para-pharyngeal flank resection does not remove pharynx tissue.

(J) IF for H3P with DAPI labeling 48 hours after no injury or para-pharyngeal flank resection. Scale bar, 200 μm. Flank resection increases mitotic activity near the pharynx.

(K) Mitotic density near pharynx 48 hours after no injury or para-pharyngeal flank resection. Data presented as mean ± SD. Dots represent values from individual animals. Significance assessed by Student's t-test (**$p<0.01$).

(L) BrdU$^+$/*ChAT*$^+$ pharynx tip cells per animal after no injury or para-pharyngeal flank resection. BrdU delivery day -1, fixation day 4 with respect to surgery. Data presented as

mean ± SD. Dots represent values from individual animals. Significance assessed by Student's t-test (**$p<0.01$).

REFERENCES

Adler, C.E., and Sánchez Alvarado, A. (2015). Types or states? Cellular dynamics and regenerative potential. Trends Cell Biol. *25*, 687-96.

Adler, C.E., Seidel, C.W., McKinney, S.A., and Sánchez Alvarado, A. (2014). Selective amputation of the pharynx identifies a FoxA-dependent regeneration program in planaria. eLife *3*, e02238.

Amamoto, R., Huerta, V.G., Takahashi, E., Dai, G., Grant, A.K., Fu, Z., and Arlotta, P. (2016). Adult axolotls can regenerate original neuronal diversity in response to brain injury. eLife *5*, e13998.

Baguñà, J. (1976). Mitosis in the intact and regenerating planarian *Dugesia mediterranea* n.sp. II. Mitotic studies during regeneration, and a possible mechanism of blastema formation. J. Exp. Zool. *195*, 65-80.

Baguñà, J., Saló, E., and Auladell, C. (1989). Regeneration and pattern formation in planarians III. Evidence that neoblasts are totipotent stem cells and the source of blastema cells. Development *107*, 77-86.

Benian, G.M., Kiff, J.E., Neckelmann, N., Moerman, D.G., and Waterston, R.H. (1989). Sequence of an unusually large protein implicated in regulation of myosin activity in *C. elegans*. Nature *342*, 45-50.

Chen, C.C., Wang, L., Plikus, M.V., Jiang, T.X., Murray, P.J., Ramos, R., Guerrero-Juarez, C.F., Hughes, M.W., Lee, O.K., Shi, S., *et al.* (2015). Organ-level quorum sensing directs regeneration in hair stem cell populations. Cell *161*, 277-90.

Cowles, M.W., Brown, D.D., Nisperos, S.V., Stanley, B.N., Pearson, B.J., and Zayas, R.M. (2013). Genome-wide analysis of the bHLH gene family in planarians identifies factors required for adult neurogenesis and neuronal regeneration. Development *140*, 4691-702.

Currie, K.W., and Pearson, B.J. (2013). Transcription factors *lhx1/5-1* and *pitx* are required for the maintenance and regeneration of serotonergic neurons in planarians. Development *140*, 3577-88.

Dubois, F. (1949). Contribution a l'étude de la migration des cellules de régénération chez les *Planaires dulcicoles*. Bull. Biol. Fr. Belg. *83*, 213-83.

Forsthoefel, D.J., Park, A.E., and Newmark, P.A. (2011). Stem cell-based growth, regeneration, and remodeling of the planarian intestine. Dev. Biol. *356*, 445-59.

Guo, T., Peters, A.H., and Newmark, P.A. (2006). A *Bruno-like* gene is required for stem cell maintenance in planarians. Dev. Cell *11*, 159-69.

Gurley, K.A., Elliott, S.A., Simakov, O., Schmidt, H.A., Holstein, T.W., and Sánchez Alvarado, A. (2010). Expression of secreted Wnt pathway components reveals unexpected complexity of the planarian amputation response. Dev. Biol. *347*, 24-39.

Hsu, Y.C., and Fuchs, E. (2012). A family business: stem cell progeny join the niche to regulate homeostasis. Nat. Rev. Mol. Cell Biol. *13*, 103-14.

King, R.S., and Newmark, P.A. (2013). *In situ* hybridization protocol for enhanced detection of gene expression in the planarian *Schmidtea mediterranea*. BMC Dev. Biol. *13*, 8.

Lapan, S.W., and Reddien, P.W. (2011). *dlx* and *sp6-9* control optic cup regeneration in a prototypic eye. PLOS Genet. *7*, e1002226.

Lapan, S.W., and Reddien, P.W. (2012). Transcriptome analysis of the planarian eye identifies *ovo* as a specific regulator of eye regeneration. Cell Rep. *2*, 294-307.

Mangel, M., Bonsall, M.B., and Aboobaker, A. (2016). Feedback control in planarian stem cell systems. BMC Syst. Biol. *10*, 17.

März, M., Seebeck, F., and Bartscherer, K. (2013). A Pitx transcription factor controls the establishment and maintenance of the serotonergic lineage in planarians. Development *140*, 4499-509.

Morgan, T.H. (1898). Experimental studies of the regeneration of *Planaria maculata*. Arch. Entw. Mech. Org. *7*, 364-97.

Newmark, P., and Sánchez Alvarado, A. (2000). Bromodeoxyuridine specifically labels the regenerative stem cells of planarians. Dev. Biol. *220*, 142-53.

Nishimura, K., Inoue, T., Yoshimoto, K., Taniguchi, T., Kitamura, Y., and Agata, K. (2011). Regeneration of dopaminergic neurons after 6-hydroxydopamine-induced lesion in planarian brain. J. Neurochem. *119*, 1217-31.

Pearson, B.J., Eisenhoffer, G.T., Gurley, K.A., Rink, J.C., Miller, D.E., and Sánchez Alvarado, A. (2009). Formaldehyde-based whole-mount *in situ* hybridization method for planarians. Dev. Dynam. *238*, 443-50.

Pellettieri, J., Fitzgerald, P., Watanabe, S., Mancuso, J., Green, D.R., and Sánchez Alvarado, A. (2010). Cell death and tissue remodeling in planarian regeneration. Dev. Biol. *338*, 76-85.

Petersen, C.P., and Reddien, P.W. (2008). *Smed-βcatenin-1* is required for anteroposterior blastema polarity in planarian regeneration. Science *319*, 327-30.

Petersen, C.P., and Reddien, P.W. (2009). A wound-induced Wnt expression program controls planarian regeneration polarity. Proc. Natl. Acad. Sci. U.S.A. *106*, 17061-6.

Poss, K.D. (2010). Advances in understanding tissue regenerative capacity and mechanisms in animals. Nat. Rev. Genet. *11*, 710-22.

Reddien, P.W. (2011). Constitutive gene expression and the specification of tissue identity in adult planarian biology. Trends Genet. *27*, 277-85.

Reddien, P.W., Oviedo, N.J., Jennings, J.R., Jenkin, J.C., and Sánchez Alvarado, A. (2005). SMEDWI-2 is a PIWI-like protein that regulates planarian stem cells. Science *310*, 1327-30.

Reddien, P.W., and Sánchez Alvarado, A. (2004). Fundamentals of planarian regeneration. Annu. Rev. Cell Dev. Bio. *20*, 725-57.

Rouhana, L., Weiss, J.A., Forsthoefel, D.J., Lee, H., King, R.S., Inoue, T., Shibata, N., Agata, K., and Newmark, P.A. (2013). RNA interference by feeding in vitro-synthesized double-stranded RNA to planarians: methodology and dynamics. Dev. Dynam. *242*, 718-30.

Sánchez Alvarado, A. (2000). Regeneration in the metazoans: why does it happen? Bioessays *22*, 578-90.

Sánchez Alvarado, A., and Newmark, P.A. (1999). Double-stranded RNA specifically disrupts gene expression during planarian regeneration. Proc. Natl. Acad. Sci. U.S.A. *96*, 5049-54.

Sánchez Alvarado, A., Newmark, P.A., Robb, S.M., and Juste, R. (2002). The *Schmidtea mediterranea* database as a molecular resource for studying platyhelminthes, stem cells and regeneration. Development *129*, 5659-65.

Schindelin, J., Arganda-Carreras, I., Frise, E., Kaynig, V., Longair, M., Pietzsch, T., Preibisch, S., Rueden, C., Saalfeld, S., Schmid, B., *et al.* (2012). Fiji: an open-source platform for biological-image analysis. Nat. Methods *9*, 676-82.

Scimone, M.L., Cote, L.E., Rogers, T., and Reddien, P.W. (2016). Two FGFRL-Wnt circuits organize the planarian anteroposterior axis. eLife *5*, e12845.

Scimone, M.L., Kravarik, K.M., Lapan, S.W., and Reddien, P.W. (2014). Neoblast specialization in regeneration of the planarian *Schmidtea mediterranea*. Stem Cell Rep. *3*, 339-52.

Scimone, M.L., Meisel, J., and Reddien, P.W. (2010). The Mi-2-like *Smed-CHD4* gene is required for stem cell differentiation in the planarian *Schmidtea mediterranea*. Development *137*, 1231-41.

Scimone, M.L., Srivastava, M., Bell, G.W., and Reddien, P.W. (2011). A regulatory program for excretory system regeneration in planarians. Development *138*, 4387-98.

Tanaka, E.M., and Reddien, P.W. (2011). The cellular basis for animal regeneration. Dev. Cell *21*, 172-85.

van Wolfswinkel, J.C., Wagner, D.E., and Reddien, P.W. (2014). Single-cell analysis reveals functionally distinct classes within the planarian stem cell compartment. Cell Stem Cell *15*, 326-39.

Wagner, D.E., Ho, J.J., and Reddien, P.W. (2012). Genetic regulators of a pluripotent adult stem cell system in planarians identified by RNAi and clonal analysis. Cell Stem Cell *10*, 299-311.

Wagner, D.E., Wang, I.E., and Reddien, P.W. (2011). Clonogenic neoblasts are pluripotent adult stem cells that underlie planarian regeneration. Science *332*, 811-6.

Wenemoser, D., and Reddien, P.W. (2010). Planarian regeneration involves distinct stem cell responses to wounds and tissue absence. Dev. Biol. *344*, 979-91.

Witchley, J.N., Mayer, M., Wagner, D.E., Owen, J.H., and Reddien, P.W. (2013). Muscle cells provide instructions for planarian regeneration. Cell Rep. *4*, 633-41.

Chapter 3

DISCUSSION

PROPORTION CONTROL WITHOUT TISSUE-SPECIFIC FEEDBACK IN PLANARIANS

Planarians restore proportion with great specificity after any injury, raising the hypothesis that cells somehow sense and respond to the relative sizes of specific tissues, tailoring production or death accordingly. The work presented in this thesis shows that eye progenitor production is target-blind – not influenced by the presence or absence of the eye, and our findings from the pharynx and ventral nerve cords (VNCs) suggest that target-blind tissue production may be a general phenomenon. In light of this, a critical re-evaluation of proportion control in planarians is necessary. Here, I consider the implications of target-blind tissue production for planarian regeneration in general, and speculate on how tissue proportion control might be implemented in the absence of tissue-specific feedback on production.

Constant progenitor production ratios maintain and restore tissue proportion in a tissue-specific manner

As a population, neoblasts give rise to progenitor types in different ratios. For example, a given population of neoblasts in the pre-pharyngeal region gives rise to a greater number of epidermal progenitors than eye progenitors. Progenitor numbers can be amplified after injury, but amplification appears to occur non-specifically for many or all tissues that are specified in a location where neoblast proliferation occurs (LoCascio et al., 2017). Together, these data suggest that within a given location, the relative numbers of

progenitor classes to one another remain relatively constant, rather than being dynamically altered in response to perturbations in specific differentiated tissues.

A static progenitor specification ratio can underlie maintenance and restoration of proportion, without being adjusted based on relative tissue size. To illustrate this, consider a set population of neoblasts that gives rise to 1 "pink" and 2 "blue" progenitors per arbitrary unit of time, which successfully incorporate into their respective tissues. Assume a constant stochastic death rate for each tissue, with each differentiated cell having a 1 in 5 probability of dying per day. Our data indicate that both age-dependent and stochastic death occur in the eye. For simplicity, I use purely stochastic death in this example, although similar conclusions are reached under the age-dependent cell death situation, as discussed in Chapter 2. At equilibrium (homeostasis), the size of the pink tissue will be 5 cells, because at that size, the rate of cell death (total dying cells per day) will be equal to the progenitor production rate, or one cell per day. The homeostatic blue tissue size will be 10 cells, because at that size the rate of blue cell death will be equal to blue progenitor production rate, or 2 cells per day. Therefore, static specification ratios can support homeostatic maintenance of tissues of different corresponding sizes (Figure 1A).

Now consider a scenario where the blue tissue is suddenly reduced to half its size (5 cells), becoming disproportionately small (Figure 1B). If each cell retains a 1 in 5 chance of dying per day, then the rate of blue cell death will be decreased to 1 cell per day. The constant rate of 2 blue progenitors produced per day will thus exceed the rate of cell death, leading to net growth specifically in the blue tissue. In contrast, consider a scenario where the blue tissue is increased in size to 15 cells (Figure 1C). At this size, 3

cells will stochastically die per day, so death will exceed production and cause net degrowth until proportion is reached. This simple example shows that constant production of progenitors at a fixed ratio without tissue-specific feedback can facilitate restoration of proportional tissue size. Interestingly, although the probability of death is fixed at the cellular level, the rate of death on the level of the entire tissue is modulated as an emergent property of tissue size.

Spatial restriction facilitates progenitor amplification specificity

Although progenitors in a given location appear to be amplified without specificity after wounding, spatial restriction of distinct progenitor types may facilitate amplification of approximately appropriate progenitor subsets. For example, pharynx resection leads to increased mitosis near the pharynx, and general non-specific amplification of nearby progenitors for tissues such as the VNCs. However, pharynx resection would not be expected to induce amplification of progenitors in the head (e.g., eye progenitors), because mitosis is localized to the wound. Therefore, on the organismal level, the spatial restriction of progenitor subsets provides specificity to the wound response (Figure 2A). Despite not being perfectly tuned to the presence and absence of specific tissues within a given region, this coarse level of specificity is likely appropriate in many natural situations, where a traumatic injury large enough to induce a sustained mitotic response is likely to damage many tissue types, rather than precisely excising a single tissue.

The amount of specificity achieved by spatial restriction depends on two primary factors. The first is the degree of compartmentalization of progenitor subsets. If two progenitor types are completely non-overlapping, then an injury near one will have a

minimal effect on the other. As progenitor types become less separated, or their borders become less defined, a corresponding decrease in the ability to amplify one and not the other occurs (Figure 2B). The second factor that determines the degree of specificity provided by spatial restriction is the distribution of the local mitotic response to wounding. A broader mitotic response will decrease the specificity of progenitor amplification (Figure 2C), since progenitors located farther from the injury will be amplified.

Based on our results from the pharynx, the restriction of progenitor location and/or the mitotic response to wounding was not sufficient to result in specific pharynx progenitor amplification, since VNC progenitors were also amplified. However, it is possible that pharynx removal increased pharynx production more than it increased VNC production. This would in fact be expected if pharynx progenitors were on average more proximal to the pharynx than VNC progenitors. More detailed investigation will be necessary to assess whether regional progenitor amplification shows bias towards particular lineages, and to what degree this bias may be explained by spatial restriction of mitosis and progenitor specification.

Progenitor restriction serves multiple advantages. First, progenitors tend to be located near the tissue they produce; pharynx progenitors surround the pharynx (Adler et al., 2014), eye and brain progenitors are located in the pre-pharyngeal region and head (Lapan and Reddien, 2011, 2012), and epidermal progenitors are distributed throughout the body, with ventral and dorsal epidermal progenitors biased ventrally and dorsally, respectively (van Wolfswinkel et al., 2014; Wurtzel et al., 2017). This arrangement allows appropriate progenitor subsets to proliferate in response to large wounds that

likely damage the tissue they produce. Another advantage is that this arrangement minimizes the distance a progenitor must migrate after being specified. Given the advantages of progenitor restriction, it is currently unclear why some progenitors are so widely distributed. For example, eye progenitors are specified broadly in the head and pre-pharyngeal region, yet they coalesce to a very specific location. This arrangement may reflect the relative scarcity of neoblasts in the anterior, thus necessitating specification further from the target tissue, or may serve additional unrecognized functions.

In conclusion, spatial restriction of progenitor specification and the mitotic response to wounding provide considerable regeneration specificity without requiring neoblasts to interpret the relative abundance of differentiated tissue types.

A global cell death response complements regional progenitor amplification

The nature of tissue production following wounding is inherently imprecise (Amamoto et al., 2016; Chen et al., 2015; Forsthoefel et al., 2011; LoCascio et al., 2017), yet somehow this imprecision does not lead to gross disproportion. For example, flank wounds increase production and incorporation of eye progenitors into intact eyes, yet fail to robustly increase eye size (LoCascio et al., 2017). Similarly, decapitation leads to increased incorporation into nearby uninjured gut tissue (Forsthoefel et al., 2011). It is therefore likely that cell death plays a complementary role to tissue production in constraining proportion, as has been extensively recognized for nervous system development elsewhere (Hamburger and Levi-Montalcini, 1949; Yamaguchi and Miura, 2015).

The regulation of wound-induced apoptosis at a tissue-specific level in planarians is largely uncharacterized, so multiple scenarios may explain why the eyes are not robustly increased in size after flank wounds. One possibility is that cell death specifically constrains maximum eye size in proportion to other tissues. For example, photoreceptor neurons may compete for a limited number of post-synaptic partners providing neurotrophins. In this scenario, cell death would be a consequence of disproportion, representing size-dependent feedback. A precise timecourse of the onset of increased incorporation and cell death might support the causality implied by this hypothesis. Alternatively, specific ablation of the neurons post-synaptic to PRNs would be expected to decrease eye size, but their identity is unknown. Importantly, irradiated animals lacking neoblasts also exhibit globally elevated wound-induced apoptosis, so feedback as a consequence of inappropriate tissue production is not necessary to explain increased death in the eye following flank wounds (Pellettieri et al., 2010).

An alternative hypothesis is that globally increased cell death does not depend on inappropriate proliferation, and is an independent consequence of large wounds. This is consistent with the neoblast-independent nature of wound-induced apoptosis. Furthermore, sustained apoptosis also occurs in regions where amplification is not observed, for example in the pharynx after decapitation (Pellettieri et al., 2010). Globally increased death following wounding might be advantageous for restoring proportion in multiple ways. First, the removal of a large amount of tissue will almost always cause remaining structures to become disproportionately large for the new total size of the body fragment. It is therefore unnecessary for specific remaining tissues to sense their disproportion, since the removal of a large amount of tissue will necessitate degrowth. An

exception to this rule may be uniformly distributed tissues such as the epidermis, pigment, protonephridia, or muscle. As opposed to discrete structures like the eyes, brain or pharynx, uniformly distributed tissues will remain relatively proportional to the new size of the body fragment after amputation. It will be interesting to determine whether the global apoptotic response selectively spares such tissues. However, regional patterns of gene expression have been documented in the epidermis and muscle (Scimone et al., 2016; Witchley et al., 2013; Wurtzel et al., 2017), calling into question whether a tissue with truly uniform distribution even exists. A second advantage of globally increased death following wounding is that progenitors for some remaining structures near the wound may be inappropriately amplified (e.g., the eyes after flank resection). Globally increased death may be a built-in mechanism to help ensure that such structures do not grow disproportionately large.

Although apoptosis appears to be global after wounding, there may yet be underlying layers of specificity that are not apparent based on general distribution of TUNEL. For example, it is possible that newly differentiated tissues are less susceptible to wound-induced cell death. Indeed, our studies of the eye suggest that young cells are less likely to undergo death than old cells during homeostasis (LoCascio et al., 2017). Susceptibility to death based on differentiation stage has also been observed elsewhere. For example, BMP4 promotes death at a specific progenitor stage in the context of mammalian olfactory epithelium neurogenesis (Shou et al., 1999). PRNs in the developing *Drosophila* eye also have different susceptibilities to cell death based on developmental stage (Fan and Bergmann, 2014). Selective resistance of young cells to wound-induced apoptosis in planarians could specifically accelerate regeneration of

amputated tissues. Determining whether developmental stage affects susceptibility to wound-induced apoptosis should be feasible, for example by performing TUNEL on FACS-sorted fractions of cells based on DNA content, or performing TUNEL in combination with markers that indicate differentiation status (e.g., *smedwi-1*). A better understanding of whether and how the specificity of death is implemented will be essential for a basic understanding of tissue proportion control in planarians.

Non-specifically increased turnover accelerates regeneration

A common feature of injuries removing significant tissue in planarians is that increased neoblast proliferation and apoptosis are sustained near the wound site (Pellettieri et al., 2010; Wenemoser and Reddien, 2010). Although counterintuitive, simultaneously and non-specifically increasing both tissue production and cell death rate could be a general strategy for accelerating restoration of tissue proportion through both tissue-specific growth and degrowth after injury. Consider a tissue that is produced at 1 cell per arbitrary unit of time, with each differentiated cell having a stochastic 1 in 10 (0.1) probability of dying per time (Figure 3A). Under these circumstances, average tissue size can be iteratively calculated using the following formula:

$$x_{t+1} = x_t + p - (d \bullet x_t)$$

where

x_{t+1} is the tissue size at time $t + 1$

x_t is the tissue size at time t

p is the rate of tissue production in cells per time

d is the probability of death per cell per time

For the proposed scenario, size will reach equilibrium at 10 cells, when $x_{t+1} = x_t$, as shown in the equation below:

$x_{t+1} = 10 + 1 - (0.1 \bullet 10) = 10$

Now consider the same tissue when both production and death rate are doubled; 2 cells are produced per time, and each cell has a stochastic 2 in 10 (0.2) probability of dying per time (Figure 3A). Again, the tissue will maintain homeostatic equilibrium at 10 cells:

$x_{t+1} = 10 + 2 - (0.2 \bullet 10) = 10$

Although both scenarios result in the same homeostatic tissue size, the scenario with doubled turnover restores proportion twice as rapidly, both after tissue removal (necessitating regenerative tissue growth) and after tissue size doubling (necessitating degrowth) (Figure 3B). For example, starting from a size of $x_t = 0$, the first scenario reaches 90% regeneration (9 cells) by $t = 22$, whereas doubling turnover reduces this time to $t = 11$. Therefore, simultaneously increasing both the production and death rate of a tissue has no effect on homeostatic size, but accelerates both regeneration and degrowth regardless of the starting point (Figure 3B).

By extension, non-specifically increasing both production and death of all tissues near a wound will accelerate restoration of proportionality. Wounds are unpredictable and represent an infinite variety of starting points for regeneration, in each case requiring the

growth or degrowth of a different combination of myriad tissue types. Measuring and responding to the precise relative abundance of each tissue after an injury would be an incredibly complex feat. As an alternative, increased general turnover would be an effective general strategy that could be easily implemented near any wound to restore proportionality without sensing relative tissue abundance. A previously unappreciated high rate of homeostatic turnover already appears to underlie tissue-specific eye regeneration after specific resection, without requiring neoblasts to sense and respond to eye absence. Elevated general regional turnover would simply be a strategy to further accelerate this process for larger wounds. The non-specificity of tissue production at wound sites is consistent with this strategy (Forsthoefel et al., 2011; LoCascio et al., 2017), but a careful analysis of cell death specificity will be necessary to determine whether it is indeed employed.

CONCLUSION

Our studies have revealed a novel mechanism for tissue-specific regeneration in the planarian eye that is facilitated by decreased cell death and constant tissue production. We have also shown that the production of eye cells is not influenced by the presence or absence of the eye, thus supporting a target-blind model for tissue production that may extend to multiple planarian tissues. Detailed case studies will be necessary to determine the extent of tissues to which this model can be applied, and it is indeed highly possible that tissue-specific feedback contributes to the efficiency of regeneration in contexts other than the eye. However, it is clear that a target-blind model for tissue production is compatible with tissue-specific regeneration, and robust maintenance and restoration of tissue proportion in planarians.

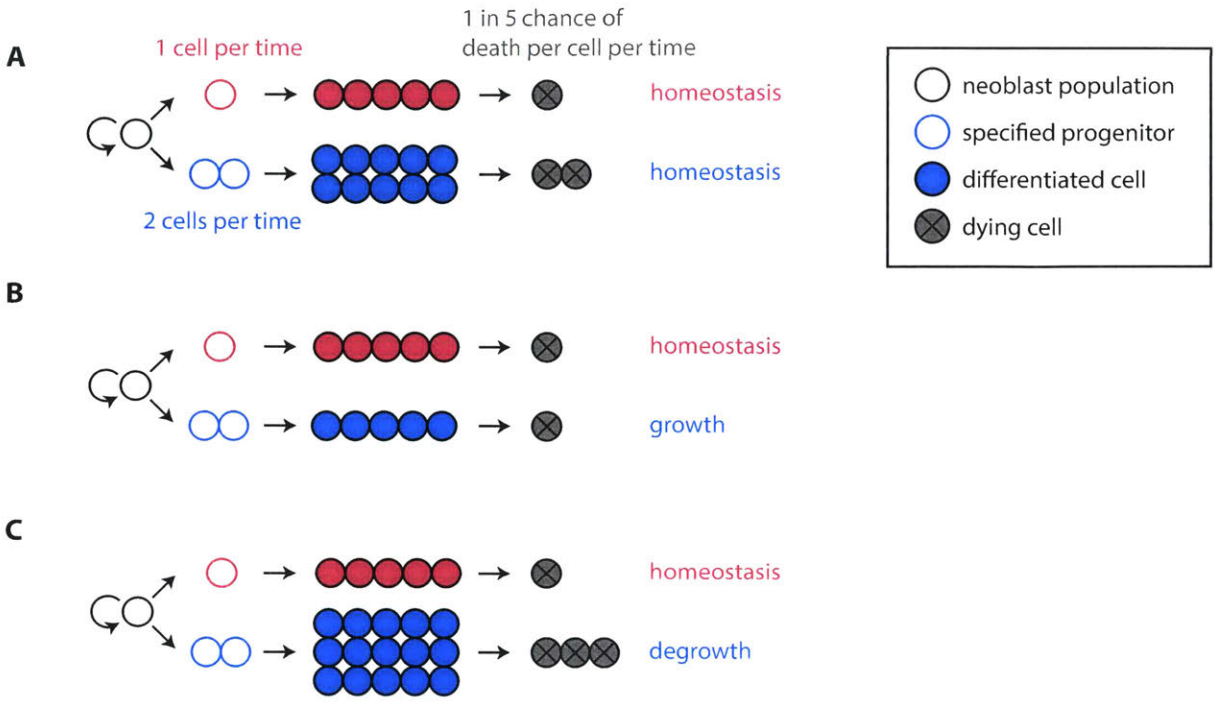
A
1 cell per time
1 in 5 chance of
death per cell per time
homeostasis
homeostasis
2 cells per time
B
homeostasis
growth
C
homeostasis
degrowth
neoblast population
specified progenitor
differentiated cell
dying cell

Figure 1. Constant progenitor production ratios maintain and restore proportion in a tissue-specific manner

In each panel, the neoblast population (white circle) produces 1 pink progenitor and 2 blue progenitors that successfully incorporate into their respective tissues per arbitrary unit time. Each cell has a fixed stochastic 1 in 5 chance of cell death per time. Expected change in tissue size given current tissue size indicated on right.

(A) Homeostasis is maintained at tissue sizes of 5 pink and 10 blue cells.

(B) Reducing blue tissue size to 5 cells results in an imbalance such that production exceeds cell death, resulting in regenerative growth specifically in the blue tissue.

(C) Increasing blue tissue size to 15 cells results in an imbalance such that cell death exceeds production, resulting in specific degrowth of the blue tissue.

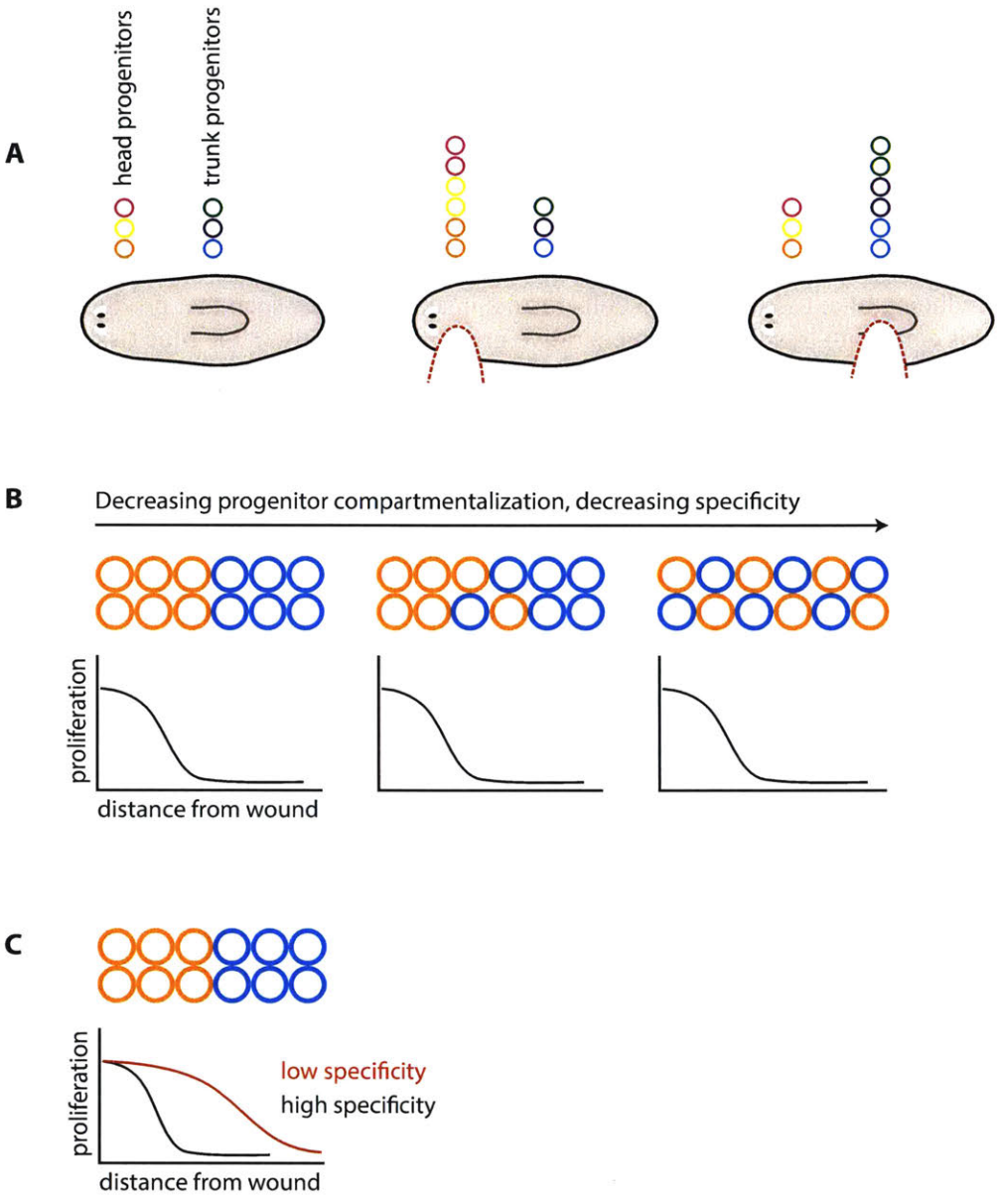
A
head progenitors
trunk progenitors
B
Decreasing progenitor compartmentalization, decreasing specificity
proliferation
distance from wound
C
proliferation
low specificity
high specificity
distance from wound

Figure 2. Spatial restriction facilitates progenitor amplification specificity

(A) Regionally restricted progenitors (colored circles) exist in the head and trunk during homeostasis (left). Large head wounds amplify head but not trunk progenitors (center), and large trunk wounds amplify trunk but not head progenitors (right).

(B) Progenitor compartmentalization facilitates specificity. Progenitors are represented by colored circles, with localized wound-induced proliferation plotted below. Progenitors that are separated by distinct borders may be amplified exclusively (left), whereas decreased compartmentalization reduces the possibility for specific progenitor amplification (center and right).

(C) Distribution of the mitotic response to wounding determines the specificity of progenitor amplification. A tight distribution of wound-induced mitosis will specifically amplify the most proximal progenitors (black curve), whereas a wide distribution (red curve) will amplify progenitors further from the wound site.

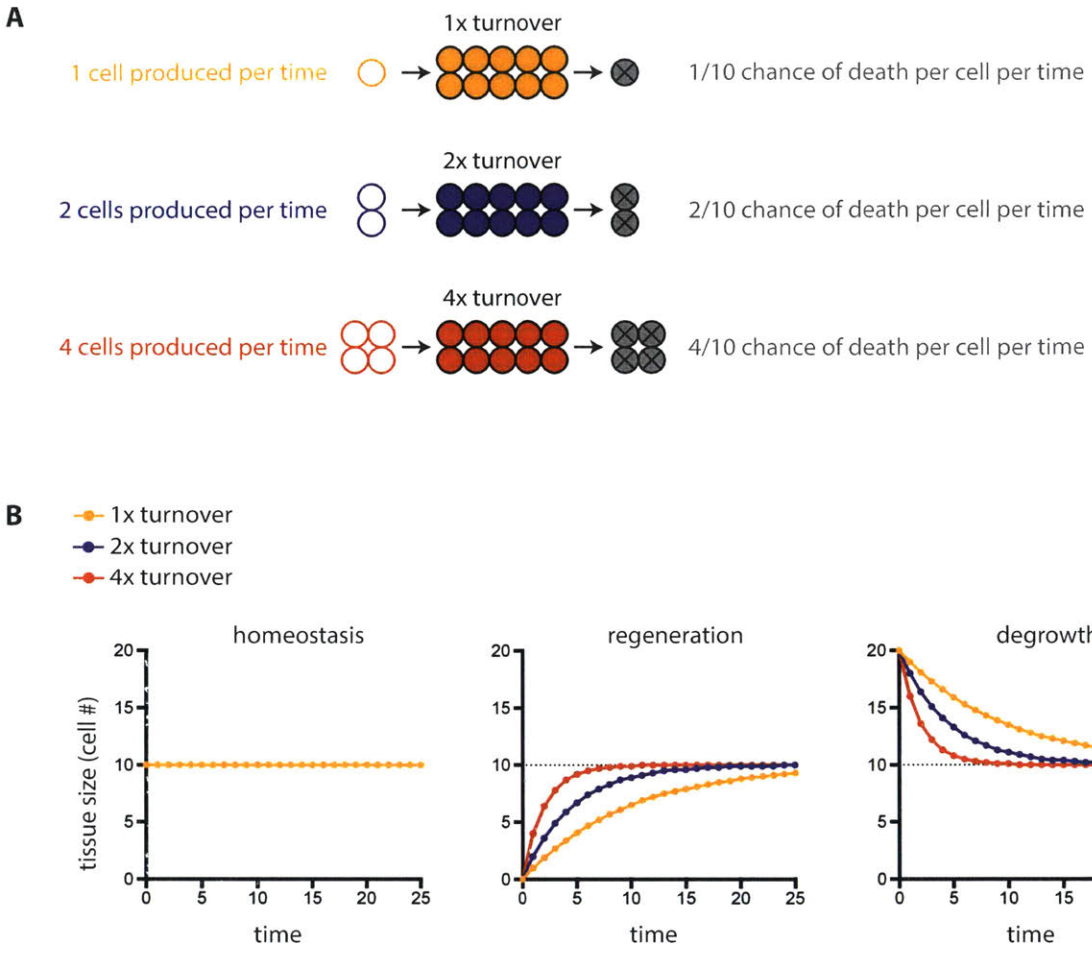
A
1x turnover
1 cell produced per time
1/10 chance of death per cell per time
2x turnover
2 cells produced per time
2/10 chance of death per cell per time
4x turnover
4 cells produced per time
4/10 chance of death per cell per time
B
1x turnover
2x turnover
4x turnover
homeostasis
regeneration
degrowth
tissue size (cell #)
time
time
time

Figure 3. Increased non-specific turnover accelerates restoration of proportion

(A) Homeostatic tissue size of 10 cells maintained under different turnover conditions. In the first condition (1x turnover) tissue is produced at 1 cell per arbitrary unit of time, with each cell having a 1 in 10 probability of cell death per time. 2x and 4x turnover conditions represent doubled and quadrupled tissue production and death probabilities, respectively.

(B) Calculated tissue size over time (see equation in text) under 1x, 2x and 4x turnover conditions described in (A) when starting from tissue size = 10 cells (homeostasis), 0 cells (regenerative growth), and 20 cells (degrowth). High turnover accelerates restoration of proportion regardless of starting size.

REFERENCES

Adler, C.E., Seidel, C.W., McKinney, S.A., and Sánchez Alvarado, A. (2014). Selective amputation of the pharynx identifies a FoxA-dependent regeneration program in planaria. eLife *3*, e02238.

Amamoto, R., Huerta, V.G., Takahashi, E., Dai, G., Grant, A.K., Fu, Z., and Arlotta, P. (2016). Adult axolotls can regenerate original neuronal diversity in response to brain injury. eLife *5*, e13998.

Chen, C.C., Wang, L., Plikus, M.V., Jiang, T.X., Murray, P.J., Ramos, R., Guerrero-Juarez, C.F., Hughes, M.W., Lee, O.K., Shi, S., *et al.* (2015). Organ-level quorum sensing directs regeneration in hair stem cell populations. Cell *161*, 277-90.

Fan, Y., and Bergmann, A. (2014). Multiple mechanisms modulate distinct cellular susceptibilities toward apoptosis in the developing *Drosophila* eye. Dev. Cell *30*, 48-60.

Forsthoefel, D.J., Park, A.E., and Newmark, P.A. (2011). Stem cell-based growth, regeneration, and remodeling of the planarian intestine. Dev. Biol. *356*, 445-59.

Hamburger, V., and Levi-Montalcini, R. (1949). Proliferation, differentiation and degeneration in the spinal ganglia of the chick embryo under normal and experimental conditions. J. Exp. Zool. *111*, 457-501.

Lapan, S.W., and Reddien, P.W. (2011). *dlx* and *sp6-9* control optic cup regeneration in a prototypic eye. PLOS Genet. *7*, e1002226.

Lapan, S.W., and Reddien, P.W. (2012). Transcriptome analysis of the planarian eye identifies *ovo* as a specific regulator of eye regeneration. Cell Rep. *2*, 294-307.

LoCascio, S.A., Lapan, S.W., and Reddien, P.W. (2017). Eye absence does not regulate planarian stem cells during eye regeneration. Dev. Cell *40*, 381-91.

Pellettieri, J., Fitzgerald, P., Watanabe, S., Mancuso, J., Green, D.R., and Sánchez Alvarado, A. (2010). Cell death and tissue remodeling in planarian regeneration. Dev. Biol. *338*, 76-85.

Scimone, M.L., Cote, L.E., Rogers, T., and Reddien, P.W. (2016). Two FGFRL-Wnt circuits organize the planarian anteroposterior axis. eLife *5*, e12845.

Shou, J., Rim, P.C., and Calof, A.L. (1999). BMPs inhibit neurogenesis by a mechanism involving degradation of a transcription factor. Nat. Neurosci. *2*, 339-45.

van Wolfswinkel, J.C., Wagner, D.E., and Reddien, P.W. (2014). Single-cell analysis reveals functionally distinct classes within the planarian stem cell compartment. Cell Stem Cell *15*, 326-39.

Wenemoser, D., and Reddien, P.W. (2010). Planarian regeneration involves distinct stem cell responses to wounds and tissue absence. Dev. Biol. *344*, 979-91.

Witchley, J.N., Mayer, M., Wagner, D.E., Owen, J.H., and Reddien, P.W. (2013). Muscle cells provide instructions for planarian regeneration. Cell Rep. *4*, 633-41.

Wurtzel, O., Oderberg, I.M., and Reddien, P.W. (2017). Planarian epidermal stem cells respond to positional cues to promote cell-type diversity. Dev. Cell *40*, 491-504.

Yamaguchi, Y., and Miura, M. (2015). Programmed cell death in neurodevelopment. Dev. Cell *32*, 478-90.